The Dissertation Committee for Alan James Dutson Certifies that this is the approved version of the following dissertation:

Functional Prototyping Through Advanced Similitude Techniques

Committee:

Kristin L. Wood, Supervisor

Joseph J. Beaman, Co-Supervisor

Richard H. Crawford

David L. Bourell

Kenneth M. Liechti

Functional Prototyping Through Advanced Similitude Techniques

by

Alan James Dutson, BSME, MSME

Dissertation

Presented to the Faculty of the Graduate School of

The University of Texas at Austin

in Partial Fulfillment

of the Requirements

for the Degree of

Doctor of Philosophy

The University of Texas at Austin

December, 2002

Dedication

To my wife, Joanna

Acknowledgements

There are many people who have encouraged and supported me in this effort. First and foremost, I must acknowledge the support of my wife, Joanna, who was willing to leave our comfortable life in industry to return to school and pursue this goal. Without her support and help, none of this would have been possible. I must also thank our parents, Bill and Faun Dutson and Michael and Maria Moody, for their encouragement and love. I would also like to thank our five beautiful children, Jonathan, Spencer, Christopher, Andrew, and little Amy, for their love and patience with me.

I must also thank my dissertation committee for their contributions and support of this work. My supervisors, Dr. Wood and Dr. Beaman, provided valuable insights and suggestions throughout the duration of this work. Their occasional redirections of the course of my research proved to be invaluable. Dr. Wood also dedicated a significant amount of time reviewing chapters and providing corrections and feedback. The other members of my committee, Dr. Crawford, Dr. Bourell, and Dr. Liechti, were always willing to take time to review my progress and give their input and ideas. I would also like to acknowledge the help of Dr. Eric Becker who, although not an official member of my committee, was generous in sharing his time and knowledge of the finite element method.

Finally, I would like to acknowledge the support of several MADlab colleagues, particularly Monty Greer, Mike VanWie, and Rodrigo Ruizpalacios. Their willingness to listen, give ideas on my research, and provide moral support was greatly appreciated.

ALAN JAMES DUTSON

The University of Texas at Austin

December, 2002

Functional Prototyping Through Advanced Similitude Techniques

Publication No._____

Alan James Dutson, Ph.D.

The University of Texas at Austin, 2002

Supervisors: Kristin L. Wood

Joseph J. Beaman

The advent of rapid prototyping (RP) technologies has led to significant improvements in many aspects of the mechanical design process. Among these enhancements is the ability to quickly evaluate the *fit* and *form* of a product. Limited material properties and part sizes available from common RP systems, however, have prevented rapid prototypes from being widely used in *functional* testing. Using rapid prototypes in place of traditional prototypes in functional evaluations of product performance has the potential to significantly reduce overall design costs and improve time to market.

Similitude techniques are proposed as a means of correlating the behavior of rapid prototypes with the behavior of a product. The research presented in this dissertation expands our understanding of the capabilities and limitations of current similitude techniques. The similitude techniques that are evaluated include

the traditional similitude method (TSM), which is also known as dimensional analysis, and the empirical similitude method (ESM). The concept of *system distortion*, which causes a model to exhibit a different behavior than the product it represents, is developed for both the TSM and the ESM. Errors in predicted product behavior that result from system distortions are illustrated through numerical and experimental examples.

An advanced ESM technique that accounts for system distortions is also presented. The advanced technique utilizes additional models to capture changes in behavior that are caused by system distortions. The increased accuracy that is available from the advanced technique comes at the price of increased effort in model fabrication and testing. Guidelines for selecting the most appropriate similitude approach for a given set of circumstances are presented.

Table of Contents

List of Tables

List of Figures

CHAPTER 1

Introduction

The product development process is defined as the set of all activities associated with the creation of a device that fulfills a set of customer needs. If the product to be designed is primarily mechanical in nature, the development process is referred to as *mechanical design*. A simple model of the mechanical design process is shown in Figure 1.

Each stage of the design process results in an updated design concept or a refined description of the final product. The results of each stage in the design

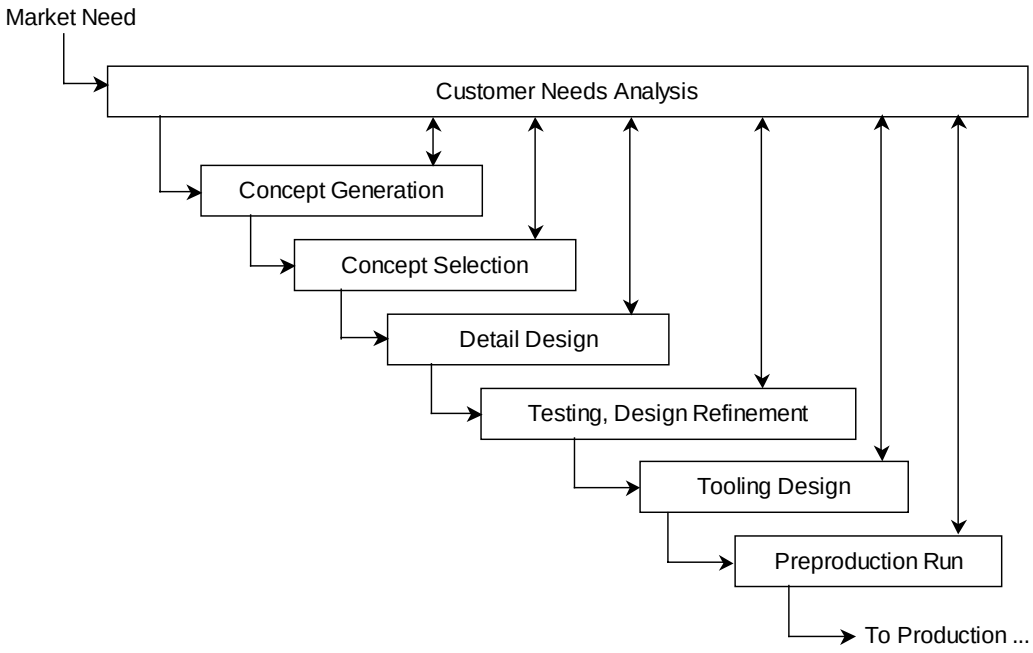

Figure 1. Simple Model of the Mechanical Design Process.

process are evaluated against the original (and new) customer needs to determine whether or not the design is on target to delight the customer. If the design is on target, then development efforts advance to the next stage of the process; if not, then previous activities are revisited in an iterative process that is characteristic of design.

The activities associated with the design process can be classified into two broad categories: *synthesis* and *analysis*. Synthesis activities relate to the creation of product concepts and the description of strategies for physically implementing those concepts. Analysis techniques are used to determine how "good" a design is, or how well a design meets a specific standard of performance (e.g. the product specifications).

One of the most common and powerful ways to analyze a mechanical design is through the construction and evaluation of a prototype. Critical engineering and business assessments of the state of a design are often centered on the performance of a prototype. Decisions to modify a design, modify a development schedule, or even terminate a design project can result from the evaluation of a prototype. The ability to use prototypes as a means of making *engineering* decisions regarding a design is the focus of this work.

1.1. THE USE OF PROTOTYPES IN PRODUCT DEVELOPMENT

A prototype may be defined as "an approximation of the product along one or more dimensions of interest" [Ullrich, 2000]. This broad definition allows nearly any representation of a product to be classified as a prototype. In order to

provide a more focused characterization of *prototype*, the following definitions will be used to distinguish between a *description of the product* and a *prototype of the product*:

Description of the product: a representation of a product that is used simply to **depict** or **define** the product or some aspect of it (e.g. specifications, drawings, etc).

Prototype of the product: a representation of a product that is used to **evaluate** the product or some aspect of it (e.g. physical models, computer simulations, etc.).

Although some aspects of design may be classified as either a *description* or a *prototype*, depending on the purpose at hand, and some exceptions to the definitions may exist (e.g. creating a physical prototype simply to fulfill a milestone), the definitions serve to emphasize that the purpose of prototypes is generally centered on *evaluation*. The results of such evaluations lead to a verification of the design or to further refinements.

1.1.1. Classification of Prototypes

Prototypes can generally be classified along two principle axes: Physical vs. Virtual; and Focused vs. Comprehensive [Ulrich, 2000; Otto, 2001] (see Figure 2). The Focused-Comprehensive axis indicates whether a prototype represents the overall product, or whether it represents some smaller subset of the product. The Physical-Virtual axis indicates whether the prototype is a physical artifact, or simply a simulation of the product. Physical prototypes can be further classified as either *traditional prototypes* or *rapid prototypes*. The distinctions

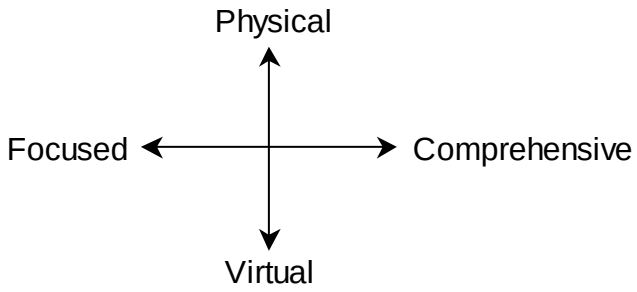

Figure 2. Classification of Prototypes, adapted from [Ulrich, 2000].

between traditional prototypes, rapid prototypes, and virtual prototypes are clarified in the following definitions:

Traditional prototype: a prototype created through typical material removal processes, net shape processes, and/or manual fabrication and assembly operations.

Rapid prototype: a prototype created through additive manufacturing processes directly from a computer model [Ulrich, 2000; Chua, 1999; Otto, 2001]. Rapid prototyping (RP) techniques are also known as *solid freeform fabrication* (SFF) [Beaman, 1997; Kochan, 1993].

Virtual prototype: a computer model, simulation, or analysis of a product.

Figure 3 summarizes the above definitions in a prototyping structure and gives several examples of each class of prototype. The examples given for rapid prototypes are all acronyms for common solid freeform fabrication processes.

1.1.2. The Prototyping Process

Virtual prototypes are often used to extract the same information for a product as can be obtained from a physical prototype [Chua, 1999]. Virtual

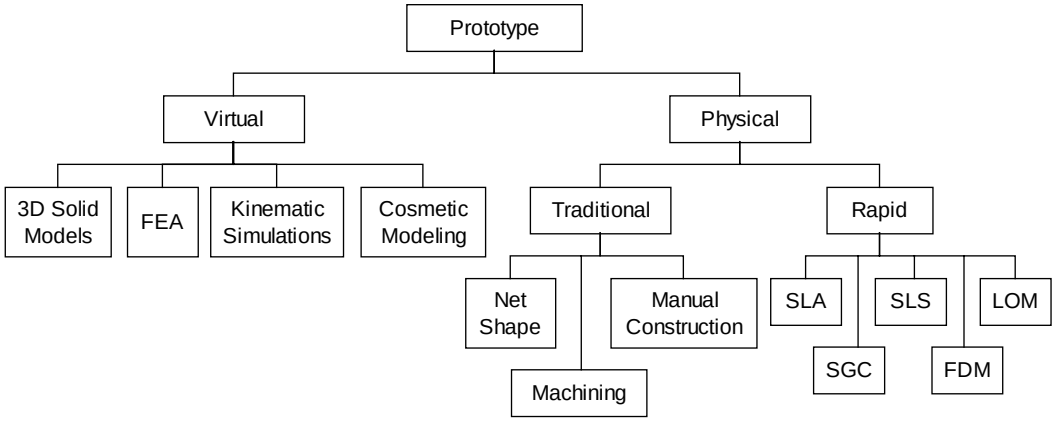

Figure 3. Prototyping Structure, adapted from [Chua, 1999].

prototypes can, at times, even provide more insight into a design than is readily available from a physical model (e.g. evaluation of various states of stress throughout a product). The benefits of virtual prototypes, which can include low cost and short cycle time, has lead to a push by many companies to replace physical prototypes with virtual prototypes [Ullman, 1997]. Physical prototypes, however, are still needed when virtual prototypes are not fully developed for a particular class of problem, or to aid in the refinement of virtual prototypes. Refinement of virtual prototypes is often needed in all but the most mature classes of problems.

For many design problems, a virtual prototype will evolve through an iterative process such as the following:

1. A virtual prototype is created and evaluated.
2. A physical prototype is created and tested.

3. The behavior of the physical prototype is compared to the behavior predicted by the virtual prototype.
4. The test results from the physical prototype are used to update/refine the virtual prototype.
5. The process is repeated until the behavior of the virtual prototype is sufficiently similar to the behavior of the physical prototype.

An effective and extensive exploration of the design space can be performed once the virtual prototype is sufficiently refined.

The integration of this *prototyping process* into product design is shown in Figure 4. As shown in the figure, evaluation of virtual and/or physical prototypes leads to iterative updates to the description of the product. Of course, actual design processes differ in the number and type of prototypes used (i.e. company A may rely more heavily on virtual prototypes, while company B uses primarily physical prototypes), but the general process shown in Figure 4 is representative of a typical design process. Figure 4 also shows the progression of physical prototypes from *engineering* or *experimental* prototypes through *pre-production*

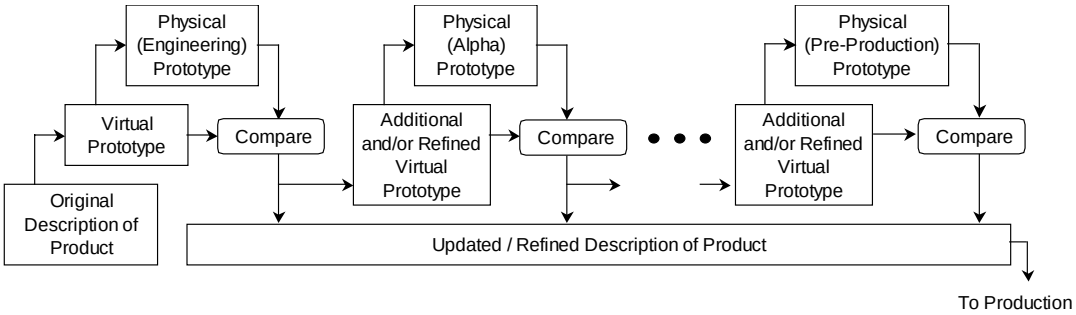

Figure 4. Typical Prototyping Process in Product Design.

prototypes as the design matures and approaches production [Ullrich, 2000]. Recent research has focused on the development of general prototyping strategies for product development. Such strategies are used to determine the appropriate number and timing of prototypes for a particular development project [Moe, 2002].

1.1.3. CyPhy Design Process

The cost and cycle time of the prototyping process shown in Figure 4 can be significantly reduced through the use of rapid prototypes in place of traditional prototypes. The use of rapid prototypes in product design has been credited with reducing development costs by as much as 40 to 70% [Dulieu-Barton, 2000]. The opportunity for such reductions in development time and cost is particularly apparent for products that involve complex geometry. The increased benefit for products with complex geometry arises from the fact that fabrication time for rapid prototypes is relatively insensitive to geometrical complexity, whereas fabrication time for traditional prototypes is very sensitive to geometric complexity (see Figure 5). The ability to effectively evaluate products using rapid prototypes in place of traditional prototypes would lead to a dramatic reduction in the overall development cycle time, thereby saving companies significant time and money.

The potential benefits of using rapid prototypes as a means of refining virtual models has lead to the introduction of a design process known as cybernetic-physical, or CyPhy (pronounced “sci-fi”). The CyPhy design process is defined as, “rapid integration of virtual and physical prototyping to produce

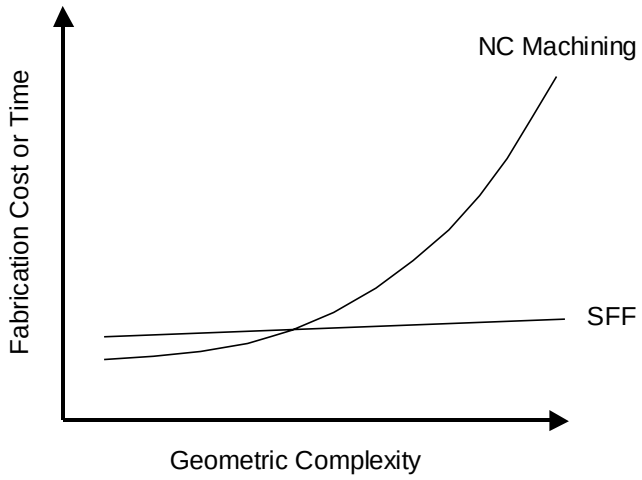

Figure 5. Geometric Complexity vs. Cost, adapted from [Cho, 1999].

tested product designs as well as realistic models for future design variants" [Wood, 1999]. The goal of CyPhy is to integrate functional testing of rapid prototypes into the design process so that virtual models of the product can be quickly refined and verified. The CyPhy process calls for the integration of embedded sensors during fabrication of rapid prototypes. Embedded sensors (as opposed to surface-mounted sensors) allow a wide range of data to be collected from physical tests. A virtual model can be quickly refined and verified by comparing the physical test data with the simulated performance of the virtual model. Once a reliable virtual model has been developed, designers can quickly and easily explore the design space of the product.

1.1.4. Functional Testing of Rapid Prototypes

Both virtual and physical prototypes are used to evaluate a product along three primary axes: Fit, Form, and Function. The current state of RP technology

allows for accurate evaluation of fit and form characteristics of a product, but provides for only limited evaluation of functional behaviors (see Figure 6, [Dornfeld, 1995]). In order to effectively utilize the CyPhy design process, the level of functional information that can be obtained from rapid prototypes must be increased.

The limited ability of RP parts to be used for functional evaluation of a product stems primarily from limitations in available part sizes and material properties in current RP systems. Two basic approaches exist for overcoming these limitations:

1. Improve the base materials and/or processes in order to increase the range of available material properties and part sizes.
2. Correlate behaviors of existing materials and part sizes to desired materials and part sizes through similitude techniques.

Significant research has been dedicated to both of the approaches mentioned above. The first approach deals with improving and expanding RP

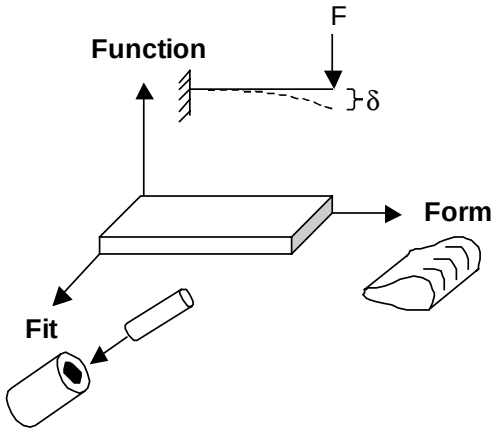

Figure 6. Capability of RP in evaluating products.

systems, while the second approach seeks to utilize the systems that are already in place. While the first approach provides a more direct means of obtaining functional information on a part, the second approach is more flexible in its ability to predict behavior for a wide range of different product sizes and materials. The second approach is the one taken for this research.

1.2. SIMILITUDE WITH RAPID PROTOTYPES

Similitude refers to any technique that utilizes a model system (e.g. scaled model) to predict the behavior of a similar system of interest (e.g. product). Perhaps the most widely used similitude technique is known as *dimensional analysis*. This technique, which is based on the Buckingham Pi theorem, uses dimensional information from the governing parameters of a behavior of interest to create scale factors between two similar systems. The scale factors are applied to one system in order to predict the behavior of the second, similar system. Another similitude technique, known as the Empirical Similitude Method, utilizes empirical test data to correlate the behavior of two similar systems [Cho, 1998; Cho, 1999].

While much research has been done on similitude techniques in general, many uncertainties still exist on how well such techniques apply to parts created through rapid prototyping processes (or, more generally, by any process). Among these uncertainties are the following:

- What is the range of application for current similitude techniques; i.e. when do they work well, and when do they not work well?

- Are there inherent characteristics in RP parts that make them unsuitable for current similitude techniques?
- Do RP processes provide material properties that are sufficiently accurate and repeatable to produce reliable results from similitude techniques?

All of the uncertainties listed above must be addressed before rapid prototypes can be used with confidence in the CyPhy design process.

1.3. RESEARCH HYPOTHESIS AND OBJECTIVES

The goal of this research is to develop a unified approach to functional testing, with particular interest in rapid prototypes. Such an approach could be used in conjunction with the CyPhy design process to produce rapid integration of physical and virtual prototypes in product development. With this goal in mind, the following research hypothesis is proposed:

> *Similitude techniques can enable rapid prototypes to be used for reliable predictions of a wide range of functional product behaviors. In addition, the range of application of such similitude techniques can be established for specific types of rapid prototypes.*

Several objectives have been developed for the purpose of evaluating the stated hypothesis. The research objectives are as follows:

1. Clearly establish the limitations and/or shortcomings of current similitude techniques in predicting selected product behaviors.

2. Develop an enhanced similitude technique to remedy the shortcomings of the current approaches.
3. Quantify the range of application for the enhanced similitude technique
4. Develop a generalized procedure for evaluating the use of similitude techniques with other RP processes and other product behaviors.

The goals of this research will be achieved when each of the above objectives has been addressed.

1.4. LAYOUT OF DISSERTATION

This dissertation is composed of a total of six chapters. Chapter 2 presents an overview of the development of current similitude techniques. Chapter 3 contains an evaluation of current similitude techniques and highlights strengths and shortcomings of each method. Chapter 4 introduces an enhanced similitude technique that improves upon current approaches. Chapter 5 integrates existing similitude techniques with the enhanced method to create a unified approach to functional testing with rapid prototypes. Chapter 6 gives conclusions and potential areas of further research.

CHAPTER 2

Similitude and Dimensional Analysis

The philosophical basis for this research stems from the cognitive science of analogical reasoning and similitude. Vosniadou stated the importance of gathering information through the use of similarities and analogies as follows:

> The ability to perceive similarities and analogies is one of the most fundamental aspects of human cognition. It is crucial for recognition, classification, and learning, and it plays an important role in scientific discovery and creativity. [Vosniadou, 1989]

Similitude allows one to make inferences about the properties of one system based on the properties of another, similar system. Gaining understanding of physical systems through similitude can provide valuable knowledge and insight with significantly less time and effort than through explicit evaluation of every system individually.

2.1. CONCEPTS OF SIMILITUDE

The principle of similitude is based on the premise that various entities can be compared on the basis of some pre-determined characteristic and classified into similar sets. Each entity within the set will be similar to all other entities in the set with respect to the specified criterion of comparison. With this in mind, it makes no sense to discuss *similitude* in general; rather, similitude must be in reference to some specific attribute or characteristic [Szuks, 1980].

Several types of similitude are discussed in the literature. Among the most common classifications of similitude are geometric, kinematic, dynamic, and physical similarity.

2.1.1. Geometric Similarity

Geometric similarity deals with the *form* of an entity or system. Euclid described the required conditions for geometric similarity as follows: “Those straight-sided geometric figures are called similar which have equal angles, and whose sides subtending equal angles are proportional” [Szucs, 1980]. Consider, for example, the two cubes shown in Figure 7. All adjacent sides of the cubes are separated by 90 degrees. The edge lengths of the cubes can be related by the following constants of proportionality:

$$\frac{A}{A'} = K_x \quad ; \quad \frac{B}{B'} = K_y \quad ; \quad \frac{C}{C'} = K_z \tag{2-1}$$

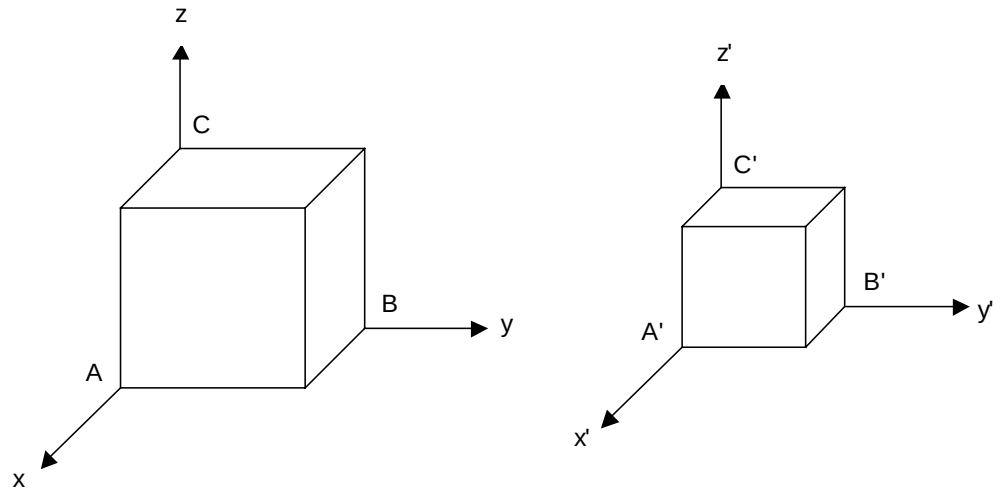

Figure 7. Geometrically Similar Objects.

The constants K_x, K_y, and K_z are the length *scale factors* (K_L) in the x, y, and z directions, respectively. The cubes are geometrically similar if $K_x = K_y = K_z$. If all of the scale factors are not equal, say $K_x = K_y \neq K_z$, then the scaling between the two cubes is said to be *distorted*, and the ratio K_x/K_z is defined as the *distortion factor* [Langhaar, 1951].

The definition of geometric similarity given by Euclid has been expanded to include general geometric shapes rather than just straight-sided figures. In general, two objects are geometrically similar if the shape of one can be mapped to the shape of the other through a continuous, linear transformation. This broader definition allows circles, spheres, and ellipses to be classified as geometrically similar in addition to straight-sided geometries [Szucs, 1980].

The linear transformation that maps one shape to another can be represented by a geometric transformation matrix *G*. A proportional transformation, which produces a geometrically similar shape, is defined with a diagonal matrix with equal values along the diagonal. A distorted transformation, which is also known as an *affine* transformation, is defined with unequal values along the diagonal of the matrix. The transformation matrix for the cubes shown in Figure 7 is defined as follows:

$$G = \begin{bmatrix} K_x & 0 & 0 \\ 0 & K_y & 0 \\ 0 & 0 & K_z \end{bmatrix} \qquad (2\text{-}2)$$

The most general case of an affine transformation is given by a fully populated transformation matrix. Several examples of proportional and affine transformations in 2D are shown in Figure 8.

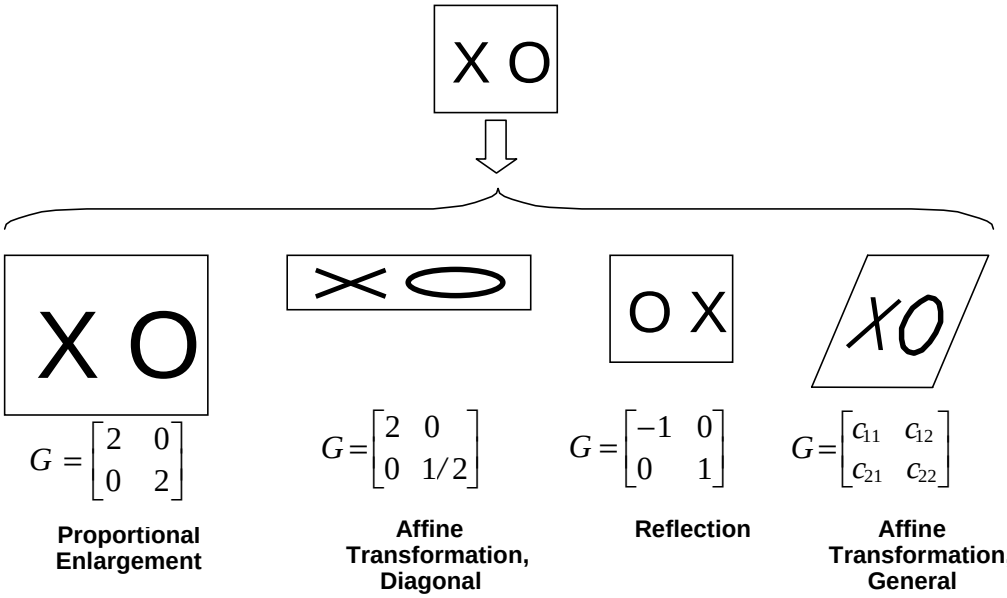

Figure 8. Various Geometric Transformations. Adapted from [Szucs, 1980].

For each geometric transformation, any point in the original system can be mapped to a corresponding point in the transformed system through the corresponding transformation matrix *G*; likewise, each point in the transformed system can be mapped back to its corresponding point in the original system through the inverse of the transformation matrix, G^{-1}. For example, in Figure 9,

$$W' = G\,W, \quad \text{and} \quad W = G^{-1}\,W' \tag{2-3}$$

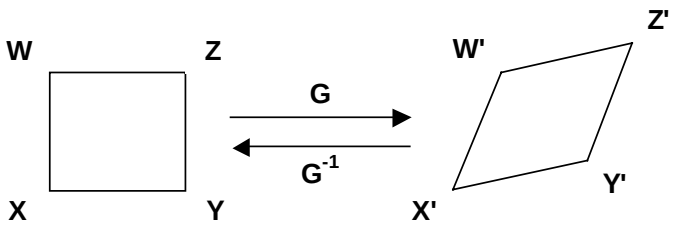

Figure 9. Geometric Mapping. Adapted from [Szucs, 1980].

Similar relationships exist for all other points in both the original and transformed systems. Equation 2-3 represents a *bi-unique mapping* between the original system and the transformed system. In other words, one and only one point in the transformed system corresponds to each point in the original system, and vice versa.

2.1.2. Kinematic Similarity

Before discussing kinematic similarity, we must first understand the concept of *homology*. Homology means, "the state of being homologous"; *homologous* means, "having the same or a similar relation; corresponding, as in relative position or structure" [Webster, 1997]. Homologous points are discussed in the previous section in connection with geometric similarity. Several corresponding, or homologous, points are labeled on the geometrically similar cubes in Figure 7. It was shown that all homologous points are related through a geometric transformation matrix *G*.

In addition to homologous points, we can also define *homologous time* as *corresponding time* between two systems. A time scale factor K_t can be defined in the same manner as a length scale factor, as follows:

$$K_t = \frac{t}{t'} \tag{2-4}$$

where *t* and *t'* are homologous times between two systems.

It is important to note that *homologous time* does not necessarily mean *equal time*. The two pendulums shown in Figure 10 illustrate this fact. The period of oscillation of a pendulum *t* is defined as the time required to complete one

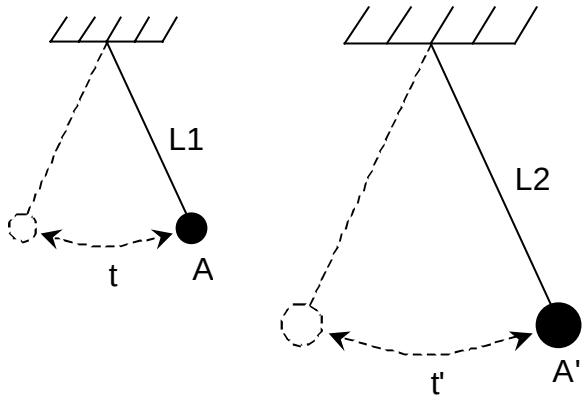

Figure 10. Two Pendulums - Example of Homologous Times.

cycle. For small amplitudes of oscillation, the period is given by the following equation:

$$t = 2\pi\sqrt{\frac{L}{g}} \qquad (2\text{-}5)$$

Since *L2* > *L1* in Figure 10, then *t'* > *t* and $K_t < 1$. The points *A* and *A'* represent homologous points, and *t* and *t'* represent homologous (not *equal*) times.

With these definitions in mind, we can now state that two systems are *kinematically similar* if homologous particles in the systems lie at homologous points at homologous times. Kinematic similarity indicates *similarity of motion* between the two systems. Kinematically similar systems will have similar velocity and acceleration scale factors (defined as $K_V = \frac{K_L}{K_t}$ and $K_a = \frac{K_L}{K_t^2}$ respectively [Langhaar, 1951]).

2.1.3. Dynamic Similarity

The concept of dynamic similarity follows closely behind that of kinematic similarity. In addition to having similarity of motion, two systems must

have similar mass distributions (and, therefore, similar net forces) in order to be classified as *dynamically similar*. If two systems have similar mass distributions, then a *mass scale factor* K_m can be defined in the same manner as all previous scale factors:

$$K_m = \frac{m}{m'} \tag{2-6}$$

where *m* and *m'* represent the masses of two parts.

If, in addition to geometric and kinematic similarity, two systems have similar mass distributions, then they will be dynamically similar and will experience similar net forces, as defined by the force scale factor K_F [Langhaar, 1951]:

$$K_F = \frac{F}{F'} = \frac{K_m K_L}{K_t^2} \tag{2-7}$$

where *F* and *F'* represent the forces experienced by the two systems. Note that the second part of the above equation is derived from Newton's second law of motion, which equates force with mass times acceleration.

2.1.4. Physical Similarity

Physical similarity, which is also known as total similarity or similarity of phenomena, deals with system behavior. A *system* in this sense is a set of objects or elements that is isolated from its surroundings by distinct boundaries. The elements within the system are associated to each other through specific physical laws or relationships. The system also responds in a specific way to stimulus from the surroundings. Analysis of a system is often focused on understanding the

relationships among the various elements within the system, as well as the response of those elements to stimulus from outside the system.

The behavior of a system can be characterized by a set of state parameters, which represents the current state or condition of the system, and by a description of how those parameters change when different stimuli are input to the system. The response of a system to a specific input is dependent on both the parameters of the system as well as the type and magnitude of the input. Taken together, the relevant system parameters and the input are defined as the *governing parameters* for a given behavior of interest. Mathematically, we can state that the system behavior is a function of the governing parameters, or

$$x = f(d_1, d_2, ..., d_n) \tag{2-8}$$

where x is the behavior of interest, and $d_1, \ldots, d_n$ are the governing parameters.

With these definitions in mind, we can now state that two systems are *physically similar* if there exists a one-to-one mapping between their states and their governing parameters. In other words, corresponding values of the governing parameters produce corresponding behaviors in the two systems. Implied in this definition is the fact that both systems must be governed by the same set of governing parameters, and that those governing parameters must follow the same mathematical model. Therefore, the governing equations for two physically similar systems must be identical.

As with geometric similarity, the states of two physically similar systems can be related through a transformation matrix T. If only one system behavior is being considered, T is a one-dimensional matrix and represents a simple scale

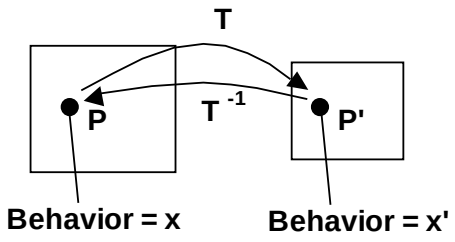

Figure 11. Behavior at Corresponding Points.

factor; in the general case, however, *x* can be a vector containing multiple system behaviors, or values of one behavior for various magnitudes of the input parameter, and *T* can be a tensor or a vector space. If ***x*** represents the state vector of an original system at some point *P*, and ***x'*** represents the state vector of a physically similar system at a corresponding point *P'* (see Figure 11), we can write the following equations relating the behavior of the two systems at the specified points:

$$\boldsymbol{x'} = \boldsymbol{T}\,\boldsymbol{x} \quad \text{and} \quad \boldsymbol{x} = \boldsymbol{T}^{-1}\,\boldsymbol{x'} \tag{2-9}$$

The above equation assumes, of course, that the state vectors ***x*** and ***x'*** are of equal dimension. In general, the transformation ***T*** can vary from point to point and from one moment in time to another. If, however, the transformation is independent of position and time, we can say that ***T*** represents a unique mapping of the states of the two systems, and that the systems are physically similar under the mapping ***T*** [Szucs, 1980].

Although physically similar systems are quite often geometrically similar as well, Szucs describes the relationship between geometric similarity and physical similarity (or *similitude*, as he calls it) as follows:

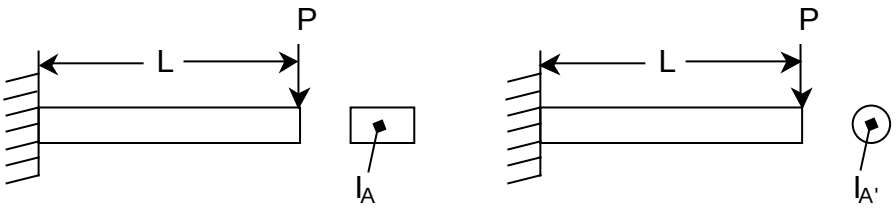

Figure 12. Cantilever Beams with Distinct Cross Sectional Geometry.

> Geometric similarity is not even a necessary condition of similitude, let alone a sufficient one: indeed, it is often an obstacle to similitude! [Szucs, 1980]

In other words, geometrically similar systems are not necessarily physically similar, and physically similar systems need not be geometrically similar (see also [Taylor, 1974]). A simple example of this fact is illustrated in Figure 12. The deflection of a cantilever beam under a concentrated force at the tip of the beam (assuming small deflections) is given by the following equation:

$$\delta = \frac{PL^3}{3EI} \tag{2-10}$$

where δ is the deflection at the end of the beam, P is the applied load, L is the length of the beam, E is the modulus of elasticity of the beam material, and I is the moment of inertia of the cross sectional area. Consider the specific case where we want to achieve identical values of deflection, rather than just corresponding values. Assuming we have identical values for P, L, and E for the two beams, one could easily adjust the dimensions of the beam cross section to achieve identical values for I as well. The beams would then be physically, although not geometrically, similar.

2.2. DIMENSIONAL ANALYSIS AND THEORY OF MODELS

Dimensional analysis is a branch of science that can be used with similitude to aid in the creation of scale models for predicting product performance. Dimensional analysis shows how physical variables can be combined, based on their dimensions, in order to reduce the number of terms in a functional equation and simplify the creation of a scale model. Dimensional analysis is the most common way of deriving the transformation matrix T that relates the behavior of physically similar systems.

2.2.1. Historical Development

The field of dimensional analysis began to develop during the sixteenth and seventeenth centuries. Some of the early contributors to the field include Galileo, Kepler, and Huyghens [Huntley, 1955]. It was Newton, however, that appears to have demonstrated the first application of what has become known as dimensional analysis. The idea behind Newton's approach was to use *ratios* of dimensional variables when comparing similar systems of differing magnitudes. For example, the equation

$$v^2 = 2\left(\frac{F}{m}\right)d \tag{2-11}$$

describes the final velocity v of an object with mass m that travels a linear distance d under a constant force F. If the ratio F / m remains constant for various values of mass m, then the ratio v^2 / s also remains constant. Newton referred to this approach for comparing similar systems of different magnitudes as the "principle of similitude" [Huntley, 1955] (see also [Astarita, 1997]).

The philosophy behind the principle of similitude lies in the concept of a *fundamental dimension*. Newton identified three entities, namely length, inertia (or mass), and time as fundamental and independent characteristics of any mechanical system. (In later years, the quantities of temperature, electric current, quantity of matter, and luminous intensity were included as fundamental dimensions for use with thermal, electrical, electrochemical, and optical systems [Szirtes, 1998]). All variables in a system are made up of combinations of these fundamental dimensions. The fact that fundamental dimensions are *independent* (i.e. the value of one does not depend on the value of another) allowed the ratios of variables used by Newton in his "principle of similitude" to remain consistent. (Note: the quantity *force* is often used as a fundamental dimension in place of *mass* in order to simplify the dimensional analysis of certain problems. We can therefore speak of the *mass system* or the *force system* when referring to a set of fundamental dimensions [Langhaar, 1951].)

Over one hundred years after Newton's work, Fourier introduced two fundamental concepts to the field of dimensional analysis. The first concept is that of a *dimensional formula*. The basis of this concept is that every physical entity can be described as a relationship among fundamental dimensions. For example, the velocity of an object is described in terms of a *length* divided by a *time*. The "exponent of the time dimension," as Fourier called it, is –1, and that of the length dimension is +1 [Huntley, 1955]. If we represent the fundamental dimensions of length, mass, and time as [L], [M], and [T] respectively, the dimensional formula for velocity is given by [L] $[T^{-1}]$, or $[LT^{-1}]$. Dimensional formulas for several

Table 1. Various Dimensional Formulas. Adapted from [Langhaar, 1951].

Physical Variable	**Dimensional Formula Mass System**	**Dimensional Formula Force System**
Velocity	$[LT^{-1}]$	$[LT^{-1}]$
Acceleration	$[LT^{-2}]$	$[LT^{-2}]$
Angular Velocity	$[T^{-1}]$	$[T^{-1}]$
Energy, Work	$[ML^{2}T^{-2}]$	[FL]
Momentum	$[MLT^{-1}]$	[FT]
Pressure and Stress	$[ML^{-1}T^{-2}]$	$[FL^{-2}]$
Power	$[ML^{2}T^{-3}]$	$[FLT^{-1}]$
Mass Density	$[ML^{-3}]$	$[FL^{-4}T^{2}]$
Dynamic Viscosity	$[ML^{-1}T^{-1}]$	$[FL^{-2}T]$
Kinematic Viscosity	$[L^{2}T^{-1}]$	$[L^{2}T^{-1}]$
Surface Tension	$[MT^{-2}]$	$[FL^{-1}]$
Modulus of Elasticity	$[ML^{-1}T^{-2}]$	$[FL^{-2}]$
Temperature	$[\theta]$	$[\theta]$
Thermal Conductivity	$[MLT^{-3}\theta^{-1}]$	$[FT^{-1}\theta^{-1}]$
Convection Coefficient	$[MT^{-3}\theta^{-1}]$	$[FL^{-1}T^{-1}\theta^{-1}]$
Heat Capacity / Volume	$[ML^{-1}T^{-2}\theta^{-1}]$	$[FL^{-2}T\theta^{-1}]$
Entropy	$[ML^{2}T^{-2}\theta^{-1}]$	$[FLT\theta^{-1}]$

common variables are shown in Table 1 (note that the fundamental dimension of temperature is represented as [θ]).

The second fundamental concept introduced by Fourier is called the *principle of dimensional homogeneity*. This principle relates to any equation

representing a physical phenomenon. The principle states that the exponent of every fundamental dimension in one term of the equation must be equal to that in every other term in the equation. The equation must be *dimensionally homogeneous* [Huntley, 1955]. In other words, if an equation has the form

$$term\ 1 = term\ 2 + term\ 3 + term\ 4 \tag{2-12}$$

then each term in the equation must have the same dimensional formula. For example, equation 2-10, which describes the deflection of a cantilever beam under a concentrated load, can be modified to include the effects of shear stresses as follows [Timoshenko, 1970]:

$$\delta = \frac{PL^3}{3EI} + \frac{PLc^2}{2IG} \tag{2-13}$$

where c is the distance from the neutral axis to the top of the beam and G is the shear modulus of elasticity. In order to be dimensionally homogeneous, each term on the right side of the equation must have the same dimensional formula as the term on the left side. In this case, each term in the equation has a dimensional formula of [L] and the equation is, in fact, dimensionally homogeneous. (All equations describing physical phenomena *must* be dimensionally homogeneous).

Although many other people contributed to the theory of dimensional analysis after Fourier's work, the next major advancement in the field is attributed to E. Buckingham for his PI theorem. The Buckingham PI theorem provides the link between the theory of dimensional analysis and the use of scale models for correlating the behavior of physically similar systems.

2.2.2. Buckingham PI Theorem

The Buckingham PI theorem states that an equation written in terms of dimensional system parameters d_j, $j = 1, \ldots, n$, can be recast in terms of a complete set of dimensionless parameters π_i, $i = 1, \ldots, N$, where $N < n$ [Bridgman, 1931; Langhaar, 1951]. In equation form,

$$g(d_1, d_2, \ldots, d_n) = 0 \quad \Rightarrow \quad f(\pi_1, \pi_2, \ldots, \pi_N) = 0 \tag{2-14}$$

Application of the PI theorem, therefore, reduces the number of independent variables in a system by converting dimensional system parameters to dimensionless parameters. A *dimensionless parameter* is described as having a dimension of *unity*. Dimensionless parameters are formed by combining dimensional variables in such a way as to make the exponent of all fundamental dimensions equal to zero, which results in a dimensional formula of [1].

Although the Buckingham PI theorem states that dimensional parameters can be converted to an equivalent set of dimensionless parameters, it does not specify *how* this conversion is to be done. Many different approaches for deriving dimensionless parameters have been proposed (see [Barr, 1979, 1982, 1984; Deb, 1986; Langhaar, 1951]). The approach used here is that presented in [Barr, 1979].

A cantilever beam with a concentrated force at the tip (see Figure 13) will be used as an example of how to develop dimensionless parameters. Suppose the behavior of interest in this system is the vertical deflection caused by a concentrated load. The first step is to determine, based on past experience or knowledge of the governing equations, which parameters affect the behavior of interest. In this case, we know that the deflection of the cantilever beam δ is

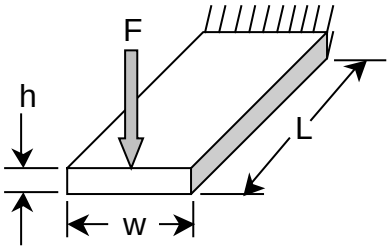

Figure 13. Cantilever Beam with Applied Load at Tip.

affected by the magnitude of the applied load *F*, the modulus of elasticity of the beam *E,* and the physical dimensions of the beam, namely height *h*, width *w*, and length *L*. With these governing parameters clearly established, we can now write a general functional equation for the deflection of the beam as follows:

$$\delta = g(F, E, h, w, L) \tag{2-15}$$

In order to recast this functional equation in terms of dimensionless parameters, we first create a matrix that lists all of the dimensional parameters along the top of the matrix and all of the relevant fundamental dimensions along the left side of the matrix. The entries in the matrix represent the power to which each fundamental dimension is raised for each dimensional variable. In other words, the entries in the matrix contain the exponents of the dimensional formula for each variable. The matrix created in this manner is referred to as the *dimensional matrix*. In the case of the cantilever beam, the dimensional matrix that is developed using the *force system* of fundamental dimensions is given as follows:

	h	E	δ	w	F	L
L	1	-2	1	1	0	1
F	0	1	0	0	1	0

(2-16)

We can see from the matrix that the dimensional formula for *h* is [L], the dimensional formula for *E* is [FL^{-2}], etc.

An *m x n* matrix (with *m* being the number of rows and *n* being the number of columns) is in *echelon form* when the leftmost *m x m* submatrix is an identity matrix. To put the dimensional matrix in equation 2-16 in echelon form, we simply replace the fundamental dimensions on the left side of the matrix with two *repeating variables*. The repeating variables are two of the original dimensional variables that we use to create ratios with the other variables in order to produce dimensionless parameters. The repeating variables should involve all of the fundamental dimensions and should not include the parameter of interest (δ in this case). The entries in the matrix now represent powers of each variable in terms of the *repeating variables* rather than in terms of the fundamental dimensions. Using height *h* and modulus of elasticity *E* as repeating variables, the dimensional matrix is converted to echelon form as follows:

	h	E	δ	w	F	L
h [L]	1	0	1	1	2	1
E [FL^{-2}]	0	1	0	0	1	0

(2-17)

We can now express the dimensions of any variable in terms of the two repeating variables. For example, the dimension of F is the same as the dimension of h^2E. We can create ratios of parameters that have a dimensional formula of [1] (i.e. dimensionless parameters) by putting each dimensional variable that is listed along the top of the echelon matrix in the numerator and the appropriate powers of the repeating variables in the denominator. Dimensionless parameters formed in this way are called *PI groups* and are represented with the symbol π. The first

two columns, which produce the ratios h / h and E / E, are trivial cases that are not included in the final set of dimensionless parameters. Starting with the third column, we develop the following set of dimensionless parameters for the cantilever beam:

$$\pi_1 = \frac{\delta}{h} \quad ; \quad \pi_2 = \frac{w}{h} \quad ; \quad \pi_3 = \frac{F}{Eh^2} \quad ; \quad \pi_4 = \frac{L}{h} \tag{2-18}$$

So, according to the Buckingham PI theorem, we have recast the original functional relationship for the cantilever beam system in terms of dimensionless parameters. In equation form:

$$\delta = g(E, h, w, L, F) \quad \Rightarrow \quad \frac{\delta}{h} = f\left(\frac{w}{h}, \frac{F}{Eh^2}, \frac{L}{h}\right) \tag{2-19}$$

Note that the set of dimensionless parameters shown above is not necessarily unique; the final form depends on the variables that are selected as repeating variables. The *number* of dimensionless parameters that are formed, however, is always the same. The number of dimensionless parameters is equal to the total number of variables minus the number of variables with independent dimensional formulas. The number of variables with independent dimensional formulas is determined by the *rank* of the dimensional matrix, which is equal to the number of independent rows or independent columns in the matrix [Strang, 1988]. By knowing the rank of the dimensional matrix, one can determine *a priori* the reduction of terms that will take place through application of the Buckingham PI theorem.

2.2.3. Scale Models and Traditional Similitude

One of the most common uses of the Buckingham PI theorem is in connection with scale models. A *scale model* (or simply *model*) is a replica of some part or object (herein called *product*) that is of interest to a designer or engineer. The model can be "scaled" in terms of size, material properties, or loading conditions. The motivation for using models instead of actual products lies in the assumption that the product of interest is relatively difficult to fabricate and evaluate. A scale model, which is really just a simplified replica of the product, is created and evaluated relatively quickly. The behavior of the model is then used to predict the behavior of the product. Dimensional analysis and the Buckingham PI theorem provide the theory behind the correlation of the model behavior with the product behavior. This theory is referred to as the *traditional similitude method (TSM).*

Suppose that two systems (a model system *m*, and a product system *p*) are physically similar (i.e. they are governed by the same set of dimensional parameters). The functional relationship for the systems can be expressed as

$$\begin{aligned} g(d_{m,1}, d_{m,2}, \ldots, d_{m,n}) &= 0 \\ g(d_{p,1}, d_{p,2}, \ldots, d_{p,n}) &= 0 \end{aligned} \tag{2-20}$$

or, in terms of a particular parameter of interest *x*, as

$$\begin{aligned} x_m &= g^*(d_{m,1}, d_{m,2}, \ldots, d_{m,n-1}) \\ x_p &= g^*(d_{p,1}, d_{p,2}, \ldots, d_{p,n-1}) \end{aligned} \tag{2-21}$$

Now, according to the Buckingham PI theorem, these functional relationships can be recast into dimensionless form as follows:

$$f(\pi_{m,1}, \pi_{m,2}, \ldots, \pi_{m,N}) = 0$$
$$f(\pi_{p,1}, \pi_{p,2}, \ldots, \pi_{p,N}) = 0 \qquad (2\text{-}22)$$

or, in terms of the specific parameter of interest x, as

$$\pi_{m,x} = f^*(\pi_{m,1}, \pi_{m,2}, \ldots, \pi_{m,N-1})$$
$$\pi_{p,x} = f^*(\pi_{m,1}, \pi_{m,2}, \ldots, \pi_{m,N-1}) \qquad (2\text{-}23)$$

For these two corresponding systems, the TSM states the following:

$$\pi_{m,x} = \pi_{p,x} \text{ if } \pi_{m,i} = \pi_{p,i} \text{ for all } i = 1, 2, \ldots, N\text{-}1 \qquad (2\text{-}24)$$

The TSM allows *similar systems* (equal dimensionless parameters) rather than *identical systems* (equal governing parameters) to be compared to one another. In other words, dimensionless parameters can be equal for two systems without all governing parameters of the two systems being equal.

Consider two physically similar cantilever beam systems. Application of dimensional analysis and the Buckingham PI theorem, as presented earlier, produced four PI groups for such a system (see equation 2-18). If we are interested in the deflection of the beam under an applied load, we can write the following relationships:

$$\delta_m = g(E_m, h_m, w_m, L_m, F_m)$$
$$\delta_p = g(E_p, h_p, w_p, L_p, F_p) \qquad (2\text{-}25)$$

or, in dimensionless form,

$$\pi_{m,1} = f(\pi_{m,2}, \pi_{m,3}, \pi_{m,4})$$
$$\pi_{p,1} = f(\pi_{p,2}, \pi_{p,3}, \pi_{p,4}) \qquad (2\text{-}26)$$

From TSM we know that

$$\pi_{m,1} = \pi_{p,1} \tag{2-27}$$

if

$$\pi_{m,2} = \pi_{p,2}\ ,\ \pi_{m,3} = \pi_{p,3}\ ,\ \pi_{m,4} = \pi_{p,4} \tag{2-28}$$

or equivalently,

$$\frac{\delta_m}{h_m} = \frac{\delta_p}{h_p} \tag{2-29}$$

if

$$\frac{w_m}{h_m} = \frac{w_p}{h_p} \quad , \quad \frac{F_m}{h_m^2 E_m} = \frac{F_p}{h_p^2 E_p} \quad , \quad \frac{L_m}{h_m} = \frac{L_p}{h_p} \tag{2-30}$$

If we now define a *scale factor K* as the value of a parameter in the product divided by the value of the same parameter in the model, or

$$K_X = \frac{X_p}{X_m} \tag{2-31}$$

we can rearrange the above equations to show the required relationships among scale factors for the cantilever beams:

$$K_\delta = K_h \tag{2-32}$$

if

$$K_w = K_h, \quad K_F = K_h^2 K_E, \quad \text{and } K_L = K_h \tag{2-33}$$

Equations 2-32 and 2-33 are known as the *model law* for the cantilever beam system. Equation 2-32 is referred to as the *prediction equation*, and equation 2-33 is referred to as the *similarity constraints*. To use the model law, a

model is constructed that satisfies all of the similarity constraints; then the behavior of the product is predicted from the behavior of the model through the prediction equation.

Although the cantilever beam problem provides a clear illustration of the TSM, it fails to capture the power of the TSM since a cantilever beam can be readily evaluated with analytical or numerical techniques. The power of the TSM can be found in situations where analytical or numerical techniques are either inaccurate or impractical approaches to predicting product behavior. Perhaps one of the most classical examples of the TSM describes how scale models can be used to predict the drag force on a ship or submarine. Complex geometries of a ship hull combined with complex fluid flow patterns make drag force a difficult quantity to evaluate analytically or numerically. However, by applying scale factors to measured drag forces on a scale model, the TSM can be used to predict drag forces on a full-scale ship.

The procedure for developing the TSM model law for a ship or submarine is the same as that presented for the cantilever beam problem. Suppose we wanted to determine the drag force on a submarine by testing a small scale model (reference [Gerhart, 1992]; see also [Cho, 1999b]). The first step is to identify the physical parameters that affect the drag force and express them as a functional equation. In this case the functional equation can be written as

$$D = g(l, V, \rho, \mu) \tag{2-34}$$

where D is the drag force, l is a characteristic length which represents the size of the submarine, V is the velocity of the submarine, ρ is the fluid density, and μ is

the (dynamic) viscosity of the fluid. Using the mass system of fundamental dimensions, the dimensional matrix can be constructed as follows:

	l	V	ρ	D	μ
M	0	0	1	1	1
L	1	1	-3	1	-1
T	0	-2	0	-2	-1

(2-35)

Selecting l, V, and ρ as repeating variable, the dimensional matrix can now be put into echelon form as follows:

	l	V	ρ	D	μ
l [L]	1	0	0	2	1
V [LT^{-1}]	0	1	0	2	1
ρ [ML^{-3}]	0	0	1	1	1

(2-36)

The dimensionless π groups can now be constructed by placing the variables along the top of the echelon matrix in the numerator and the appropriate powers of the repeating variables in the denominator. The non-trivial π groups are given as

$$\pi_1 = \frac{D}{l^2 V^2 \rho} \quad ; \quad \pi_2 = \frac{\mu}{lV\rho} \tag{2-37}$$

The original functional equation for the drag force can now be written in dimensionless form as

$$\pi_1 = f(\pi_2) \quad or \quad \frac{D}{\rho V^2 l^2} = f\left(\frac{\mu}{\rho V l}\right) \tag{2-38}$$

For two physically similar systems (a product, p and a model, m) we can state that

$$\left(\frac{D}{\rho V^2 l^2}\right)_p = \left(\frac{D}{\rho V^2 l^2}\right)_m \quad if \quad \left(\frac{\mu}{\rho V l}\right)_p = \left(\frac{\mu}{\rho V l}\right)_m \tag{2-39}$$

By recognizing that the two π terms in this example represent common dimensionless parameters in fluid dynamics ($\frac{\rho Vl}{\mu}$ is defined as Reynolds number, R, and $\frac{D}{1/2\rho V^2 l^2}$ is defined as the drag coefficient, C_D) we can state that

$$C_{D,p} = C_{D,m} \quad if \quad R_p = R_m \tag{2-40}$$

The examples given above illustrate the power and versatility of the TSM. There are, however, many situations in which the required similarity constraints are difficult to satisfy (e.g. attaining identical values of Reynolds number for two different systems). When the similarity constraints of two systems are not satisfied, the scaling between the two systems is said to be *distorted*; if the similarity constraints are satisfied, the systems are said to be *well-scaled*. A similar definition of distortion was presented earlier in describing geometrically similar objects (see section 2.1.1). We will refer to the distortion between geometric shapes as *geometric distortion* and the distortion in scale factors between a product and a model as *model distortion*. Several sources of model distortion exist, including the following:

1. **Non-constant scale factor over range of application**. Note that the TSM requires *constant* scale factors over the entire range of application. A scale factor is simply a ratio of parameters, and any deviation in one of the parameters will result in a deviation from the constant value required for the scale factor. For example,

$$E_m = constant, \quad E_p = variable, \quad \Rightarrow \quad K_E = \frac{E_m}{E_p} \neq constant \tag{2-41}$$

Since the TSM assumes constant scale factors, such variations result in inaccurate TSM predictions.

2. **Scale factor that cannot be realized physically**. Some scale factors that are required by the model law in a well-scaled system may not be physically realizable or practical. For example, a problem in fluid dynamics might require a specific ratio of viscosities between two fluids. Two fluids that satisfy the required ratio may not exist or may not be readily available.
3. **Omission of one or more dominant system parameters**. The accuracy of the TSM depends on one's ability to recognize and include all of the relevant system parameters in the creation of the model laws. If one or more of the dominant system parameters is inadvertently omitted, the resulting set of dimensionless parameters and model laws will be incomplete and inaccurate. If, for example, beam length was not included as one of the governing parameters for beam deflection (see equation 2-15), then the model beam would not be constructed according to the required length scale factor $K_L = K_h$ (see equation 2-33) and application of the TSM would again produce inaccurate results.
4. **Different governing parameters for the model and product**. In some instances, the process of scaling causes different parameters to become relevant in the model than are relevant in the product. For example, surface tension might be a relevant parameter in determining

the drag force on a small-scale model of a ship, but be totally irrelevant in determining the drag force on the corresponding full size ship. This phenomenon is known as *scale effects*. Scale effects cause the model and the product systems to be governed by different parameters, which results in physical dissimilarity.

5. **Other sources of physical dissimilarity**. There are many other potential sources of distortion that can cause two systems to behave differently. For example, one system may exhibit pure isotropic material behavior while the other exhibits orthotropic behavior; one system may have variation in material properties within a part (possibly due to a specific manufacturing process, such as injection molding) while the other system does not; one system could have inconsistent material behavior between parts (as with a statistical material such as concrete) while the other system does not; etc. In each case, the differences in behavior produce inaccurate or inconsistent scaling factors between the systems, and the actual scale factor is different than the theoretical scale factor developed through TSM.

Developing a well-scaled model can often be difficult in practice. The various sources of distortion listed above can either be anticipated or they can be entirely unexpected. The fact that unexpected distortions in a model can produce inaccuracies in predicted product performance, use of the TSM carries with it an inherent risk. Confidence in TSM results requires significant *a priori* knowledge about the material properties and governing parameters of the systems involved.

Since such knowledge is often not available, direct product testing is frequently used in place of similitude techniques, which results in longer and more expensive development cycles.

2.2.4. Empirical Similitude

In an attempt to overcome the inherent difficulties and inaccuracies in the TSM, a new similitude technique known as the *empirical similitude method*, or *ESM*, has been developed [Cho, 1999]. The ESM develops a correlation between a model and product empirically, rather through dimensional information alone.

The primary areas of application of the ESM is for systems with the following characteristics:

1) The product and model systems are distorted. Product performance can therefore not be predicted accurately through TSM.
2) The geometry of the product is such that fabrication and testing of the product directly is difficult. Prediction of product performance through some type of similitude technique would therefore be beneficial.
3) Fabrication of a simplified version of the product (with regard to geometric shape) requires significantly less effort than fabrication of the product itself.

The fundamental concept of the ESM is shown in Figure 14. Rather than creating just a scale model of the product, as is done in the TSM, the ESM also uses a simplified specimen pair to correlate the behavior of the model and the product. One specimen, called the *model specimen*, is a geometrically simplified version of the model; the other specimen, called the *product specimen*, is a

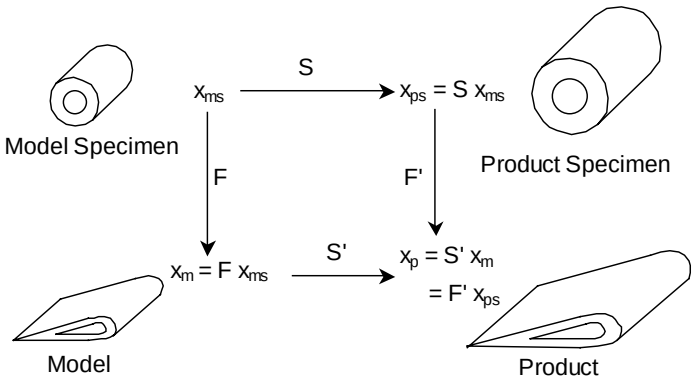

Figure 14. Empirical Similarity Method. Adapted from [Cho, 1999].

geometrically simplified version of the product. The model specimen is created from the same material and manufacturing process as the model, while the product specimen is created from the same material and manufacturing process as the product.

The concept of the ESM is to create a correlation between distorted systems through empirical testing. The states of the model specimen x_{ms}, the product specimen x_{ps}, and the model x_m, are used to predict the state of the product, x_p. In other words,

$$x_p = f(x_m, x_{ms}, x_{ps}) \tag{2-42}$$

If the behavior of each system is measured at several different geometric points or at several different loading conditions, then the states must be represented as vectors rather than as single numerical values. By representing vectors in bold type, the above equation is rewritten in vector form as follows:

$$\boldsymbol{x_p} = f(\boldsymbol{x_m}, \boldsymbol{x_{ms}}, \boldsymbol{x_{ps}}) \tag{2-43}$$

The relationship between any two state vectors can be given, in the most general case, with a fully populated transformation matrix. The theory of the ESM, which relies on the creation and use of such transformation matrices, makes use of the following assumptions:

1. The model and the model specimen can be tested to determine the state variation caused by changes in geometric shape, or *form.* Since material properties, size, and loading conditions are the same for the model and the model specimen, variations in state between the model and the model specimen are due entirely to the change in geometric shape. A *form transformation matrix F* can be created which represents the variation in the state vector caused by the change in geometric shape [Wood, 2002].
2. The model specimen and the product specimen can be tested to determine the state variation caused by changes in material properties, size, and loading conditions (all of the parameters that are typically scaled between a product and a model). A *scale transformation matrix S* can be created which represents the variation in the state vector caused by changes in size, material properties, and loading conditions, independent of geometric shape [Wood, 2002]. Changes in *size*, in this case, refer to parametric scaling of the overall length dimensions, rather than inherent size changes that accompany changes in shape.
3. The transformation matrices *F* and *S* are independent (i.e. there is no coupling between material behavior and geometric shape).

By testing the model, the model specimen, and the product specimen, we can extract the transformation matrices *F* and *S* from the following relationships:

$$\begin{aligned} \boldsymbol{x}_{ps} &= \boldsymbol{S}\, \boldsymbol{x}_{ms} \\ \boldsymbol{x}_{m} &= \boldsymbol{F}\, \boldsymbol{x}_{ms} \end{aligned} \tag{2-44}$$

We can solve equation 2-44 by using the inverse of the model specimen state vector as follows:

$$\begin{aligned} \boldsymbol{S} &= \boldsymbol{x}_{ps}\ \boldsymbol{x}_{ms}^{-1} \\ \boldsymbol{F} &= \boldsymbol{x}_{m}\ \boldsymbol{x}_{ms}^{-1} \end{aligned} \tag{2-45}$$

However, since $\boldsymbol{x}_{ms}$ is an n x 1 vector rather than an n x n matrix (with n being the number of measurement points taken), we cannot calculate the inverse of $\boldsymbol{x}_{ms}$ directly (recall that we can only take the inverse of a square matrix). We therefore need to use one of two important concepts from linear algebra. The first is the concept of a *pseudoinverse*; the second is the concept of a *circulant matrix*.

The pseudoinverse $\boldsymbol{x}^{+}$ of a vector $\boldsymbol{x}$ is given by the following equation [Strang, 1988]:

$$\boldsymbol{x}^{+} = (\boldsymbol{x}^{T}\, \boldsymbol{x})^{-1}\, \boldsymbol{x}^{T} \tag{2-46}$$

By using the pseudoinverse of $\boldsymbol{x}_{ms}$, the transformation matrices *S* and *F* can be derived as follows:

$$\begin{aligned} \boldsymbol{S} &= \boldsymbol{x}_{ps}\, \boldsymbol{x}_{ms}^{+} \\ \boldsymbol{F} &= \boldsymbol{x}_{m}\, \boldsymbol{x}_{ms}^{+} \end{aligned} \tag{2-47}$$

The second approach to solving equation 2-44 is to convert the *n x 1* state vectors into *n x n* circulant matrices. Transforming a vector into a circulant matrix

can be thought of as a simple matrix manipulation (similar, for example, to taking the transpose of a matrix). The circulant form of a vector $\boldsymbol{x}$ is defined as follows:

$$x = \begin{bmatrix} x_1 \\ x_2 \\ \vdots \\ x_n \end{bmatrix} \quad \Rightarrow \quad cir(x) = \begin{bmatrix} x_1 & x_n & \cdots & x_2 \\ x_2 & x_1 & \cdots & x_3 \\ \vdots & \vdots & & \vdots \\ x_n & x_{n-1} & \cdots & x_1 \end{bmatrix} \tag{2-48}$$

Since the circulant form of a vector is a square matrix, an inverse can be calculated directly. The circulant form of equation 2-44 is given by

$$\begin{aligned} cir(\boldsymbol{x_{ps}}) &= \boldsymbol{S}\ cir(\boldsymbol{x_{ms}}) \\ cir(\boldsymbol{x_{m}}) &= \boldsymbol{F}\ cir(\boldsymbol{x_{ms}}) \end{aligned} \tag{2-49}$$

and the transformation matrices S and F can be calculated as follows:

$$\begin{aligned} \boldsymbol{S} &= cir(\boldsymbol{x_{ps}})\ cir(\boldsymbol{x_{ms}})^{-1} \\ \boldsymbol{F} &= cir(\boldsymbol{x_{m}})\ cir(\boldsymbol{x_{ms}})^{-1} \end{aligned} \tag{2-50}$$

[Wood, 2002b] compares the accuracy of various approaches of calculating the transformation matrices S and F.

Since the transformation matrices are considered to be independent, the same scale transformation matrix S that relates the model specimen to the product specimen can also be used to relate the model to the product. Likewise, the same form transformation matrix F that relates the model specimen to the model can also be used to relate the product specimen to the product. In other words, we assume that $S = S'$ and $F = F'$, as shown in Figure 14. The state of the product can therefore be predicted by either one of the following equations:

$$\boldsymbol{x_p} = \boldsymbol{S}\,\boldsymbol{x_m}$$
$$\boldsymbol{x_p} = \boldsymbol{F}\,\boldsymbol{x_{ps}} \qquad (2\text{-}51)$$

The advantage of the ESM approach over the TSM is that model distortions can be captured in the scale transformation matrix *S*. This approach is contrasted with the TSM which relies solely on dimensional information to correlate systems, with no means of compensating for system distortion. In addition to capturing system distortion, the ESM allows for prediction of product behavior with no *a priori* knowledge about material properties of the product or model systems. The major disadvantage of the ESM is the additional effort required to construct and test the model specimen and product specimen, and calculate the appropriate transformation matrices *S* and *F*.

The position of the ESM in functional testing of products is considered to lie between the TSM and full-scale testing, as shown in Figure 15. The ESM is presented as a more accurate approach, in general, than the TSM. The ESM is

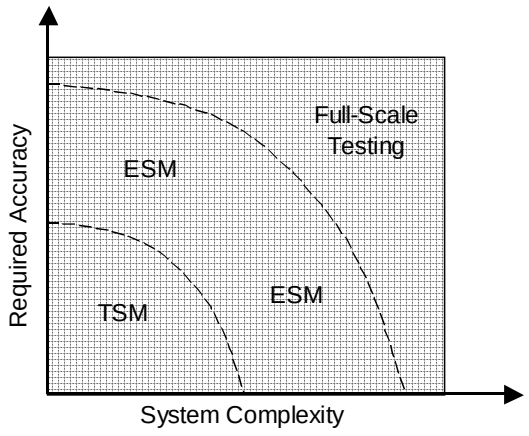

Figure 15. TSM vs. ESM.

also presented as a better approach for correlating complex systems whose governing parameters may not be well known, as required by the TSM. The boundaries of the ESM (i.e. limitations, range of beneficial applications, etc.) are illustrated qualitatively in Figure 15. These boundaries, however, are currently not clearly defined. The boundaries of the ESM are explored in the following chapter.

CHAPTER 3

Range of Application of the Empirical Similitude Method

The purpose of the ESM is to provide more accurate predictions of product performance, as compared with the TSM, when two systems are distorted. Several sources of model distortion were presented in Chapter 2. Additional sources of distortion have been identified, and a classification structure that groups all known sources of model distortion into classes or families has been created. This classification structure is shown in Figure 16.

The classification scheme in Figure 16 is by no means unique. The structure proposed by [Murphy, 1950], for example, is made up of geometrical, loading, and material distortions, while that proposed by [Cho, 1999] consists of functional and parametric distortions. [Farrar, 1994] discusses distortions that result from limitations in experimental equipment. Figure 16 represents a compilation of all such sources of model distortion. Keep in mind, however, that regardless of the terminology used, each type of distortion simply represents a situation in which the TSM similarity constraints are not satisfied (i.e. when one of the π terms in the model is not equal to the corresponding π term in the product [Murphy, 1950]).

Although Figure 16 appears to be the most complete compilation of model distortions to date, it is not presumed to be a complete set. In other words, additional sources of model distortion may exist that have not yet been identified. The wide range of model distortions that have been identified, however, indicates

the likelihood that many models will contain some type of distortion, and emphasizes the importance of being able to compensate for such distortions.

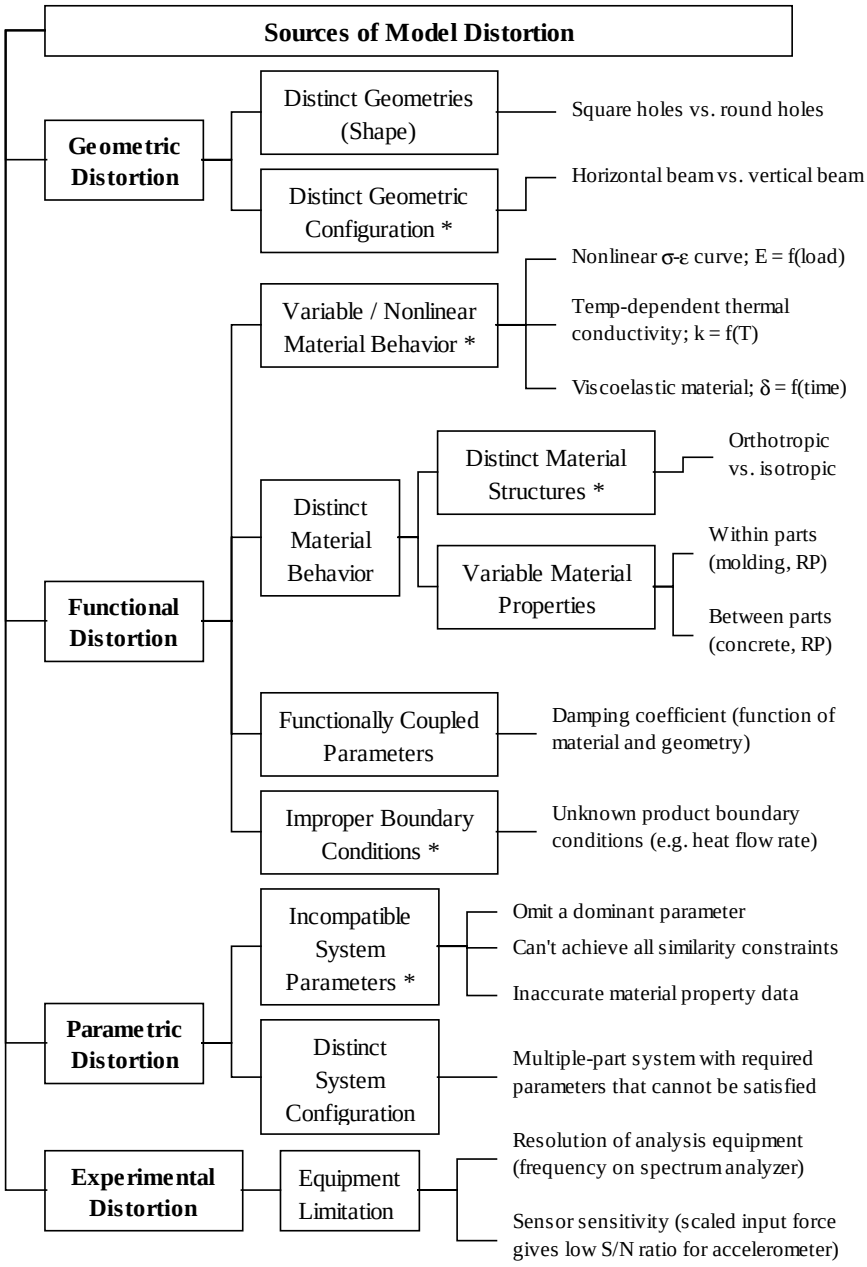

Figure 16. Classification of Model Distortion.

A brief description of each of the main classes of model distortion, as shown in Figure 16, is presented below:

Geometric Distortion: Systems that are different geometrically, either with regard to shape or to geometrical configuration (e.g. horizontal beam vs. vertical beam), are categorized as being *geometrically distorted*. (Note that distortions in *size* are categorized under *parametric distortions*, as described below, since size values are considered to be explicit governing parameters).

Functional Distortion: Two systems are classified as *functionally distorted* if the behavior of the systems is not governed by the same physical laws or principles. Functional distortion can occur even when two systems are governed by the same physical parameters if those parameters behave differently in the two systems. For example, functional distortion occurs when a parameter of one system exhibits linear behavior while the corresponding parameter of the "similar" system exhibits nonlinear behavior.

Parametric Distortion: *Parametric distortion* occurs when proper ratios of the dominant system parameters, as required by the TSM, cannot be achieved. Parametric distortion results when, for example, a dominant system parameter is inadvertently omitted or when a required ratio of system parameters is physically impossible to achieve.

Experimental Distortion: A test setup in which input or output signals required by the TSM are at levels that are difficult or impossible to achieve with available equipment results in *experimental distortion*. Experimental distortion

often results from sensors that have inadequate sensitivity or analysis equipment that has inadequate resolution.

It is important to note that the ESM is not intended to resolve all of the model distortions described in Figure 16. For example, experimental distortion is an artifact of the experimental setup and the resolution of the equipment, and cannot be circumvented by applying the ESM. Experimental distortion must be resolved instead by redesigning the experiment or by improving the equipment. Geometric distortion that is caused by distinct geometric shapes between the product and the model can also not be resolved with the ESM. Such geometric distortions must be resolved by redesigning the experiment such that geometric similarity can be achieved. So even though all TSM similarity constraints need not be satisfied when applying the ESM, there are still some conditions (such as geometric similarity between the product and the model) that must be met. The types of model distortions that are effectively resolved through application of the ESM are highlighted with an asterisk in Figure 16.

Application of the ESM in product testing falls between the TSM and full-scale testing, as was shown in Figure 15 in the preceding chapter. The purpose of this chapter is to clearly establish the boundaries of the ESM. The lower boundary will indicate when the ESM is not necessary (i.e. when the TSM is sufficient). The upper boundary will indicate when the ESM is no longer applicable (i.e. when full-scale testing is more appropriate).

The boundaries of the current ESM technique will be established in two ways: first, the theoretical foundations of both the TSM and the ESM will be

reviewed, and situations which violate the theories will be identified (situations which violate the TSM theory indicate where the lower boundary of the ESM lies; situations which violate the ESM theory indicate where the upper boundary of the ESM lies); second, several numerical examples will be provided which illustrate the limits of application of the ESM. The numerical examples are intended to clarify situations in which the ESM is not appropriate that may not be easy to recognize intuitively. The numerical examples are used for illustrative purposes only and are not intended to be a comprehensive representation of the ESM boundaries.

All of the numerical examples are developed through the use of finite element analysis (FEA) with ABAQUS™ software. In order to maintain consistency and simplicity in the numerical examples, all examples deal with the deflection of a cantilever beam under a concentrated load at the tip. This simple example provides an effective means of illustrating the desired concepts and clarifying the boundaries of the ESM. Other applications of the ESM are provided in later chapters.

3.1. LOWER BOUNDARY OF ESM

Chapter 2 develops the theory of the TSM and presents the conditions that are required for the TSM to be valid. This section gives a brief review of the TSM and presents two numerical examples that clarify its application.

The TSM states that two physically similar systems (a product *p* and a model *m*) whose behavior of interest *x* is influenced by the same governing parameters d_i, as in

$$x_p = f(d_1, d_2, ..., d_n) \qquad x_m = f(d_1, d_2, ..., d_n) \tag{3-1}$$

can be recast into an equivalent dimensionless form as follows:

$$\pi_{x,p} = g(\pi_{1,p}, \pi_{2,p}, ..., \pi_{N,p}) \qquad \pi_{x,m} = g(\pi_{1,m}, \pi_{2,m}, ..., \pi_{N,m}) \tag{3-2}$$

where $N < n$. Now,

$$\pi_{x,p} = \pi_{x,m} \; if \; \pi_{i,p} = \pi_{i,m} \; \forall \; i \tag{3-3}$$

Scale factors relating the governing parameters of the product to the corresponding parameters of the model can be determined from the similarity constraints in equation 3-3. If all of the similarity constraints can be satisfied, the performance of the product can be predicted by testing the model and applying the appropriate scale factor.

The theory of the TSM is valid only for those systems whose dimensionless parameters (π_i) are *exactly equal over the entire range of application*. This strict requirement of the TSM demands that all of the governing parameters be constant over the entire range of application (or, if there is variation in one of the governing parameters, that the variation be exactly equivalent in the corresponding parameter of the other system). Such strict requirements are often difficult to satisfy in practice. Cases in which the TSM requirements are not satisfied (which are summarized in Figure 16) represent the lower boundary of the ESM. In other words, any time a system includes one of the distortions listed in

Figure 16, the TSM no longer gives accurate predictions of product performance. Of course, the magnitude of the distortion will determine the magnitude of the error in the TSM prediction.

After reviewing the literature, there appears to be two issues related to the TSM that need further clarification. The first is the notion that geometric complexity is a source of model distortion. The second is the idea that large differences in size can lead to model distortions. (For example, will a very long product beam involve large deflection effects while a short model beam, even though well-scaled, exhibit no such effects?) The theory of TSM asserts that neither of the two situations presented above will result in model distortions. In other words, nothing in the theory of TSM restricts geometric complexity or size scales. The following sections use finite element studies to illustrate (not *prove*) that the TSM does in fact produce accurate results in both cases (the *proof* lies in the TSM theory itself).

3.1.1. TSM Study 1: Effect of Geometric Complexity

The deflection of a cantilever beam under a concentrated load at the tip is described by the functional relationship in equation 2-15, which is repeated here for convenience:

$$\delta = g(F, E, h, w, L) \tag{3-4}$$

where δ is the deflection of the beam at the tip, F is the applied load, E is the elastic modulus of the material, h is the height of the beam, w is the width of the beam, and L is the length of the beam. The equivalent dimensionless form of equation 3-4 is given as follows:

$$\frac{\delta}{h} = f\left(\frac{w}{h}, \frac{F}{Eh^2}, \frac{L}{h}\right) \tag{3-5}$$

Suppose the product beam has material properties of aluminum, and the model beam has properties of polycarbonate. All material properties are assumed to be constant over the range of application. The material properties and beam parameters used in this study are summarized in Table 2. Substituting values from Table 2 into equation 3-5 shows that all TSM constraints are indeed satisfied (all corresponding dimensionless parameters between the product and the model are identical). The difference in Poisson's ratio is considered to be insignificant.

The TSM procedure described in Chapter 2 is applied to several different beam geometries. A total of six test cases are run using various geometric features in the beams, included combinations of tapers, evenly-spaced holes, and unevenly-spaced holes. The various beam geometries, which are shown in Figure 17, represent different levels of geometric complexity. Note that geometric similarity is maintained between product and model beams, as required by TSM.

Table 2. Properties and Parameters used in Beam Study.

	Product Beam	**Model Beam**
Elastic Modulus, E (ksi)	10,150	320
Poisson Ratio, ν	0.33	0.39
Height, h (in)	0.125	0.215
Width, w (in)	1.00	1.72
Length, L (in)	8.00	13.76
Applied Force, F (lb)	10.0	0.933

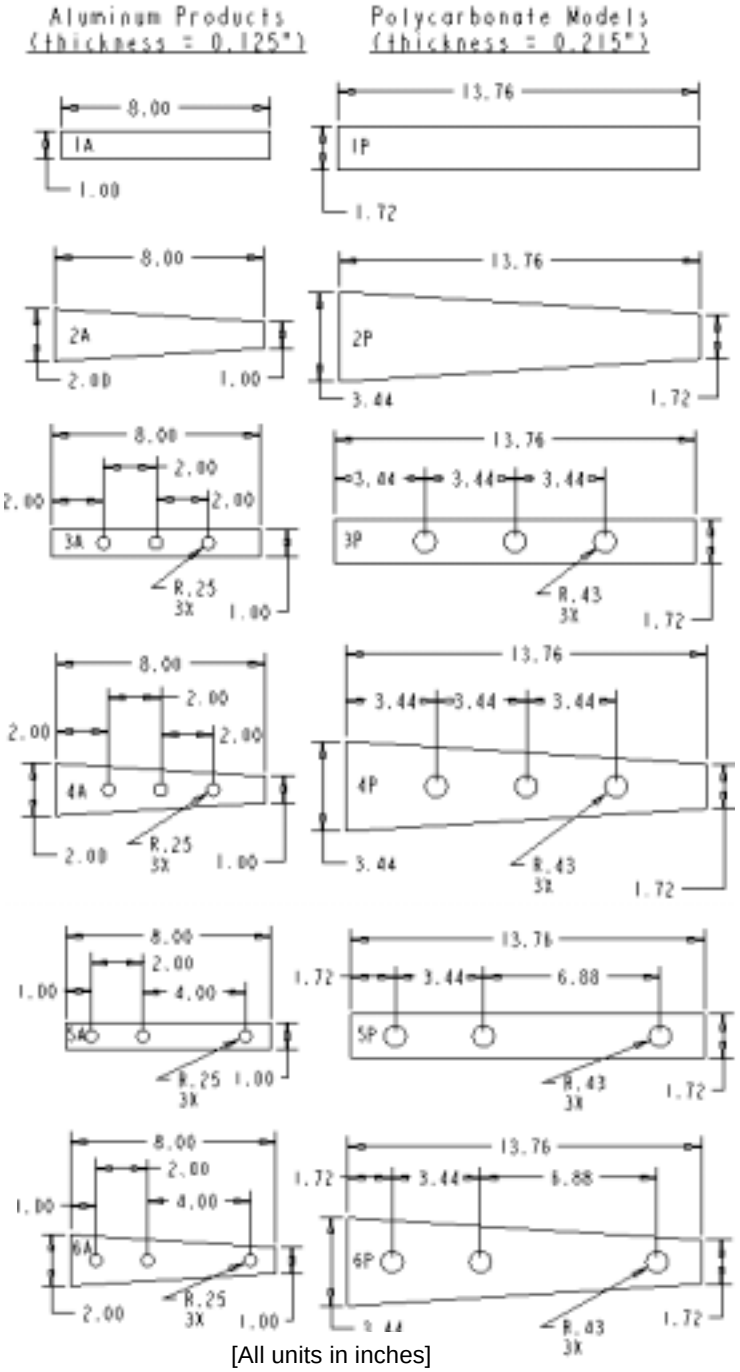

[All units in inches]

Figure 17. Various Beam Geometries used in Finite Element Study.

The finite element models for each test case are created as follows:

- Symmetry is used for each beam; therefore, only half of the beam is modeled and half of the load is applied.
- Linear shell elements with reduced integration are used (S4R elements).
- Large deflection effects are included.
- Twenty equally-spaced increments are used in the loading step (this is done so that correlations can be made at equivalent points between the model and the product).
- The deflection of the load point is monitored at each increment.

A sample finite element model is shown in Figure 18.

The TSM deflection scale factor K_δ (calculated as 0.5814) is multiplied by the deflection of the model beam at each load increment, and that result is compared with the actual deflection of the product beam. A percent error between the actual deflection of the product beam and the deflection predicted by the TSM is calculated. Table 3 illustrates how the results are tabulated for the first set of

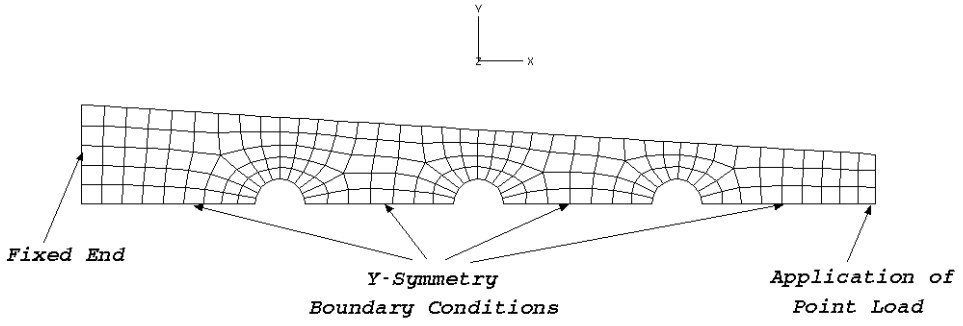

Figure 18. Sample Finite Element Model.

Table 3. Tabulation of Results for TSM Study 1.

Load Increment	δ_{model}	$\delta_{TSM,predicted}$ (δ_{model} x 0.5814)	$\delta_{product}$	**Error (%)**
1	0.0870	0.0506	0.0510	0.82
2	0.1750	0.1017	0.1020	0.25
3	0.2620	0.1523	0.1530	0.44
⋮	⋮	⋮	⋮	⋮
20	1.720	1.000	1.000	0.00
			Average	0.47

beams. This procedure is repeated for all six sets of beam geometries. A summary of the errors for each of the six beam geometries is shown in Table 4. Note that the TSM error is never above 1%, which is considered to be within the accuracy of the finite element models.

The results of the study illustrate that geometric complexity by itself is not a source of model distortion. These results confirm the theory of TSM since, in each case, all properties and parameters are well scaled and geometric similarity

Table 4. Results of TSM Study 1.

Case	**Average TSM Error**
1	0.47 %
2	0.87 %
3	0.14 %
4	0.60 %
5	0.20 %
6	0.59 %

is maintained. It should be noted, however, that this study deals with *pure changes in geometric shape*, meaning changes in geometric shape that are completely independent of all other system parameters and material behaviors. When all material properties are linear, as is true in this study, then this condition holds true; when material properties are nonlinear, however, then changes in geometric shape can effect material behavior, as will be illustrated in later studies. The point to be taken from this study is that *geometric complexity alone does not constitute a source of model distortion*.

3.1.2. TSM Study 2: Effect of Size Scales

The next study explores the effects of changes in size on TSM results. Recall from Chapter 2 that a change in size is defined as a *parametric scaling of overall length dimensions*. The question to be addressed in this study is whether or not a significantly different size scale between the product and the model affects TSM results. For the specific case of deflection of a cantilever beam, we want to see if the large size difference between the two beams results in different degrees of large deflection effects, which may lead to errors in the TSM predictions.

A cantilever beam with five holes along its length is selected as the product beam to be analyzed. The size scale between the model and the product is chosen to be 10:1, which is considered to be relatively large. All relevant material properties, such as Young's modulus, are held constant over the entire range of application so that only the effects of the size change can be evaluated. The finite element procedure used in this study is the same as that presented in the previous

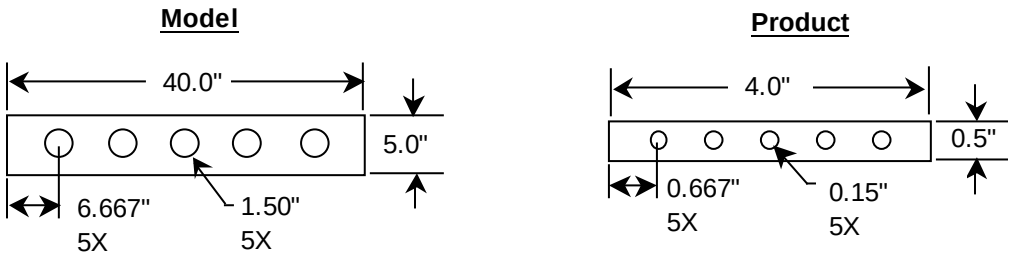

Figure 19. Model and Product Beams for TSM Study 2.

section, except that only ten load increments are evaluated for each beam instead of twenty. The model and product beams are shown in Figure 19. Additional information on the beams is contained in Table 5. As in the previous study, the values of all system parameters are selected so as to satisfy all TSM constraints.

The TSM prediction of beam deflection is calculated in the same way as described in Study 1, except that in this case the deflection scale factor K_δ is 0.1. Table 6 shows a tabulation of the study results. Note that average TSM error is less than 0.01%, which is easily within the numerical error of the finite element method. This result confirms that pure size changes, or changes in geometric size scale only, produce no error in TSM results. This result validates the TSM theory

Table 5. Properties and Parameters for TSM Study 2

	Product Beam	**Model Beam**
Elastic Modulus, E (ksi)	1,000	100
Poisson Ratio, ν	0.33	0.33
Height, h (in)	0.05	0.5
Applied Force, F (lb)	1.0	10.0

Table 6. Tabulation of Results for TSM Study 2.

Load Increment	δ_{model}	$\delta_{TSM,predicted}$ (δ_{model} * 0.1)	$\delta_{product}$	Error (%)
1	4.345	0.4345	0.4345	0.000
2	8.389	0.8389	0.8388	0.012
3	11.94	1.194	1.194	0.000
⋮	⋮	⋮	⋮	⋮
10	24.86	2.486	2.486	0.000
			Average	0.007

since, in each case, all properties and parameters are again well scaled and geometric similarity is maintained. It is true that large deflection effects influence the deflection results, but *the influence is identical in both beams*. Figure 20 shows a plot of the force-deflection curve for the product beam, as well as the

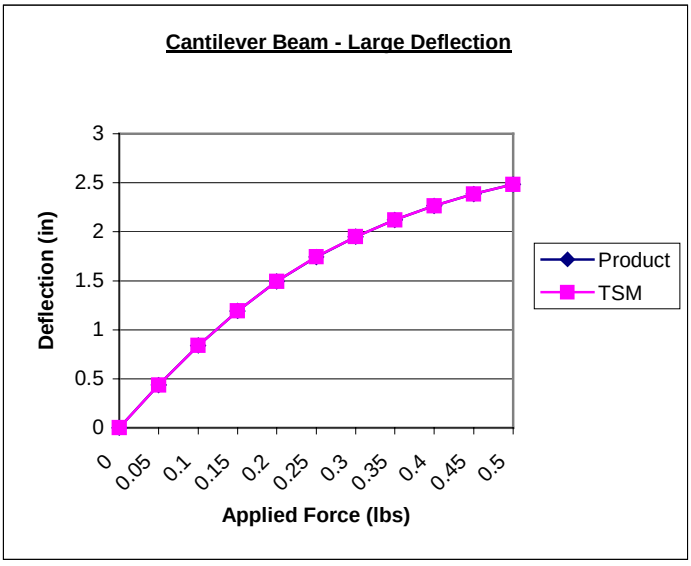

Figure 20. Force-Deflection Curves for TSM Study 2.

TSM prediction obtained from the model beam. (Note that the results are so similar that they appear as one curve in the figure). The nonlinear nature of the force-deflection curve is evidence of large deflection effects. The degree of nonlinearity, however, is the same for both curves.

The curves which describe the final deflected shape of the beams would also be the same for the model and the product; the only difference in the curves would be in their *size*. Figure 21 shows a simple sketch of how the final deflected shape of both beams might appear. One might think of the relationship between the two beams as simply a *change of units*.

It is important to emphasize that this study involves a *pure size change*; none of the other governing parameters is affected. It was pointed out in Chapter 2 that size changes are often accompanied by a change in some other governing parameter of the system. For instance, surface tension may be an important parameter in determining the drag force on a small-scale model of a ship, but may be completely irrelevant in determining the drag force on the corresponding full size ship. This phenomenon is known as *scale effects*. Scale effects cause two systems to become physically dissimilar, or distorted. The study just conducted,

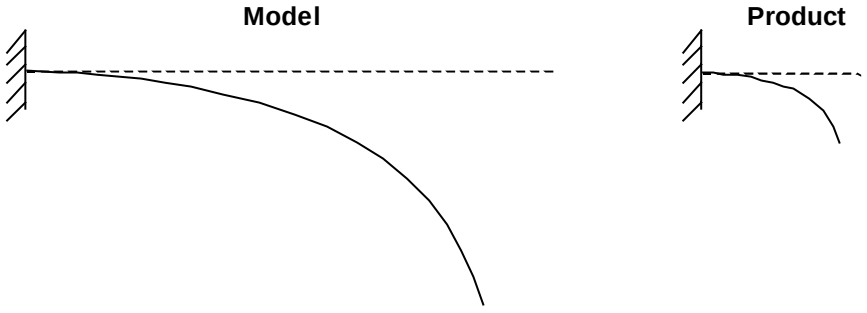

Figure 21. Illustration of Corresponding Deflection Curves.

however, illustrates that *it is not the change in size itself that causes the distortion*, but the accompanying change in some other governing parameter. A change in the size scale of a model, by itself, causes no distortion, even when large deflection effects are present. This result is in accordance with the theory of TSM.

The two studies in this section illustrate situations in which the TSM is an appropriate approach, and when application of the ESM is not necessary. The ESM becomes necessary only when a distortion exists between the model and the product. When model distortions exist, a single, constant scale factor no longer provides accurate predictions of product performance. In such cases the TSM becomes inaccurate, and the ESM becomes a more appropriate approach. This condition describes the *lower boundary* of the ESM, or the point at which the TSM is no longer a valid approach. The following section examines the range of application of the ESM and establishes its *upper boundary*, or the point at which the ESM is no longer a valid approach.

3.2. UPPER BOUNDARY OF ESM

In order to establish the range of application of the ESM and define an upper boundary, we must first examine the ESM theory and determine the conditions under which that theory is valid. A graphical representation of the ESM approach, which was introduced in Chapter 2, is repeated here for convenience (see Figure 22).

The major assumption of the ESM is that the “scale” transformation matrix S, which relates the model specimen to the product specimen, can also be

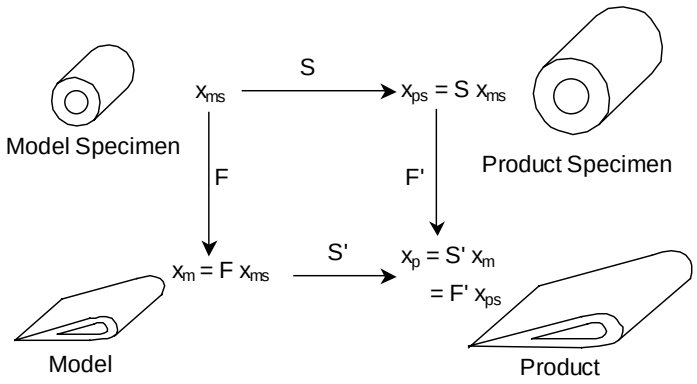

Figure 22. Empirical Similarity Method. Adapted from [Cho, 1999].

used to relate the model to the product. In other words, S = S' in Figure 22. In addition, the "form" transformation matrix F, which relates the model specimen to the model, can also be used to relate the product specimen to the product. In other words, F = F' in Figure 22 [see also Wood, 2002].

In order to ensure that S = S' and F = F', three conditions must be satisfied. The first condition is that all scaling must be done in a consistent manner. This means that the scaling between the model specimen and the product specimen, in terms of size, material properties, and applied loads, must be identical to that between the model and the product. Also, the "scaling" between the model specimen and the model, in terms of changes in geometric shape, must be identical to that between the product specimen and the product (i.e. the model and the product must be geometrically similar, as must the model specimen and the product specimen). This requirement stems from the fact that changes in scaling must be isolated from changes in form in order to extract independent scale and form transformation matrices. In other words, the change in state

between the model and the model specimen must be due only to changes in *form*, and the change in state between the product specimen and the model specimen must be due only to changes in *scale*.

Although the scaling must be *consistent*, there is no requirement for the scaling to be equal to that required by the TSM. The effect of any "distorted scaling" between the model and the product (scaling that does not satisfy the TSM constraints) should be captured in the transformation matrix between the model specimen and the product specimen, provided that the same "distorted scaling" is applied between the specimen pair. It is assumed that the model and the specimen pair can be designed with consistent scaling, and that this ESM condition can always be satisfied.

The second condition that is required to ensure that S = S' and F = F' is that material properties must be consistent between the model and the model specimen, as well as between the product and the product specimen. This requirement may seem trivial since the model and model specimen are made from the same material, as are the product and the product specimen. However, inconsistencies in material properties can occur with different types of materials and different manufacturing processes. Some materials (such as concrete) are considered to be *statistical materials* since there can be significant variation in material properties from one batch to the next [Farrar, 1994]. Some processes (such as injection molding) can produce variation in material properties within parts depending on fill patterns, locations of weld lines, etc. Parts created through

rapid prototyping processes can exhibit variations in material properties between parts as well as within individual parts.

The third condition that is required to ensure that S = S' and F = F' is that material behavior and geometric shape must be *independent*. This requirement is emphasized in Figure 22 where the form transformation matrix F is independent of the scale transformation matrix S. In other words, a change in form must not affect the way in which a material behaves. If a change in geometric shape *does* affect material behavior, then the change in behavior must be identical in both the model and product systems in order to maintain S = S' and F = F'. This type of situation is descriptive of a well-scaled system (one in which TSM applies). However, for systems that are not well-scaled (those which contain model distortions), and in general, any change in material behavior that results from a change in geometric shape will not be identical in the model system and the product system. If this situation occurs, then we can no longer say that *scale* and *form* are independent. This brings us back to the ESM requirement that *changes in geometric shape must not affect material behavior* (in either the model or product system) in order to ensure that S = S' and F = F'.

It is important to notice the subtle distinction that is made between material properties and material behavior: *material properties* refer to the global properties of the material; *material behavior* refers to the response of the material under some specific loading or boundary condition. For example, the material property of a stress-softening material can be described with a nonlinear stress-strain curve. The material behavior – whether it behaves as a "flexible" material

or a “stiff” material – depends on the specific operating point along the curve that results from a given loading condition.

If any of the three conditions given above is not satisfied, we cannot guarantee that S = S’ and F = F’, and the ESM theory is violated. When this situation occurs, the ESM can no longer be used as a reliable approach for predicting product performance. The three conditions that cause the ESM theory to be violated are shown in Figure 23 along with several specific examples. We will label these conditions as *specimen distortions* since they involve inconsistencies between the product / model system and the specimen pair. This type of distortion is in contrast to the *model distortions* presented earlier in this

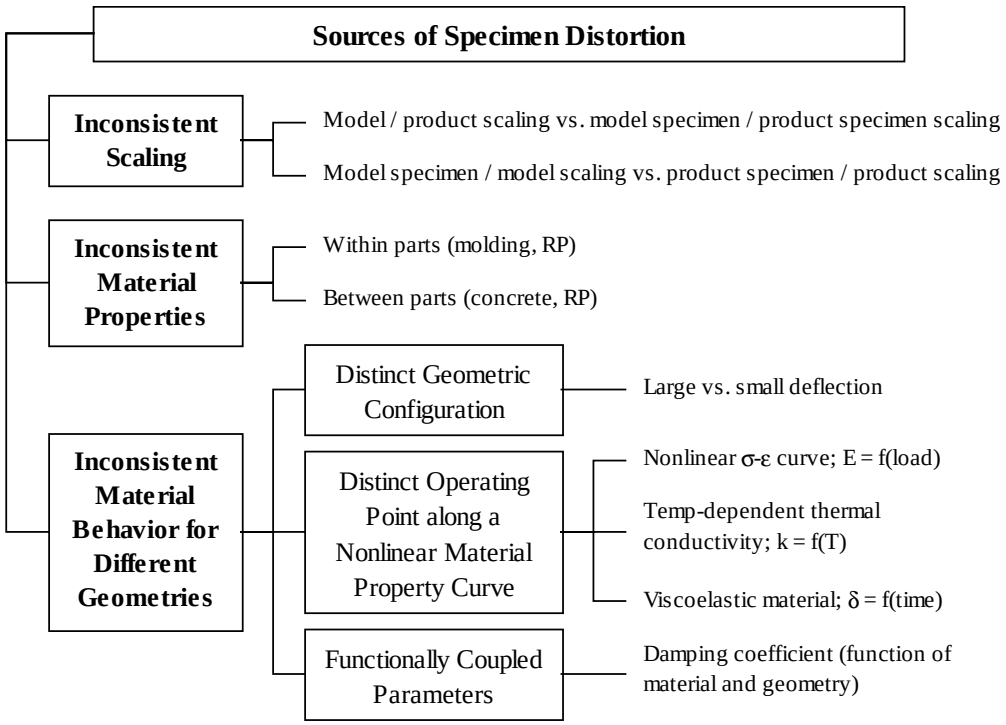

Figure 23. Sources of Specimen Distortion.

chapter that describe distortions between a model and a product. The three main classes of *Inconsistent Material Behavior* shown in Figure 23 are discussed below.

Distinct Geometric Configuration: Systems whose geometric configurations change in different proportions during testing are defined as being *geometrically distorted*. Note that *differing geometric shapes* are not included in this definition of geometric distortion since the specimens will have, by design, a different geometric shape than the model or product. The geometric shape is assumed to remain constant during testing. The *geometric configuration*, however, can change during testing, and this change can be different in the specimen than in the model or the product. The geometry of a cantilever beam, for example, can produce different levels of large deflection effects in the model and the model specimen. It was shown earlier in this chapter that large deflection effects are equivalent when two systems are well scaled and geometrically similar. But since a model is not geometrically similar to its specimen, large deflection effects will not necessarily be equivalent between the two systems, and distinct geometric configurations can result.

Distinct Operating Point along a Nonlinear Material Property Curve: Whenever a nonlinear material property curve describes the behavior of the model or product system, then the model or product will demonstrate a different behavior then the respective specimen if the specimen is operating at a different point along that curve. Three specific examples of this situation are shown in Figure 23. Note that geometry is not the only factor that causes specimen

distortion in these cases. For example, the behavior of a viscoelastic material is dependent on *time*. If a viscoelastic model is tested in a different time period than its corresponding model specimen, ESM results will be distorted.

Functionally Coupled Parameters: Some parameters, such as the damping coefficient of a structure, are inherently functions of both material properties and geometric shape. In such cases, changes in geometric shape can affect the way in which a system behaves and lead to specimen distortion.

The sources of specimen distortion described above define the upper boundary of the ESM approach. In other words, systems that involve specimen distortion can no longer rely on the ESM technique for reliable predictions of product performance. Of course, the *degree* of distortion will determine the degree of error in the ESM approach, but *any* amount of specimen distortion defines the theoretical bound or limit of ESM. In practice, one may accept a small degree of specimen distortion and still use the ESM to obtain much better results than with the TSM. But that situation is left for discussion in a later chapter; here we are only concerned with establishing the theoretical limits of the ESM.

The following sections present three numerical studies that illustrate the effects of specimen distortion. A simple cantilever beam system is again used to demonstrate the principles presented above. Each study involves some type of model distortion between the product and the model (otherwise we would not even be using the ESM). Results of the studies show how ESM predictions of product performance vary as the degree of model distortion increases and as the change in geometric shape increases. The studies are carried out in a similar

manner to those presented earlier (ABAQUS finite element software is used, shell elements are used to model the beams, etc). Specific details of the studies are included in each respective section.

3.2.1. ESM Study 1: Linear vs. Nonlinear Material Properties

The first study investigates the effects of distortions in material properties. Specifically, the product system is modeled with linear material properties (a linear stress-strain curve, representing a constant value of Young's modulus) and the model system is modeled with nonlinear material properties (a nonlinear stress-strain curve, representing a variable value of Young's modulus). The nonlinear stress-strain behavior of the model system is defined with a Ramberg-Osgood curve, which is described by the following equation [see ABAQUS, 2001]:

$$\varepsilon = \frac{\sigma}{E}\left(1+\alpha\left(\frac{\sigma}{\sigma^0}\right)^{n-1}\right) \qquad (3\text{-}6)$$

where σ = stress

ε = strain

E = Young's modulus (defined as the slope of the stress-strain curve at zero stress)

α = "yield" offset

σ^0 = yield stress in the sense that, when $\sigma = \sigma^0$, $\varepsilon = ((1+\alpha)\sigma^0)/E$

n = hardening exponent for the "plastic" (nonlinear) term: $n > 1$

By varying the parameters in the Ramberg-Osgood equation, three different material properties that exhibit increasing degrees of nonlinearity are

Table 7. Parameters for Ramberg-Osgood curve.

	E (ksi)	α	σ^0 (ksi)	n
Material 1	150	0.40	3	2.0
Material 2	320	0.43	3	3.0
Material 3	500	2.00	3	2.5

defined. The parameters used to define these material properties are shown in Table 7, and the resultant stress-strain curves are shown in Figure 24. The straight lines in Figure 24 represent the slopes of the stress-strain curves at zero stress (given by *E* in Table 7), which is the traditional definition of Young's modulus for a nonlinear stress-strain curve. The three curves shown in Figure 24 represent three different material property cases for the model and the model specimen in this study. The product and product specimen maintain a linear stress-strain relationship, with a Young's modulus of 10,150 ksi (equal to that of aluminum).

The "degree of nonlinearity" in the stress-strain curves (which represents the "degree of model distortion") can be quantified through a residual sum of

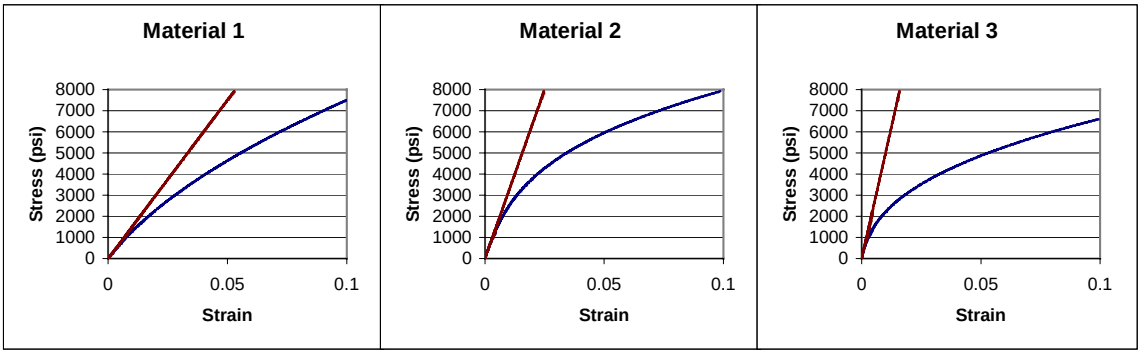

Figure 24. Nonlinear Stress-Strain Curves for ESM Study 1.

squares between the points that define the linear curves and those that define the corresponding nonlinear curves [see DeVor, 1992]. Each linear curve in Figure 24 is defined by calculating strain at every 10 psi increment of stress using the linear relationship $\varepsilon = \sigma / E$. Each corresponding nonlinear curve in Figure 24 is defined by calculating strain at every 10 psi increment of stress using equation 3-6. The residual sum of squares is then calculated as follows:

$$SS(residual) = \sum_{i=1}^{n} (\varepsilon_{nl} - \varepsilon_{l})^2 \qquad (3\text{-}7)$$

where ε_{nl} is the nonlinear value of strain at each increment of stress, ε_{l} is the linear value of strain at each increment of stress, and n is the total number of stress increments. Table 8 shows the calculated residual sum of squares for each nonlinear stress-strain curve in Figure 24. The values in Table 8 indicate that each successive material exhibits a higher degree of nonlinearity, which signifies that each successive material represents a higher degree of model distortion.

Three different geometric cases are also considered in this study. The geometry of the model, product, model specimen, and product specimen are shown in Figure 25. The three different geometric cases involve different sizes of holes in the product (and, correspondingly, in the model). The three hole sizes

Table 8. Residual Sum of Squares for Model Materials.

	Range of Stress (psi)	**SS(residual)**
Material 1	0 - 8000	0.52
Material 2	0 - 8000	0.67
Material 3	0 - 8000	2.60

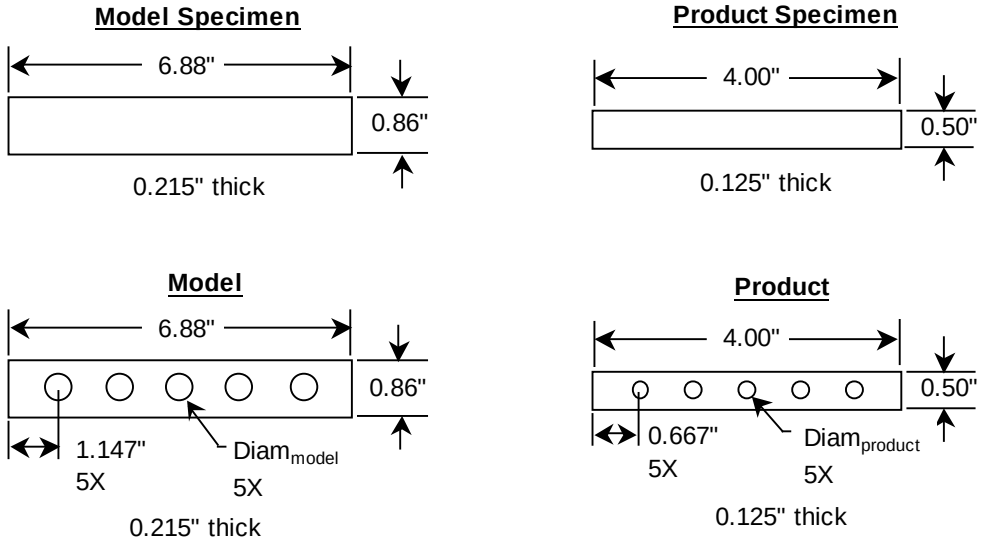

Figure 25. Setup for ESM Study 1.

considered in the study are shown in Table 9. Notice that a constant scale factor of 0.5814 relates all geometric features of the model to the product. The only distortion between the model family and the product family is in the value and behavior of Young's modulus.

A total of nine cases have now been defined for the study (three different hole sizes for each of the three different material properties). The goal of the study is to determine the influence that changes in geometric shape and changes

Table 9. Three Geometric Cases for ESM Study 1.

	Diam$_{product}$ (in)	**Diam$_{model}$ (in)**
Geometry 1	0.150	0.258
Geometry 2	0.250	0.430
Geometry 3	0.350	0.602

in model distortion have on ESM results. In each case a load of 20 lbs is applied to one end of the product beam while the other end of the beam is held fixed. (The required load for the model beam was determined from TSM scale factors assuming a constant value for Young's modulus). The deflection of the tip of the beam, which is recorded at ten equal load increments (at 2 lbs, 4 lbs, 6 lbs, … 20 lbs), represents the *state vector* for each beam. The transformation matrices S and F are derived from the state vectors of the model, model specimen, and product specimen, as outlined in Chapter 2. Both the pseudo-inverse (*pi*) approach and the circulant matrix (*cir*) approach are used in deriving the transformation matrices. The ESM technique is then used to predict the state of the product. The error in the ESM approach is determined by comparing the ESM prediction with the actual state of the product. The state of the product is also predicted using the TSM approach in order to demonstrate the improvement that can be realized with the ESM when model distortions are present. Table 10 shows how results are tabulated for each case. (The values in Table 10 are for Material 2, Geometry 2).

Table 10. Tabulation of Results for ESM Study 1.

Load Inc.	**δ_{model}**	**$\delta_{product}$**	**δ_{TSM}**	**Error TSM,%**	**δ_{pi}**	**Error pi,%**	**δ_{cir}**	**Error cir,%**
1	0.115	0.066	0.067	0.56	0.068	2.05	0.067	0.44
2	0.230	0.133	0.134	0.82	0.135	2.02	0.134	0.57
3	0.247	0.199	0.202	1.37	0.203	2.11	0.200	0.80
⇓	⇓	⇓	⇓	⇓	⇓	⇓	⇓	⇓
10	1.218	0.646	0.708	9.64	0.667	3.26	0.671	3.82
			Ave.	**4.20**		**2.50**		**1.90**

The average errors from the TSM, ESM pseudo-inverse (*pi*), and ESM circulant matrix (*cir*) approaches for all nine cases are compiled in Table 11. A review of the table shows that, for any given material, prediction errors increase as the change in geometric shape increases (with Geometry 1 having the least change and Geometry 3 having the greatest). Likewise, for any given geometric shape, prediction errors tend to increase as the degree of material distortion increases (with Material 1 having the least distortion and Material 3 having the greatest). The only exceptions to this trend, which are due to the fact that the model distortion for Material 2 is actually smaller than that for Material 1 at low values of stress, are highlighted with an asterisk. Note that, in every case, the ESM predictions produce less error than the TSM prediction.

Table 11. Average Errors from Various Similitude Approaches.

	Geometry 1		Geometry 2		Geometry 3	
Material 1	TSM	4.06 %	TSM	4.86 %	TSM	6.26 %
	ESM_{pi}	0.53 %	ESM_{pi}	1.31 %	ESM_{pi}	2.41 %
	ESM_{cir}	0.54 %	ESM_{cir}	1.31 %	ESM_{cir}	2.64 %
Material 2	TSM *	2.79 %	TSM *	4.20 %	TSM	7.94 %
	ESM_{pi}	0.67 %	ESM_{pi}	2.50 %	ESM_{pi}	7.62 %
	ESM_{cir} *	0.52 %	ESM_{cir}	1.90 %	ESM_{cir}	5.54 %
Material 3	TSM	36.48 %	TSM	45.88 %	TSM	67.66 %
	ESM_{pi}	3.44 %	ESM_{pi}	11.89 %	ESM_{pi}	28.00 %
	ESM_{cir}	2.88 %	ESM_{cir}	10.10 %	ESM_{cir}	26.88 %

Figure 26 contains a plot of ESM error as a function of model distortion (we assume zero prediction error for zero model distortion in this case). Recall that model distortion in this case is represented by the residual sum of squares of the nonlinear stress-strain curves for the various materials, as shown in Table 8. The plot in Figure 26 reflects the results obtained from the circulant matrix approach, although TSM or ESM pseudo-inverse results would show similar trends. The results shown in Figure 26 lead to the same conclusions that can be drawn from Table 11 - that prediction error tends to increase with increased changes in geometric shape and with increased levels of model distortion.

The source of the TSM error in this study is obvious: material properties (specifically Young's modulus) are not well-scaled between the product and the model and, consequently, the TSM constraints are not satisfied. The source of the

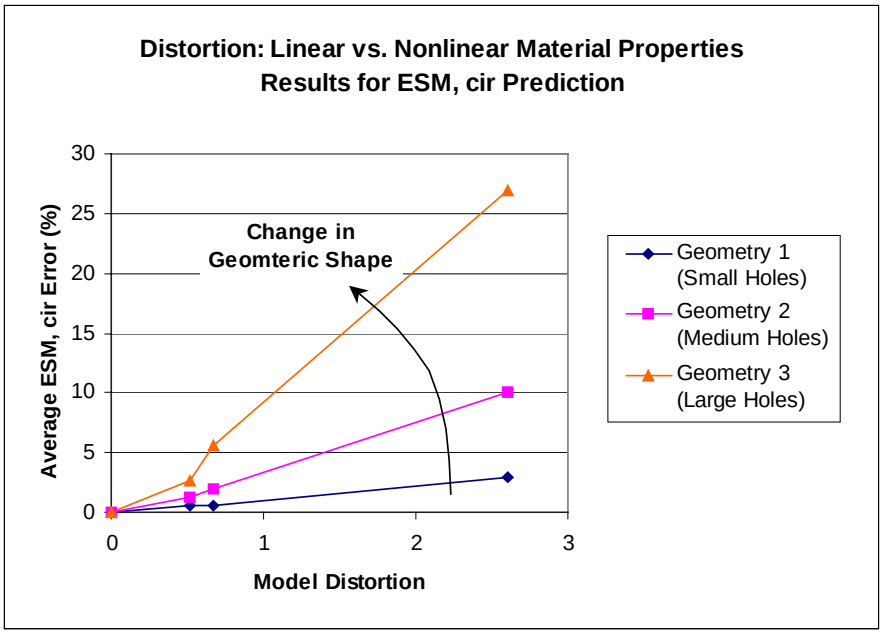

Figure 26. Prediction Error vs. Model Distortion for ESM Study 1.

ESM error was alluded to earlier in the chapter. It lies in the fact that the nonlinear stress-strain curve of the model material causes a change in geometry to produce a different effect in the model family than it does in the product family.

The source of the ESM error can be understood more clearly by plotting the location of maximum stress for each geometric shape, as shown in Figure 27.

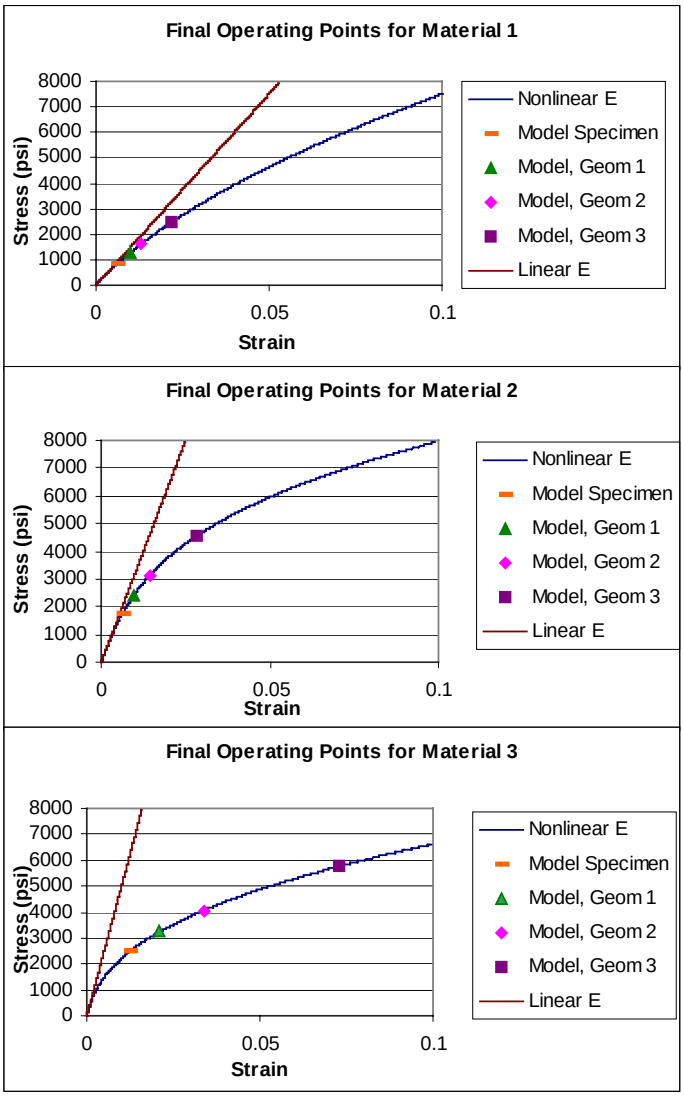

Figure 27. Maximum Stress Resulting from Different Geometries.

Notice that as the holes get bigger, the maximum stress (which occurs at the stress concentration around the first hole) increases. As the maximum stress increases, the model material behaves in a more flexible manner (i.e. the effective value of Young's modulus decreases) while the product material remains the same (with a constant value of Young's modulus). Since the material behavior is dependent on geometric shape, the ESM assumption is violated and specimen distortion is introduced into the ESM approach.

3.2.2. ESM Study 2: Distortion of Beam Length

The second ESM study investigates the effect of distorting one of the physical dimensions of the system. In this case the *length* of the model and the model specimen is distorted (equally, of course), and the effect of the distortion on TSM and ESM results is evaluated. The setup for the study is shown in Figure 28.

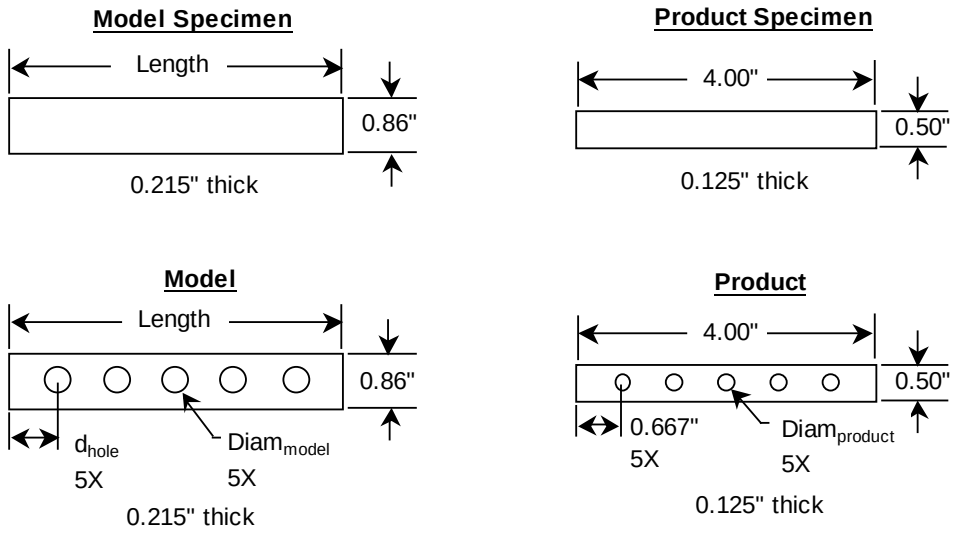

Figure 28. Setup for ESM Study 2.

Table 12. Length Values for ESM Study 2.

	Length (in)	**d_{hole} (in)**	**Distortion (%)**
Length 1	4.00	0.667	-41.9
Length 2	6.88	1.147	0.00
Length 3	8.00	1.333	16.3
Length 4	12.0	2.000	74.4
Length 5	16.0	2.666	133

The setup for this study is very similar to that of the previous study except that, in this case, the material properties are well-scaled (with constant values for Young's modulus of 10,150 ksi for the product family and 320 ksi for the model family) and the model distortion comes from length changes in the model family. Five different values of length are considered, as shown in Table 12.

Note that the second length shown in Table 12 corresponds to a well-scaled system, and we would expect no error in either the TSM or the ESM results. The first length value represents a model beam that is "too short," and the last three length values represent model beams that are "too long." The degree of model distortion that corresponds to each length can be quantified by calculating the percent change in length with respect to the well-scaled value. In other words,

$$distort_L = \frac{L_i - L_{WS}}{L_{WS}} * 100, \quad i = 1,2,3,4,5 \tag{3-8}$$

where $distort_L$ is the amount of distortion in length, L_i is the length of each beam, and L_{WS} is the length of the well-scaled beam. The calculated values of length distortion, as described by equation 3-8, are included in Table 12. According to

ESM theory, the effects of the distortion in beam length should be captured with the simplified specimen pair.

As with the last study, three different geometric shapes (resulting from different hole sizes) are considered for the model and the product. The hole sizes for the three geometric cases are listed in Table 9.

A total of fifteen different cases have now been defined for this study (three different geometric cases for each of the five levels of length distortion). The goal of the study is once again to determine the influence of changes in geometric shape and changes in model distortion on TSM and ESM results. The procedures for carrying out the study, and for calculating TSM and ESM errors, are the same as those used in the previous study. Results of the study, which include prediction errors from the TSM, ESM pseudo-inverse (*pi*), and ESM circulant matrix (*cir*) approaches, are shown in Table 13.

A review of Table 13 shows that, for any given length, ESM prediction errors increase as the change in geometric shape increases (TSM errors decrease slightly as changes in geometric shape increase, for a reason that will be explained later in this section). Also, for any given geometric shape, prediction errors increase as the degree of distortion in beam length increases. The ESM in each case produces significantly more accurate results than the TSM, especially as the degree of model distortion increases (except for the numerical “noise” in the well-scaled case).

Table 13. Average Errors for ESM Study 2.

	Geometry 1		Geometry 2		Geometry 3	
Length 1	TSM	79.0%	TSM	77.0 %	TSM	74.6 %
	ESM_{pi}	6.58 %	ESM_{pi}	16.7 %	ESM_{pi}	28.8 %
	ESM_{cir}	6.61 %	ESM_{cir}	16.8 %	ESM_{cir}	29.1 %
Length 2	TSM	0.07 %	TSM	0.04 %	TSM	0.20 %
	ESM_{pi}	0.09 %	ESM_{pi}	0.42 %	ESM_{pi}	1.51 %
	ESM_{cir}	0.09 %	ESM_{cir}	0.05 %	ESM_{cir}	0.18 %
Length 3	TSM	54.5 %	TSM	51.2 %	TSM	45.2 %
	ESM_{pi}	1.43 %	ESM_{pi}	3.87 %	ESM_{pi}	8.59 %
	ESM_{cir}	1.28 %	ESM_{cir}	3.41 %	ESM_{cir}	7.24 %
Length 4	TSM	387 %	TSM	351 %	TSM	295 %
	ESM_{pi}	4.48 %	ESM_{pi}	12.2 %	ESM_{pi}	24.6 %
	ESM_{cir}	4.14 %	ESM_{cir}	11.2 %	ESM_{cir}	22.2 %
Length 5	TSM	946 %	TSM	838 %	TSM	674 %
	ESM_{pi}	6.20 %	ESM_{pi}	16.7 %	ESM_{pi}	33.0 %
	ESM_{cir}	5.71 %	ESM_{cir}	15.3 %	ESM_{cir}	30.1 %

Figure 29 contains a plot of ESM_{cir} error as a function of length distortion. We see from the plot that prediction error tends to increase as the degree of distortion increases *and* as the change in geometric shape increases. This result again indicates a coupling between geometric shape and material behavior, which violates the ESM assumptions and results in errors.

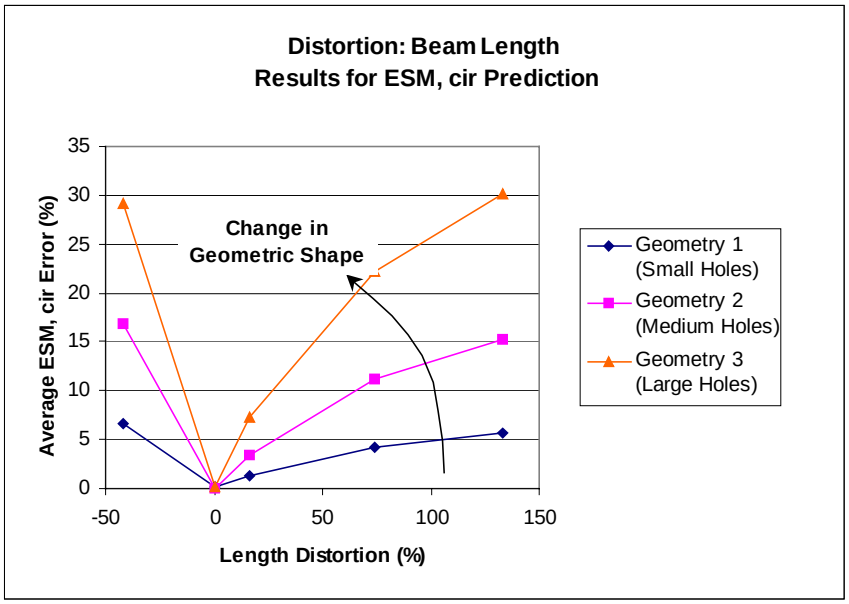

Figure 29. Plot of Average Errors for ESM Study 2.

The cause of the ESM prediction error in this study lies in the fact that differences in the *geometric configuration* of the model and the model specimen cause the material to behave differently in each case. The large deflection effects, which cause different geometric configuration in the model and the model specimen, can be represented by the nonlinear curve shown in Figure 30.

The vertical axis in Figure 30 represents deflection of the beam for a given load, while the horizontal axis represents changes in geometric shape or material properties. The dashed horizontal line represents the maximum deflection of the beam (the point where the beam becomes completely vertical). Note that the actual deflection of the beam approaches this theoretical maximum in an asymptotic fashion (which results in a much steeper slope at the start of the curve than at the end). Suppose that point A represents the product specimen. By

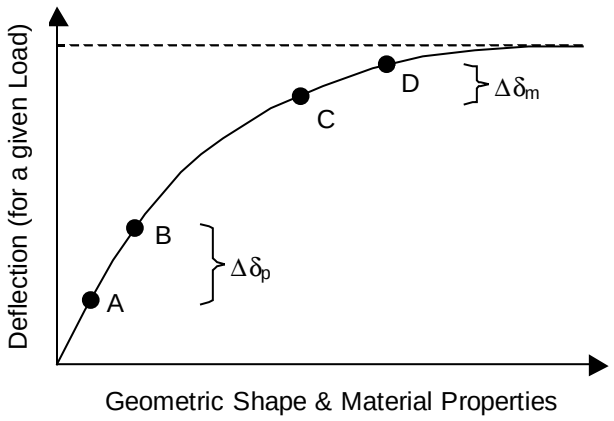

Figure 30. Large Deflection Phenomenon.

changing the geometry of the product specimen (e.g. adding holes for the product beam, represented by point B), the deflection of the beam increases by some $\Delta\delta_p$ for the same applied load. Now suppose that point C represents the model specimen, which, because of its distorted length, has a much larger deflection than the corresponding product specimen. By making the same geometric changes to the model specimen as was done to the product specimen (e.g. adding holes for the model beam, represented by point D), the deflection of the model beam increases by some $\Delta\delta_m$ for the same applied load. Because the initial geometric configuration of the model beam (large deflection) is different than that of the product beam (small deflection), the same change in beam geometry produces a different increase in deflection in the model and product systems (in this case $\Delta\delta_m < \Delta\delta_p$). This difference in material behavior between the model system and the product system is the source of the specimen distortion and the cause of the ESM error.

One more clarification is in order before we move on to the final study. The actual deflection of the model beams whose lengths are "too long" are much larger than they would have been had they been properly scaled. For this reason the TSM "over-predicts" the deflection of the corresponding product beams. As the holes in the product and model beams grow larger, the resultant increase in deflection is larger in the product beam than in the (already highly-deflected) model beam because of the large deflection phenomenon just described. The relatively larger increase in the deflection of the product beam actually causes a reduction in the TSM error (since the TSM "overshoots" on its predicted deflection of the product beam). This is the reason that, for a given length, the TSM error shown in Table 13 tends to decrease with increased hole sizes. This decrease in the TSM error is of little consolation, however, since the error is still extremely high for highly distorted beams.

3.2.3. ESM Study 3: Distortion in Material Structure

The final study in this section involves different material structures in the product and model families. The product family exhibits isotropic material properties, while the model family exhibits a form of orthotropy known as *transverse isotropy*. A material that has a transverse isotropic structure has a plane of isotropy at every point in the material [ABAQUS, 2001]. To clarify the differences in material structure, consider a beam with three orthogonal coordinates, as shown in Figure 31. An isotropic material is characterized by $E_1 = E_2 = E_3$; an orthotropic material is characterized by $E_1 \neq E_2 \neq E_3$; a transverse isotropic material is characterized by $E_1 = E_2 \neq E_3$.

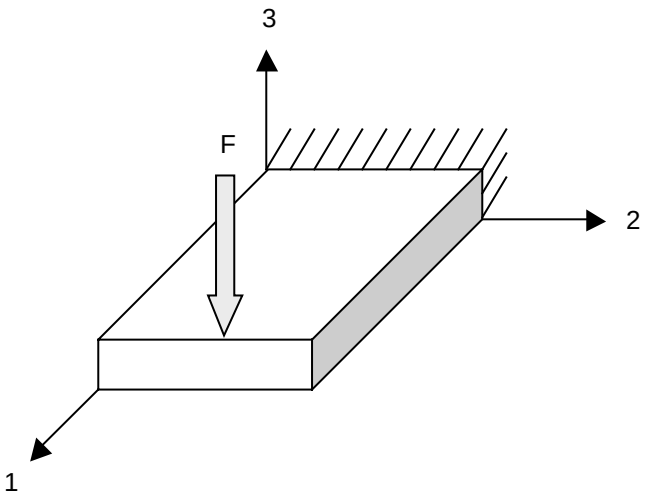

Figure 31. Coordinates for Cantilever Beam.

The distortion in this case comes from variations in the out-of-plane shear modulus of the beam (direction "3" in Figure 31). The study involves changing the degree of distortion in the shear modulus and evaluating the effect on the ESM prediction accuracy. The material properties for both the model and product beams are shown in Table 14. Note that, since the cantilever beam is modeled under plane stress assumptions using shell elements, the out-of-plane tensile modulus parameters (E_3, ν_{13}, ν_{23}) are not relevant and need not be specified. However, the out-of-plane shear modulus values (G_{13} and G_{23}) must be specified in order to account for transverse shear deformation in the shell elements [ABAQUS, 2001].

As in the previous studies, the properties of the product beam are held constant while the properties of the model beam change from case to case. Note that the values of shear modulus in the product beam correspond to an isotropic

Table 14. Material Properties for ESM Study 3.

		Model				
Parameter	**Product**	**Case A**	**Case B**	**Case C**	**Case D**	**Case E**
E_1 (ksi)	10,150	320	320	320	320	320
E_2 (ksi)	10,150	320	320	320	320	320
ν_{12}	0.3	0.3	0.3	0.3	0.3	0.3
G_{12} (ksi)	3904	123	123	123	123	123
G_{13} (ksi)	3904	500	250	123	50	5
G_{23} (ksi)	3904	500	250	123	50	5
Model Distortion (%)		307	103	0	-59	-96

material in which G = E / (2 (1 + ν)). Note also that the values of shear modulus are well scaled for Case C of the model beam. Case A and Case B represent situations in which the model beam is "too stiff" in shear, and Case D and Case E represent situations in which the model beam is "too flexible" in shear. The degree of distortion caused by changes in the out-of-plane shear modulus can be quantified as a percent deviation from the well-scaled value, as follows:

$$distort_{G,OP} = \frac{G_{OP,i} - G_{OP,WS}}{G_{OP,WS}} * 100, \quad i = A, B, C, D, E \tag{3-9}$$

where $distort_{G,OP}$ is the distortion in the out-of-plane shear modulus, $G_{OP,i}$ is the out-of-plane shear modulus for each case, and $G_{OP,WS}$ is the well-scaled value of out-of-plane shear modulus. The degree of model distortion for each case, as described by equation 3-9, is included in Table 14.

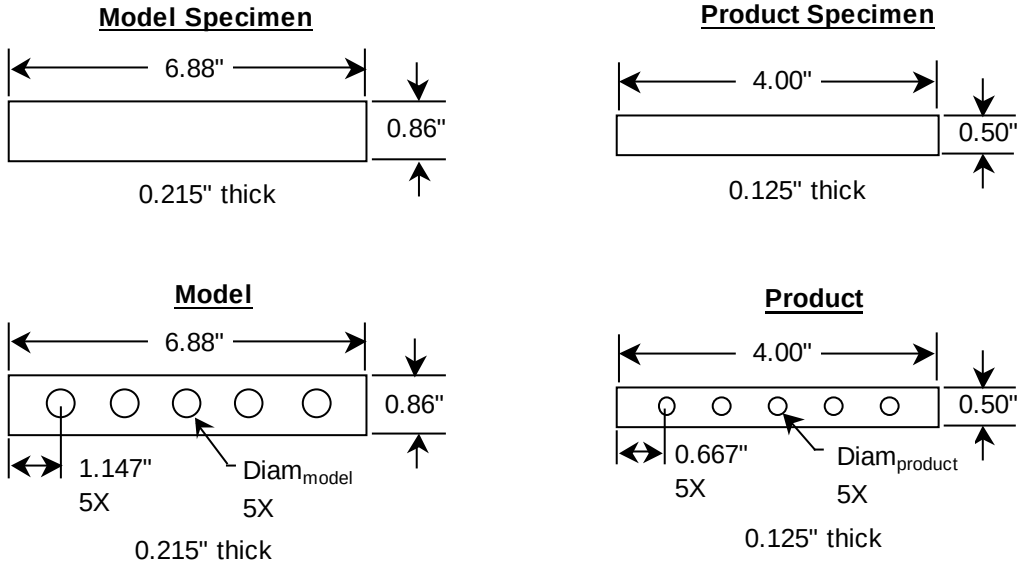

Figure 32. Beam Dimensions for ESM Study 3.

The dimensions of the beam used in this study are shown in Figure 32. The same three geometric cases, which correspond to three different hole sizes in the product and model beams (as shown in Table 9), are considered in this study. A total of fifteen different cases (three different geometric cases for each of the five levels of model distortion) are evaluated. The procedure for carrying out the study is the same as that used in the previous two studies.

The average errors that result from the TSM, ESM pseudo-inverse (*pi*), and ESM circulant matrix (*cir*) approaches are listed in Table 15. A review of the table shows that, for any particular case, average errors increase as the change in geometric shape increases (except for the "numerical noise" in Case C). Also, for any particular geometric shape, average errors tend to decrease from Case A to Case C and then increase again from Case C to Case E. In other words, Case C (in

Table 15. Average Errors for ESM Study 3.

	Geometry 1		Geometry 2		Geometry 3	
Case A	TSM	0.77 %	TSM	1.57 %	TSM	3.20 %
	ESM_{pi}	0.58 %	ESM_{pi}	1.60 %	ESM_{pi}	3.85 %
	ESM_{cir}	0.49 %	ESM_{cir}	1.30 %	ESM_{cir}	2.93 %
Case B	TSM	0.31 %	TSM	0.74 %	TSM	1.93 %
	ESM_{pi}	0.24 %	ESM_{pi}	0.90 %	ESM_{pi}	2.73 %
	ESM_{cir}	0.16 %	ESM_{cir}	0.59 %	ESM_{cir}	1.77 %
Case C	TSM	0.29 %	TSM	0.39 %	TSM	0.01 %
	ESM_{pi}	0.19 %	ESM_{pi}	0.34 %	ESM_{pi}	1.42 %
	ESM_{cir}	0.29 %	ESM_{cir}	0.38 %	ESM_{cir}	0.02 %
Case D	TSM	1.26 %	TSM	2.42 %	TSM	3.79 %
	ESM_{pi}	0.87 %	ESM_{pi}	1.77 %	ESM_{pi}	2.13 %
	ESM_{cir}	0.97 %	ESM_{cir}	2.13 %	ESM_{cir}	3.50 %
Case E	TSM	5.09 %	TSM	10.61 %	TSM	18.81 %
	ESM_{pi}	2.54 %	ESM_{pi}	7.56 %	ESM_{pi}	14.36 %
	ESM_{cir}	2.66 %	ESM_{cir}	8.05 %	ESM_{cir}	16.06 %

which the shear modulus is well scaled) shows the smallest average error. A plot of the average ESM error (as obtained through the circulant matrix approach) as a function of model distortion is shown in Figure 33. The form of the plot is similar to those of the previous two studies with the average error increasing with both increased model distortion and increased changes in geometric shape.

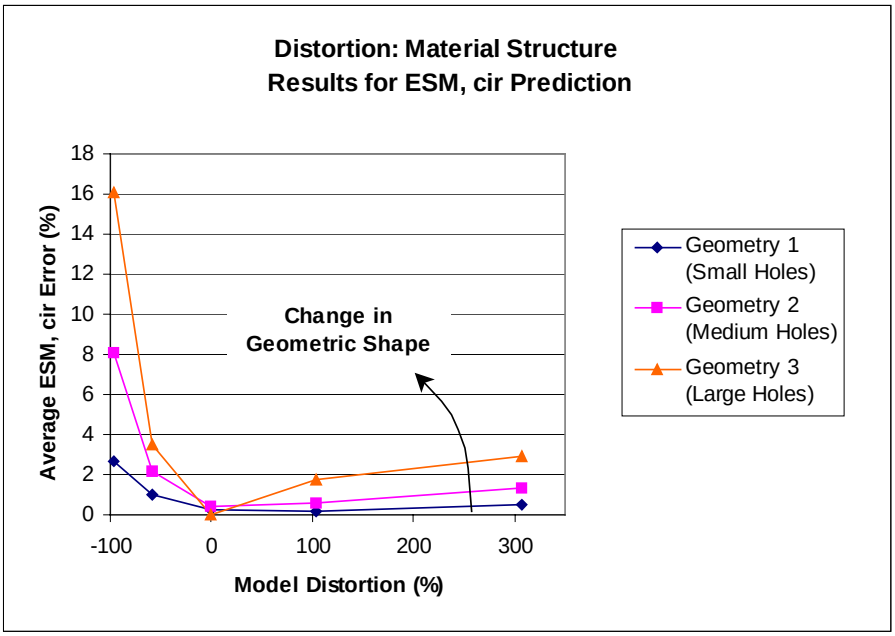

Figure 33. Plot of Average Error for ESM Study 3.

The source of the ESM prediction errors for this study can be found in the fact that beam deflection is a function of tensile modulus *and* shear modulus, as described by the following equation [see Timoshenko, 1970]:

$$\delta = \frac{FL^3}{3EI} + \frac{FLh^2}{8GI} \qquad (3\text{-}10)$$

The second term on the right hand side of equation 3-10 represents deflection of the beam due to shear stresses. As the geometric shape of the beam changes (as from the model specimen to the model) the amount of deflection due to shear also changes. Since the deflection due to shear varies with shear modulus, the *contribution of deflection due to shear* becomes different in the model family than in the product family as the value of shear modulus deviates from its well-scaled value. The difference in this contribution of deflection due to shear is the source

of the specimen distortion and the errors in the ESM approach. This type of situation, in which system behavior is inherently a function of both material properties and geometric shape, is classified in the "functionally coupled parameters" category of the specimen distortion structure shown in Figure 23.

Figure 33 shows that the ESM error is relatively insensitive to distortion in shear modulus, except when those distortions become extremely small. This insensitivity is due to the fact that deflection due to shear is a relatively small percentage of overall deflection, especially when the height of the beam is small. Although the sensitivity of ESM error to model distortion is smaller in this study than in the previous two studies, the trend of increased errors with increased model distortion and with increased changes in geometric shape is the same.

It should be noted that, although Figure 33 shows the absolute error increasing for both positive and negative system distortion, the "direction of error" is different in these two cases. For those cases in which the system distortion is defined as negative (when the shear modulus is "too low" and the beams are too flexible in shear), the predictions of the similitude methods are too high. Likewise, for those cases in which the system distortion is defined as positive (when the shear modulus is "too high" and the beams are too stiff in shear), the predictions made with the similitude methods are too low.

It is also interesting to note that the improvement of the ESM over the TSM is not as significant as in the previous two studies. This result indicates that the specimen distortion is relatively high in this case (the specimen pair fails to capture a significant portion of the model distortion). Since the effect of the model

distortion on system behavior is relatively small, however, the overall ESM error remains small as well.

3.3. NOTES ON STUDY FINDINGS

Several comments about the studies in this chapter are now presented as points of clarification and discussion. These comments are presented as notes in the following paragraphs.

Note 1: The studies presented in this chapter simply serve as illustrations that specimen distortions *can* cause the ESM to produce inaccurate predictions of product performance. In no way does this result imply that specimen distortions always exist. There are many situations in which the ESM can effectively resolve model distortions with little or no error caused by specimen distortions.

Suppose, for example, that we have a model with a nonlinear stress-strain curve and a product with a linear stress-strain curve, similar to the ESM Study 1. Now suppose that the simplified geometry for the specimen pair does not increase the maximum stress in the deflected beam (see, for example, Figure 34). The change in geometry between the model and model specimen will not cause a

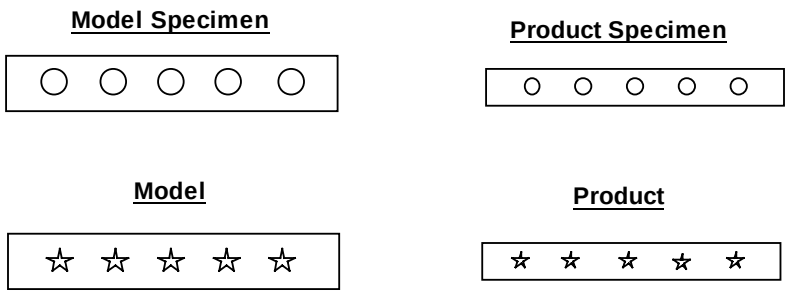

Figure 34. Specimens with Similar Operating Stresses.

change in how the material behaves since both will be operating at the same point on the nonlinear stress-strain curve. Consequently, no specimen distortion will occur, and the ESM will give accurate predictions of product performance.

Note 2: The plots of ESM prediction error as a function of model distortion that are presented for the three ESM studies show a resemblance to the Taguchi loss function. The Taguchi loss function expresses the idea that, in product design, there is an increased loss in overall quality that comes with increased variation from the nominal functional performance of the product. The concept of the Taguchi loss function is shown in Figure 35. By labeling the vertical axis as "ESM Prediction Error" and the horizontal axis as "Model Distortion," we can represent the error in ESM predictions as a function of model distortion with a loss function similar to that shown in Figure 35. The shape of the function will depend on the change in geometric shape between the model and model specimen, as was illustrated in the three ESM studies presented earlier in this chapter. The error in the TSM predictions can also be modeled with a similar

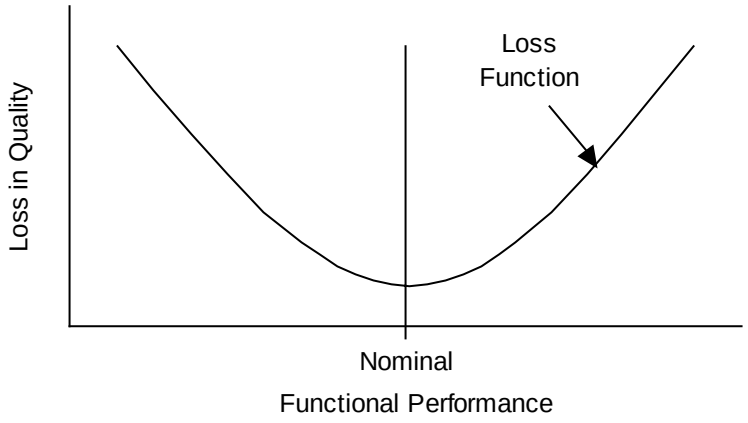

Figure 35. Quality Loss Function [Adapted from DeVor, 1992].

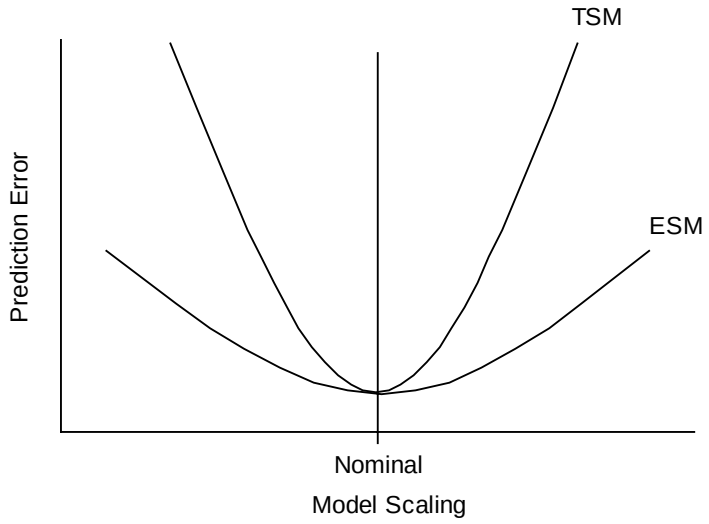

Figure 36. TSM and ESM Loss Functions.

loss function. Since the TSM error is larger than the ESM error (at least for the studies presented in this chapter), the slope of the TSM loss function is greater than that for the ESM loss function, as illustrated in Figure 36.

The interpretation of the ESM loss function is that, for cases in which specimen distortion exists, the error in the ESM prediction can be minimized by scaling the model as closely as possible to the nominal values (as given by the TSM). In addition, since the shape of the loss function depends on the degree of change in geometric shape between the model or product and the respective specimen, the error in the ESM prediction can be reduced by minimizing the change in geometric shape for the specimen pair. The interpretation of the TSM loss function is obvious: error in TSM predictions can be minimized by reducing model distortions.

Note 3: The ESM pseudo-inverse and circulant matrix approaches produce similar, but not identical, results. The error in the circulant matrix approach is less than that for the pseudo-inverse approach in the majority of cases in the three ESM studies presented in this chapter. However, there is no indication as to which method is better for a particular situation. Differences in the various approaches for creating the *S* and *F* transformation matrices are discussed in the following chapter.

Having established the limitations of the current ESM technique, we must now look for an enhanced approach that will correct or compensate for those limitations. Such an enhanced approach to the ESM is presented in the following chapter.

CHAPTER 4

Advanced Empirical Similitude Method

Limitations in the current ESM approach have been established by identifying sources of specimen distortion that cause ESM assumptions to be violated. Several examples in Chapter 3 serve to illustrate the effect of various types of specimen distortion in terms of ESM prediction errors. Our attention now turns to the development of an advanced similitude technique that extends the range of ESM application, as illustrated in Figure 37.

Before presenting the advanced similitude technique, it is important to determine, if possible, the most appropriate method of constructing the ESM transformation matrices. As discussed in the previous chapter, the standard methods of constructing transformation matrices, namely the pseudo-inverse approach and the circulant matrix approach, do not yield identical results. The

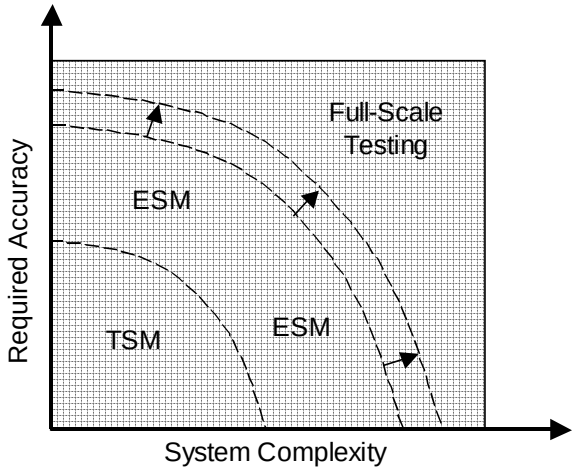

Figure 37. Extension of ESM Boundary.

following sections evaluate the pseudo-inverse and circulant matrix techniques, and present an alternative approach to constructing the transformation matrices.

4.1. CREATION OF TRANSFORMATION MATRICES

Three methods of creating transformation matrices for the ESM are presented below. The three methods include the pseudo-inverse approach, the diagonal matrix approach, and the circulant matrix approach. The purpose of this section is to enhance our understanding of each method and provide guidance as to which method is most appropriate in various circumstances.

4.1.1. Pseudo-inverse

The need for a pseudo-inverse of a matrix arises when one seeks to invert a rectangular matrix. Recall that a "true" inverse is only defined for square matrices. The ESM presents a need for a pseudo-inverse since the state vector of the model specimen, which is rectangular in general, must be inverted in order to derive either of the transformation matrices (**S** or **F**).

A matrix **X** is said to be a *generalized inverse* of a matrix **B** if it satisfies one or more of the following properties [Usmani, 1987]:

$$\begin{aligned} \mathbf{B\,X\,B} &= \mathbf{B} \\ \mathbf{X\,B\,X} &= \mathbf{X} \\ \mathbf{(B\,X)}^{H} &= \mathbf{B\,X} \\ \mathbf{(X\,B)}^{H} &= \mathbf{X\,B} \end{aligned} \tag{4-1}$$

The notation $(\mathbf{B\,X})^{H}$ in Eqn. 4-1 represents the conjugate transpose of the matrix product (**B X**). If the entries in **B** and **X** are real (which we will assume in the

discussion that follows), the simple transpose $(\mathbf{B}\ \mathbf{X})^{T}$ can be used in place of the conjugate transpose $(\mathbf{B}\ \mathbf{X})^{H}$. The matrix **X** is said to be a *Moore-Penrose generalized inverse* of **B** if it satisfies all four conditions of Eqn. 4-1 [Usmani, 1987]. We refer to the Moore-Penrose generalized inverse of **B** as the *pseudo-inverse* of **B** and represent it as $\mathbf{B}^{+}$.

In order to direct our development of the pseudo-inverse, consider a system of equations **Ax = b** that has the following form:

$$\begin{bmatrix} a_{11} & a_{12} \\ a_{21} & a_{22} \\ a_{31} & a_{32} \end{bmatrix} \begin{bmatrix} x_1 \\ x_2 \end{bmatrix} = \begin{bmatrix} b_1 \\ b_2 \\ b_3 \end{bmatrix} \tag{4-2}$$

Since the number of equations (i.e. the number of rows in **A**) is greater than the number of unknowns (i.e. the number columns in **A**), the system of equations is said to be *inconsistent* and will likely not have a unique solution. In order to envision why the system of equations is inconsistent, consider the system as a single vector equation where each column in **A** represents a vector, and the unknown variables (x_1 and x_2) represent the coefficients that are required for the summation of the column vectors to equal the vector **b**. In other words,

$$x_1 \begin{bmatrix} a_{11} \\ a_{21} \\ a_{31} \end{bmatrix} + x_2 \begin{bmatrix} a_{12} \\ a_{22} \\ a_{32} \end{bmatrix} = \begin{bmatrix} b_1 \\ b_2 \\ b_3 \end{bmatrix} \tag{4-3}$$

The two column vectors of **A** define a plane in three-dimensional space that is known as the *column space* of **A** [Strang, 1988]. The system of equations described by Eqn. 4-3 is illustrated graphically in Figure 38. As shown in Figure

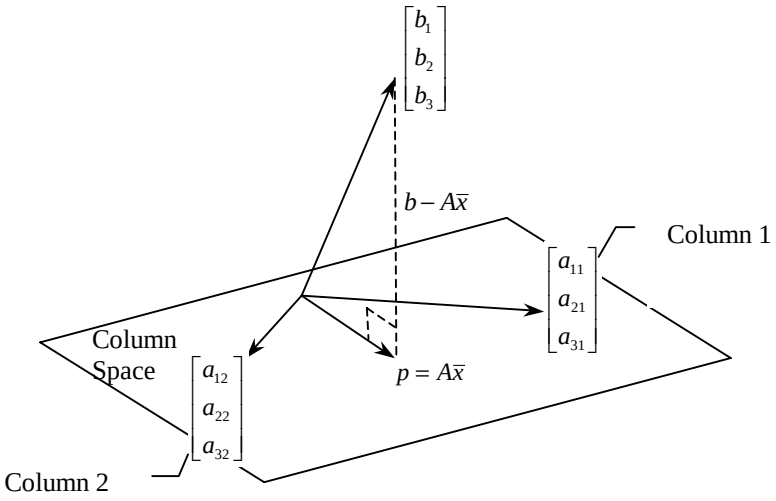

Figure 38. Inconsistent System of Equations, adapted from [Strang, 1988].

38, the vector **b** will not, in general, lie within the column space of **A**. When **b** does not lie in the column space of **A**, it is impossible to find values of x_1 and x_2 that will produce the proper combination of the column vectors of **A** to equal vector **b**. The best we can do, then, is to find the values $\bar{x}_1$ and $\bar{x}_2$ that produce the vector **p** (which lies within the column space of **A**) that comes *as close as possible* to the vector **b**. In linear algebra terms, the vector **p** represents the projection of **b** onto the column space of **A**.

In order to determine the values of $\bar{x}_1$ and $\bar{x}_2$ that produce the vector **p**, we notice that the error vector (which is labeled as $b - A\bar{x}$ in Figure 38) must be as short as possible. From geometry we know that the shortest distance from the tip of vector **b** to the column space of **A** is *perpendicular* to the column space of **A**. For the error vector to be perpendicular to the column space of **A** requires that it be perpendicular to every column in **A**. If we recall from linear algebra that the

inner product of two vectors **x** and **y** (calculated as $\mathbf{x}^T\mathbf{y}$) is zero when the vectors are perpendicular to each other, we can write the perpendicularity requirement for the error vector as follows:

$$\begin{aligned} A_1^T(b - A\bar{x}) &= 0 \\ A_2^T(b - A\bar{x}) &= 0 \end{aligned} \tag{4-4}$$

where $\mathbf{A}_1$ and $\mathbf{A}_2$ represent the first and second column vectors of **A**, respectively. Equation 4-4 can be written equivalently as

$$A^T(b - A\bar{x}) = 0 \tag{4-5}$$

or as

$$A^T A\bar{x} = A^T b\,. \tag{4-6}$$

Equation 4-6, which is known as a *normal equation*, is equivalent to multiplying both sides of the original equation $\boldsymbol{Ax = b}$ by $\mathbf{A}^T$. The product $\mathbf{A}^T\mathbf{A}$ in Eqn. 4-6 is a square matrix whose inverse $(\mathbf{A}^T\mathbf{A})^{-1}$ can be readily calculated (provided that none of the columns are linearly dependent). Multiplying both sides of Eqn. 4-6 by $(\mathbf{A}^T\mathbf{A})^{-1}$ gives

$$(A^T A)^{-1}(A^T A)\bar{x} = (A^T A)^{-1}A^T b \tag{4-7}$$

which is equivalent to

$$I\,\bar{x} = (A^T A)^{-1}A^T b \tag{4-8}$$

where I is the identity matrix. Equation 4-8 simplifies to

$$\bar{x} = (A^T A)^{-1}A^T b\,. \tag{4-9}$$

The quantity $(\mathbf{A}^T\mathbf{A})^{-1}\mathbf{A}^T$ in Eqn. 4-9 is defined as the *pseudo-inverse* of **A**. As shown in the development of Eqn. 4-9, the pseudo-inverse represents the optimal solution to an inconsistent system of equations. The solution to Eqn. 4-9 is often referred to as the *least squares* solution to the system of equations.

Now suppose that the original system of equations is of the form

$$\begin{bmatrix} a_{11} & a_{12} & a_{13} \\ a_{21} & a_{22} & a_{23} \end{bmatrix} \begin{bmatrix} x_1 \\ x_2 \\ x_3 \end{bmatrix} = \begin{bmatrix} b_1 \\ b_2 \end{bmatrix}. \tag{4-10}$$

In this case there are more unknowns (i.e. number of columns of **A**) then there are equations (i.e. number of rows of **A**). Unlike the inconsistent set of equations discussed previously, not only will this system *have* a solution, but it will have *infinitely many* solutions. In other words, the solution to this system is not unique.

The type of system represented by Eqn. 4-10 is referred to as *over determined*. In order to envision why Eqn. 4-10 is over determined, again consider the system of equations as a single vector equation given by

$$x_1 \begin{bmatrix} a_{11} \\ a_{21} \end{bmatrix} + x_2 \begin{bmatrix} a_{12} \\ a_{22} \end{bmatrix} + x_3 \begin{bmatrix} a_{13} \\ a_{23} \end{bmatrix} = \begin{bmatrix} b_1 \\ b_2 \end{bmatrix}. \tag{4-11}$$

Since each column vector of **A** has a dimension of 2, all of the vectors lie in a single plane. The system in Eqn. 4-11 is represented graphically in Figure 39. Note that, in a plane, three independent column vectors are not necessary to describe the vector b – any two would suffice. Since there is an "extra" column vector, there are an infinite number of combinations of the column vectors of **A** that will produce the vector **b**.

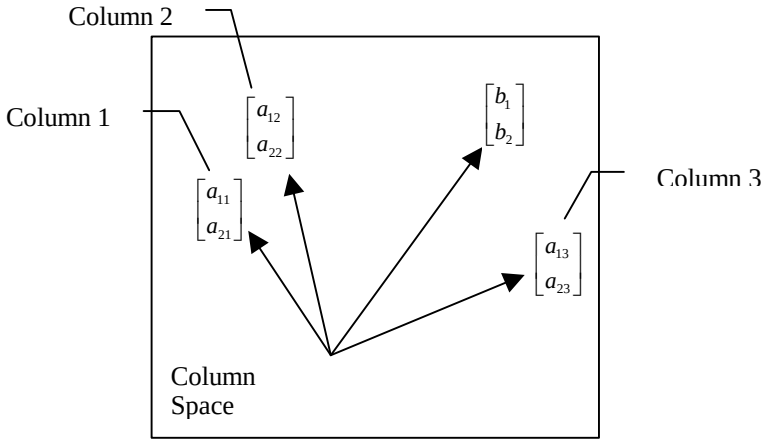

Figure 39. Over Determined System of Equations.

As a simple example of the infinite number of solutions that are possible with an over determined system, suppose that the system of equations contains the following values:

$$\begin{bmatrix} 1 & 0 & 1 \\ 0 & 1 & 1 \end{bmatrix} \begin{bmatrix} x_1 \\ x_2 \\ x_3 \end{bmatrix} = \begin{bmatrix} 2 \\ 2 \end{bmatrix}. \qquad (4\text{-}12)$$

Solutions to Eqn. 4-12 include

$$\begin{bmatrix} x_1 \\ x_2 \\ x_3 \end{bmatrix} = \left\langle \begin{bmatrix} 1 \\ 1 \\ 1 \end{bmatrix}, \begin{bmatrix} 2 \\ 2 \\ 0 \end{bmatrix}, \begin{bmatrix} 0 \\ 2 \\ 2 \end{bmatrix}, \begin{bmatrix} -1 \\ -1 \\ 3 \end{bmatrix}, \begin{bmatrix} -2 \\ -2 \\ 4 \end{bmatrix}, \begin{bmatrix} 2/3 \\ 2/3 \\ 4/3 \end{bmatrix}, \cdots \right\rangle \qquad (4\text{-}13)$$

along with an infinite number of additional solutions. The condition illustrated by Eqn. 4-13 is typical of over determined systems in which the number of unknowns is larger than the number of equations.

The pseudo-inverse technique, which is used to find the least squares solution to an inconsistent system of equations, can also be applied to an over determined system (both situations involve rectangular matrices for which no "true" inverse can be calculated). The same formula for the pseudo-inverse, as contained in Eqn. 4-9, can be applied in either situation. We should note, however, that there is a slight difference in the interpretation of the results, depending on whether the system is inconsistent or over determined. When the system is inconsistent, we can argue that the result from the pseudo-inverse approach is the "best" result since it comes as close to the actual solution as possible. When the system is over determined, however, it is more difficult to say that the result from the pseudo-inverse approach is the "best" solution since there are many solutions that satisfy the system of equations exactly. (The last result shown in Eqn. 4-13 is obtained with the pseudo-inverse approach; can we argue that it is "better" than any of the other solutions in Eqn. 4-13?) We can, however, still refer to the pseudo-inverse result as the *least squares* solution since it is obtained through the use of the normal equations described in Eqn. 4-6. We can think of the least squares solution as "normalizing" the contributions of the (too many) column vectors of **A**. This normalizing effect can be seen in the least squares solution in Eqn. 4-13.

We now examine how the pseudo-inverse technique is applied to the ESM. The ESM is based on the idea that transformation matrices can be extracted from measured system states, according to the following equations:

$$\begin{aligned} \boldsymbol{x}_{ps} &= \boldsymbol{S}\, \boldsymbol{x}_{ms} \\ \boldsymbol{x}_{m} &= \boldsymbol{F}\, \boldsymbol{x}_{ms} \end{aligned} \qquad (4\text{-}14)$$

Once the transformation matrices are computed (at least one of them), the state of the product can be predicted through one of the following equations:

$$\begin{aligned} \boldsymbol{x_p} &= \boldsymbol{S}\, \boldsymbol{x_m} \\ \boldsymbol{x_p} &= \boldsymbol{F}\, \boldsymbol{x_{ps}} \end{aligned} \qquad (4\text{-}15)$$

Let's suppose that we want to derive the scale transformation matrix **S** from the first of Eqns. 4-14, and that the state vectors are of length *n*. At first glance, use of the pseudo-inverse may seem unnecessary since the *n* by *n* matrix **S** in the system of equations $\boldsymbol{S x_{ms}} = \boldsymbol{x_{ps}}$ is a *square matrix*. However, our approach to solving this system of equations is slightly different than that used in deriving the pseudo-inverse; instead of being given **S** and $\mathbf{x_{ps}}$ and solving for $\mathbf{x_{ms}}$, we are given $\mathbf{x_{ms}}$ and $\mathbf{x_{ps}}$ and must solve for **S**. Since **S** is, in general, a fully populated matrix with n^2 unknowns, and the system only has *n* equations, we are faced with an over determined system of equations (more unknowns than equations). Since there are infinitely many solutions to an over determined system of equations, we know that *there is no unique solution for the transformation matrix* ***S*** (or **F**, for that matter).

One way to derive the matrix **S** is to use the least squares approach, as presented earlier in this section. Since $\mathbf{x_{ms}}$ is not square, we cannot solve for **S** by calculating $\boldsymbol{S} = \boldsymbol{x_{ps}}\, \boldsymbol{x_{ms}}^{-1}$; instead we must resort to the pseudo-inverse and solve for **S** by calculating $\boldsymbol{S} = \boldsymbol{x_{ps}}\, \boldsymbol{x_{ms}}^{+}$, where $\boldsymbol{x_{ms}}^{+}$ is given as follows:

$$x_{ms}^{+} = (x_{ms}^{T} x_{ms})^{-1} x_{ms}^{T}. \qquad (4\text{-}16)$$

The transformation matrix **S** calculated in this way represents the least squares solution to the system $\boldsymbol{S x_{ms}} = \boldsymbol{x_{ps}}$. We see later in this chapter that other solutions

to **S** are indeed possible; the least squares approach is, however, a consistent method for calculating the transformation matrices.

Extensions to the least squares approach have been suggested by [Cho, 1999]. If, for example, we assume that the system behavior follows a 1st order polynomial, we can represent the system states as 1st order polynomials rather than as single points. Under this assumption, a 3 x 3 system $\boldsymbol{x_{ps} = S x_{ms}}$ is represented as

$$\begin{bmatrix} 1 & x_{ps,1} \\ 1 & x_{ps,2} \\ 1 & x_{ps,3} \end{bmatrix} = \begin{bmatrix} s_{11} & s_{12} & s_{13} \\ s_{21} & s_{22} & s_{23} \\ s_{31} & s_{32} & s_{33} \end{bmatrix} \begin{bmatrix} 1 & x_{ms,1} \\ 1 & x_{ms,2} \\ 1 & x_{ms,3} \end{bmatrix}. \qquad (4\text{-}17)$$

If we assume the system behavior follows a 2nd order polynomial, the system of equations is represented as

$$\begin{bmatrix} 1 & x_{ps,1} & x_{ps,1}^{\,2} \\ 1 & x_{ps,2} & x_{ps,2}^{\,2} \\ 1 & x_{ps,3} & x_{ps,3}^{\,2} \end{bmatrix} = \begin{bmatrix} s_{11} & s_{12} & s_{13} \\ s_{21} & s_{22} & s_{23} \\ s_{31} & s_{32} & s_{33} \end{bmatrix} \begin{bmatrix} 1 & x_{ms,1} & x_{ms,1}^{\,2} \\ 1 & x_{ms,2} & x_{ms,2}^{\,2} \\ 1 & x_{ms,3} & x_{ms,3}^{\,2} \end{bmatrix} \qquad (4\text{-}18)$$

and so forth. In each case the pseudo-inverse technique can be used to derive the least squares solution to the system of equations. Further discussion on the use of polynomials in connection with ESM transformation matrices is provided by [Wood, 2002].

Although the pseudo-inverse technique provides a consistent way of calculating the ESM transformation matrices, the matrices that are derived in this way fail to satisfy one of the core assumptions of the ESM: **SF** = **FS**. Figure 22 in

Chapter 3 shows that the two paths for predicting the state of the product should be identical (i.e. assuming that **S** = **S'** and **F** = **F'**, $\mathbf{x_p} = \mathbf{SFx_{ms}}$ and $\mathbf{x_p} = \mathbf{FSx_{ms}}$; therefore **SF** must equal **FS**). Since matrix multiplication is not commutative in general (**SF** ≠ **FS**), this assumption of the ESM is violated when the pseudo-inverse technique is used in deriving the transformation matrices.

4.1.2. Diagonal Matrix

The concept behind the diagonal matrix approach is that the value of each entry in a state vector is dependent *only on the value of the corresponding entry* of the related state vector. For example, consider the system $\boldsymbol{x_{ps} = Sx_{ms}}$ where each state vector has three entries (i.e. the vectors have a dimension of 3). In the general case, **S** is a fully populated matrix, and the system is represented as

$$\begin{bmatrix} x_{ps,1} \\ x_{ps,2} \\ x_{ps,3} \end{bmatrix} = \begin{bmatrix} s_{11} & s_{12} & s_{13} \\ s_{21} & s_{22} & s_{23} \\ s_{31} & s_{32} & s_{33} \end{bmatrix} \begin{bmatrix} x_{ms,1} \\ x_{ms,2} \\ x_{ms,3} \end{bmatrix}. \tag{4-19}$$

We see in Eqn. 4-19 that $\mathbf{x_{ps,1}}$, for example, is not determined just from $\mathbf{x_{ms,1}}$; rather, it is calculated as a linear combination of $\mathbf{x_{ms,1}}$, $\mathbf{x_{ms,2}}$, and $\mathbf{x_{ms,3}}$. If we assume, however, that each entry of $\mathbf{x_{ps}}$ can be determined entirely from the corresponding entry of $\mathbf{x_{ms}}$, we can modify Eqn. 4-19 to take the following form:

$$\begin{bmatrix} x_{ps,1} \\ x_{ps,2} \\ x_{ps,3} \end{bmatrix} = \begin{bmatrix} s_{11} & 0 & 0 \\ 0 & s_{22} & 0 \\ 0 & 0 & s_{33} \end{bmatrix} \begin{bmatrix} x_{ms,1} \\ x_{ms,2} \\ x_{ms,3} \end{bmatrix}. \tag{4-20}$$

We now have

$$x_{ps,1} = s_{11} x_{ms,1}$$
$$x_{ps,2} = s_{22} x_{ms,2} \qquad (4\text{-}21)$$
$$x_{ps,3} = s_{33} x_{ms,3}$$

where each point in the product specimen is simply a scaled value of the corresponding point in the model specimen. In this case, no specific relationship is assumed to exist among the points of the state vectors; rather, the value of each point depends solely on the value of the corresponding point and the scale factor for that particular entry.

When the transformation matrix **S** is diagonal, as in Eqn. 4-20, the procedure for calculating **S** given $\mathbf{x_{ps}}$ and $\mathbf{x_{ms}}$ is much more straightforward than it is with the pseudo-inverse approach. For the diagonal case, each row in Eqn. 4-21 is simply solved for the respective scale factor s_{ii}, as follows:

$$s_{11} = x_{ps,1} / x_{ms,1}$$
$$s_{22} = x_{ps,2} / x_{ms,2} \qquad (4\text{-}22)$$
$$s_{33} = x_{ps,3} / x_{ms,3}$$

Each scale factor is then placed in the appropriate location along the diagonal, and the transformation matrix **S** is complete.

It is important to emphasize the relationship between this ESM diagonal method and the TSM method, and to point out the valuable insight about model distortion that can be obtained with the diagonal method. Suppose that scale factors are calculated according to Eqn. 4-22 and that *they are all the same*; this situation represents a well-scaled system (the degree of model distortion is zero). Now suppose that scale factors are calculated for a different system according to

Eqn. 4-22 and that *they have different values*; this situation represents a system with model distortions (the degree of model distortion is characterized by the variation in the scale factors). Recall that the need for the ESM arises from distorted systems for which a constant scale factor fails to accurately correlate the two systems. The entries of the diagonal matrix show how the scale factor changes as you move from point to point within the system (a *point* in this case can represent a physical location in the system, a specific loading condition, or any other independent variable for which one is measuring system behavior).

Another important aspect of the diagonal matrix approach is that the ESM requirement that **SF** = **FS** is always satisfied. The fact that diagonal matrices are always commutative for matrix multiplication can be illustrated with the following example:

$$\begin{bmatrix} a_{11} & 0 \\ 0 & a_{22} \end{bmatrix}\begin{bmatrix} b_{11} & 0 \\ 0 & b_{22} \end{bmatrix} = \begin{bmatrix} b_{11} & 0 \\ 0 & b_{22} \end{bmatrix}\begin{bmatrix} a_{11} & 0 \\ 0 & a_{22} \end{bmatrix} = \begin{bmatrix} a_{11}b_{11} & 0 \\ 0 & a_{22}b_{22} \end{bmatrix} \qquad (4\text{-}23)$$

Equation 4-23 can easily be extended to *n* dimensions.

4.1.3. Circulant Matrix

The final method for constructing ESM transformation matrices that is presented in this chapter uses the circulant matrix technique. As mentioned in Chapter 2, transforming a vector into a circulant matrix can be thought of as a matrix manipulation, similar to taking the transpose of a matrix. The motivation for applying the circulant technique to the ESM is that *the circulant form of a vector is a square matrix* that can readily be inverted (provided that none of the columns are linearly dependent). The circulant matrix technique is an ideal

approach for deriving the transformation matrices in the ESM since the derivation of the transformation matrices requires taking the inverse of a vector, which cannot be done directly.

The circulant form of a vector is constructed as follows:

$$x = \begin{bmatrix} x_1 \\ x_2 \\ \vdots \\ x_n \end{bmatrix} \quad \Rightarrow \quad cir(x) = \begin{bmatrix} x_1 & x_n & \cdots & x_2 \\ x_2 & x_1 & \cdots & x_3 \\ \vdots & \vdots & & \vdots \\ x_n & x_{n-1} & \cdots & x_1 \end{bmatrix} \tag{4-24}$$

By using the circulant form of each state vector, the basic ESM relationships shown in Eqn. 4-14 become

$$\begin{aligned} cir(\mathbf{x}_{ps}) &= \mathbf{S}\ cir(\mathbf{x}_{ms}) \\ cir(\mathbf{x}_{m}) &= \mathbf{F}\ cir(\mathbf{x}_{ms}) \end{aligned} \tag{4-25}$$

Since a circulant matrix is square by definition, the inverse of cir($\mathbf{x}_{ms}$) can be calculated (provided its columns are linearly independent) and multiplied to both sides of Eqn. 4-25 to give

$$\begin{aligned} \mathbf{S} &= cir(\mathbf{x}_{ps})\ cir(\mathbf{x}_{ms})^{-1} \\ \mathbf{F} &= cir(\mathbf{x}_{m})\ cir(\mathbf{x}_{ms})^{-1} \end{aligned} \tag{4-26}$$

Since the inverse of a circulant matrix is also a circulant matrix, and the product of two circulant matrices is also a circulant matrix [Davis, 1979; Fuhrmann, 1996], we conclude that Eqn. 4-26 produces *circulant* transformation matrices **S** and **F**. The fact that **S** and **F** are circulant is an important conclusion since *circulant matrices also commute under matrix multiplication* [Davis, 1979; Fuhrmann, 1996]. This means that **SF** = **FS** as required by the ESM.

4.2. EVALUATION OF TRANSFORMATION MATRICES

The three previous subsections contain details of various approaches for constructing the ESM transformation matrices. Although the form of the transformation matrices is entirely different with each approach (the *pseudo-inverse* produces fully-populated, general matrices; the *circulant* produces fully-populated, circulant matrices; and the *diagonal* produces diagonal matrices), all three approaches produce matrices that satisfy the basic ESM relationships shown in Eqn. 4-14 (recall that, since Eqn. 4-14 represents an over determined system, there is not one unique solution to the system). It is difficult to say which approach produces the "best" results; indeed, the "best" approach could vary depending on the nature of each situation. An evaluation of the different techniques for constructing transformation matrices is presented in this section in order to clarify the conditions under which each technique should be applied.

The pseudo-inverse appears to be the first approach used in deriving transformation matrices for the ESM [Cho, 1997]. However, since the pseudo-inverse technique fails to satisfy the requirement that **SF** = **FS**, we abandon this approach for the present time. It should be noted, however, that the pseudo-inverse technique has shown good potential for accurately predicting certain types of product behaviors, especially when those behaviors can be described with polynomial relationships (see [Cho, 1999]). In order to use the pseudo-inverse technique with confidence, however, we must be able to separate the error in the technique itself (the fact that $\mathbf{SF} \neq \mathbf{FS}$) from the error that comes from specimen distortions in the system. For example, the difference in the products **SF** and **FS**

could be used as a measure of the inherent error in the pseudo-inverse technique and compared with the overall ESM error. If the error in the technique is small relative to the overall error, the pseudo-inverse approach could still be used with confidence. Further research is needed to formalize such a procedure for quantifying the error in the pseudo-inverse approach.

We turn now to an evaluation of the circulant and diagonal matrix approaches, both of which satisfy the ESM requirement that **SF** = **FS**. We recall that the diagonal matrix associates each point in the state vector only with the *corresponding point* in the related vector, while the circulant matrix associates each point in the state vector with a *linear combination of all the points* in the related vector. Each point in a vector that is formed with a circulant matrix (say, $\mathbf{x_p}$) can be thought of as a *weighted sum* of all the points in the corresponding vector (say, $\mathbf{x_m}$). The unique form of the circulant matrix, as described in Eqn. 4-24, tends to smooth the variation between the points in $\mathbf{x_p}$. *Variation,* in this sense, is a measure of the difference in the values of adjacent points in a vector. The variation V of a vector $\mathbf{z}$ is formally defined by [Davis, 1979] as follows:

$$V(z) = |z_1 - z_2|^2 + |z_2 - z_3|^2 + \cdots + |z_{n-1} - z_n|^2 + |z_n - z_1|^2 . \qquad (4\text{-}27)$$

The smoothing effect of circulant matrices, as compared to diagonal matrices, is illustrated with two simple examples in the following subsections. It is important to note that the examples simply serve to illustrate the effect that circulant matrices can exhibit with regards to the variation of a vector; they do not

prove that circulant matrices smooth variation in all situations (such as for vectors that represent non-monotonic functions).

4.2.1. Heat Transfer Application

We first consider a steady state heat transfer problem similar to that presented in [Cho, 1999]. In this case, we want to predict the steady state temperature of the product at several internal points by measuring the steady state temperature at corresponding points in the model. Suppose that the product, which is fabricated out of high temperature material, is to be exposed to a temperature of 600 K at the external surfaces and 300 K at the internal surfaces (see Figure 40). Suppose also that the model, which is fabricated out of low temperature material, can only withstand temperatures up to 450K. The TSM constraints for steady state heat transfer require that $\left(\frac{T_o}{T_i}\right)_p = \left(\frac{T_o}{T_i}\right)_m$; however, since $\left(\frac{600K}{300K}\right) \neq \left(\frac{450K}{300K}\right)$, the system is distorted, and we resort to the ESM to predict product performance. The simplified geometry of the specimen pair, along with the overall ESM setup for the problem, is shown in Figure 40.

ABAQUS™ software is used to construct a finite element model for each system shown in Figure 40. The finite element models for both the product/model system and the specimen system are shown in Figure 41. The finite element models are made up of 2-D, four node thermal elements. The steady state temperature is measured at the nodal points from Node 1 to Node 9, as shown in Figure 41. Note that the increments between nodal points in the product / model pair tend to increase from Node 1 to Node 9, so that one increment in the product

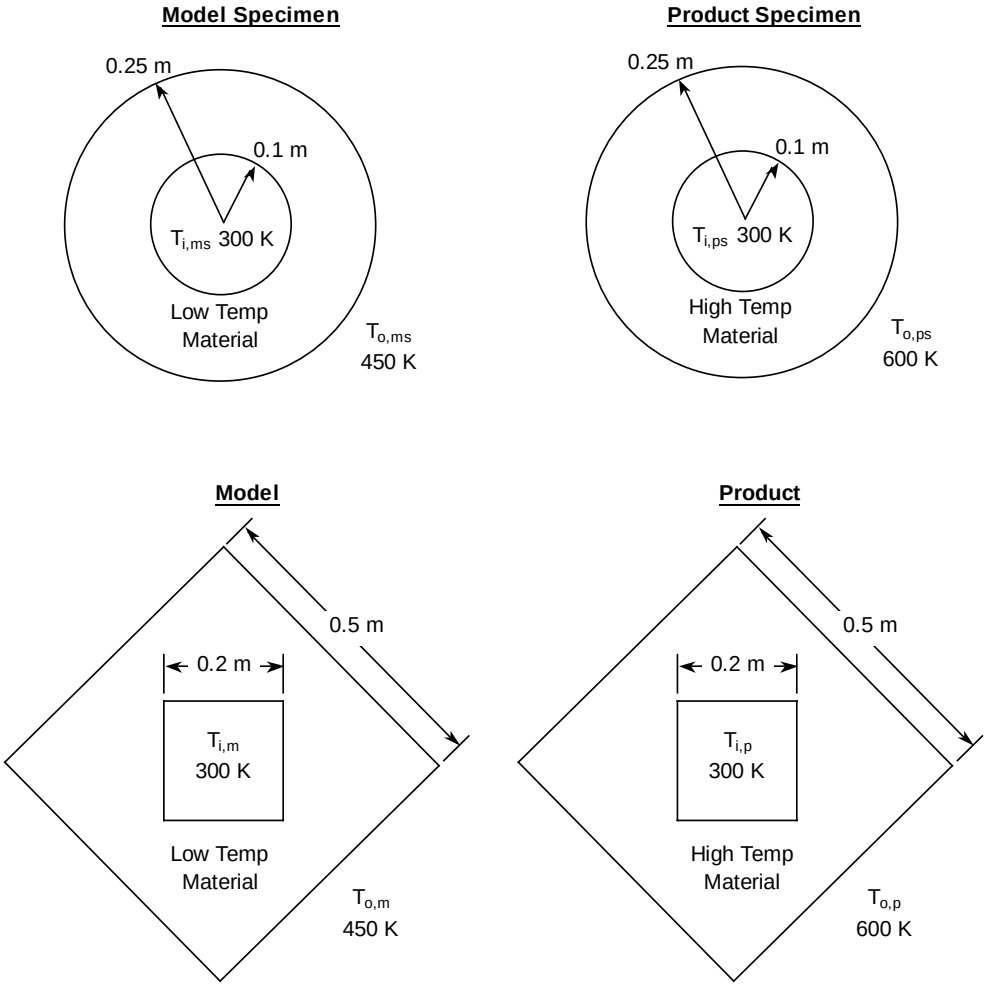

Figure 40. ESM Setup for Steady State Heat Transfer Problem.

/ model pair does not necessarily represent the same geometric distance as the corresponding increment in the specimen pair.

In order to evaluate the effect of measurement point selection on ESM results, several different nodal increments are used as measurement points for the state vectors. Three different cases that involve various nodal increments are

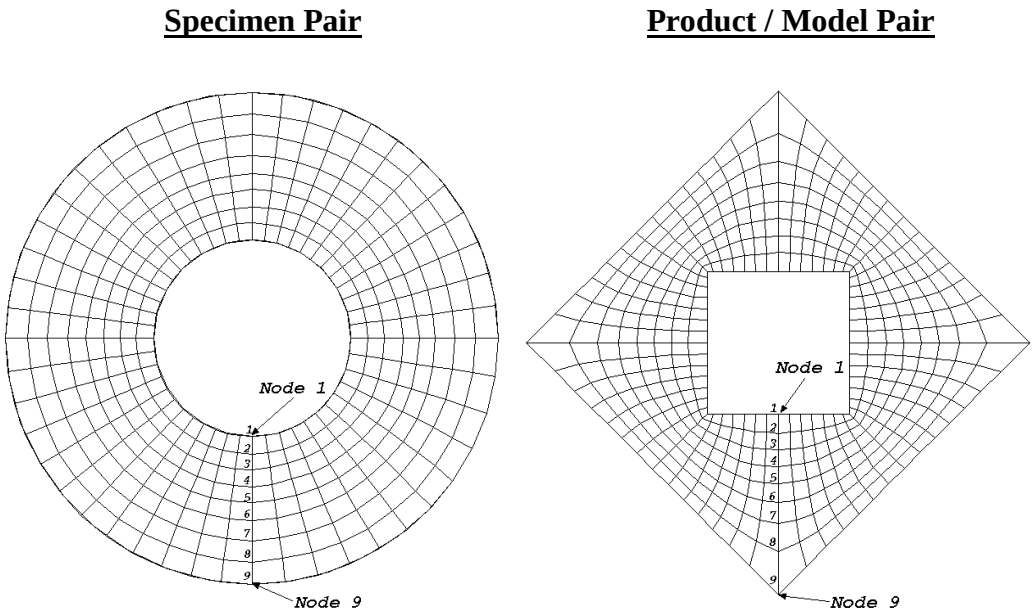

Figure 41. Finite Element Models for Steady State Heat Transfer Problem.

shown in Table 16. In each case the selected nodal points for the product / model pair are the same while those for the specimen pair are varied.

Table 16. Measurement Points for Heat Transfer Application.

	Product / Model Pair	**Specimen Pair**		
Measurement Point	Node # (All Cases)	Node # Case 1	Node # Case 2	Node # Case 3
1	1	1	1	1
2	3	3	2	2
3	5	5	3	7
4	7	7	6	8
5	9	9	9	9

The purpose of using different node sets as measurement points for the ESM is to demonstrate the ability of the circulant matrix to smooth the variation in the product state vector. The physical distance in one "step," or nodal increment, in the product / model pair is not the same as the corresponding distance in the specimen pair. Case 1 in Table 16 involves evenly spaced nodal increments; Case 2 involves uneven nodal increments biased towards the center of the product; and Case 3 involves uneven nodal increments biased towards the outside of the product. Results from other uneven nodal point selections should fall within the (nearly) extreme cases represented by Case 2 and Case 3.

The situation represented in Table 16 has important practical implications that are relevant to the general application of the ESM. The major implications include the following:

1. The location of corresponding points between a product or model and the respective specimen is not easy to determine in general (see Figure 42). In many situations, one increment in the product /

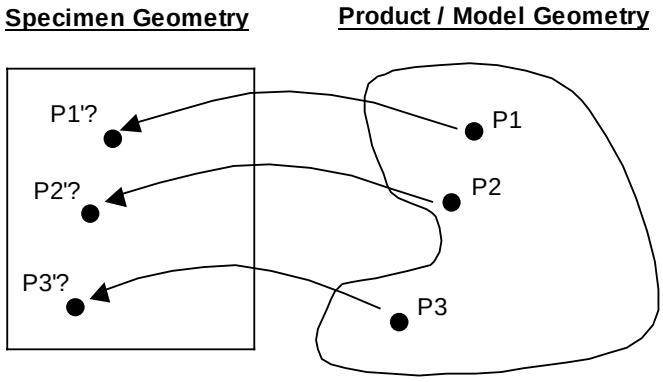

Figure 42. Corresponding Points for General Changes in Geometric Shape.

model pair may not be equivalent to a corresponding increment in the specimen pair.

2. Even in situations where corresponding points can be precisely defined, the experimental process of placing sensors for taking measurements involves inherent variability and error. We are interested in the effect that deviations from the "true" measurement location has on ESM prediction error.

The steady state temperature of the product is predicted at each of the five measurement points defined in Table 16 using both the circulant and diagonal matrix approaches. The steady state temperature of the product is also calculated directly and compared with the ESM predictions. Plots of the ESM predictions using the diagonal matrix approach and the circulant matrix approach are shown in Figure 43 and Figure 44, respectively.

Figure 43 shows that the diagonal matrix approach predicts the steady state temperature exactly at the boundaries (where the measurement points correspond perfectly), but produces errors at the internal points (where the measurement points do not correspond perfectly). Figure 44 shows that the circulant matrix approach "smooths" the variation between measurement points. The prediction curve in Figure 44 shifts up or down, depending on the set of measurement points that is used for the state vector, but the *form* of the prediction curve remains the same. The consistent form of the prediction curve is a result of the unique structure of the circulant matrix.

Figure 45 and Figure 46 contain plots of the ESM error for the diagonal and circulant matrix approaches, respectively. These figures emphasize the fact

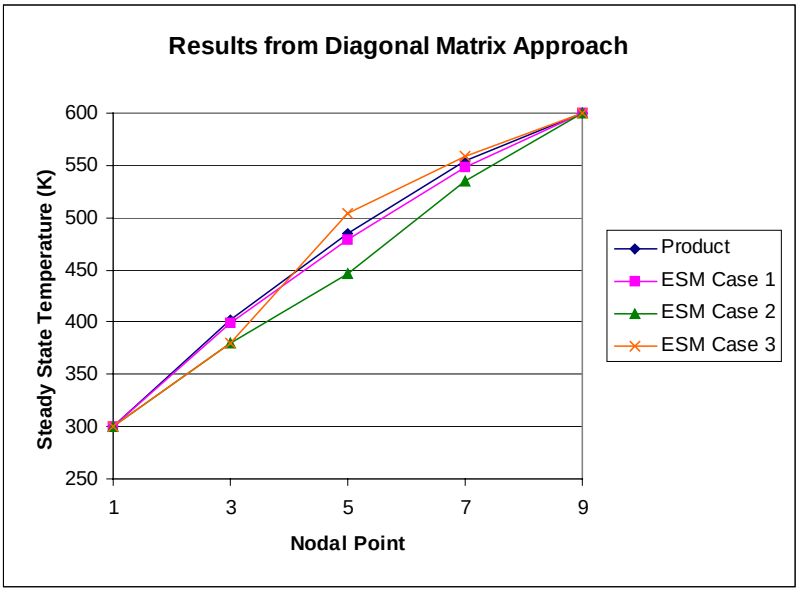

Figure 43. Steady State Temperature Prediction Using Diagonal Matrix.

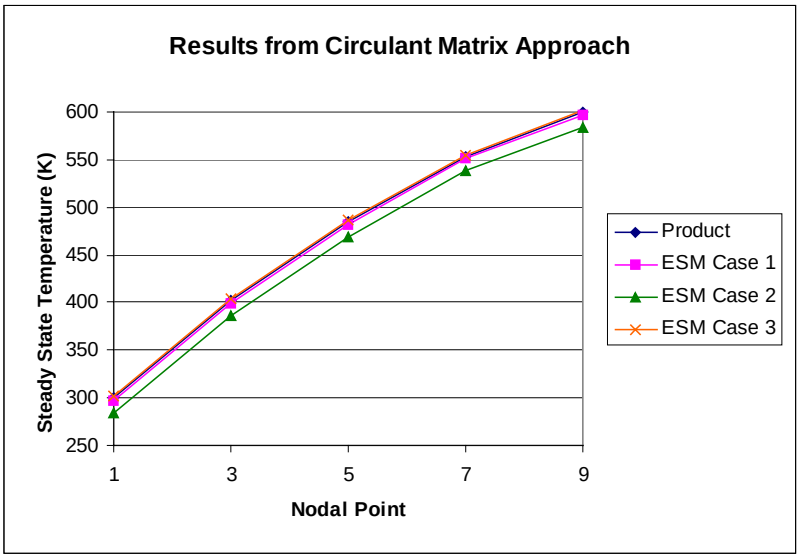

Figure 44. Steady State Temperature Prediction Using Circulant Matrix.

that the circulant matrix approach smooths out the error among all of the measurement points while the diagonal matrix approach produces different levels

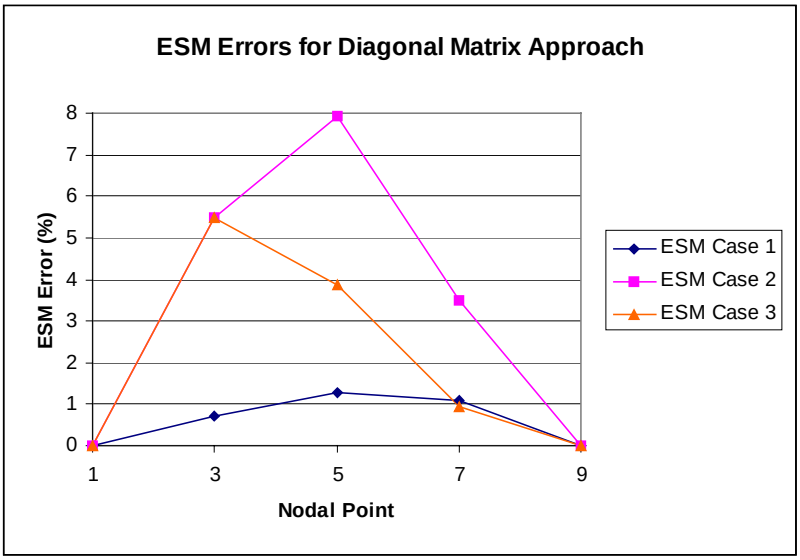

Figure 45. ESM Errors for Diagonal Matrix Approach.

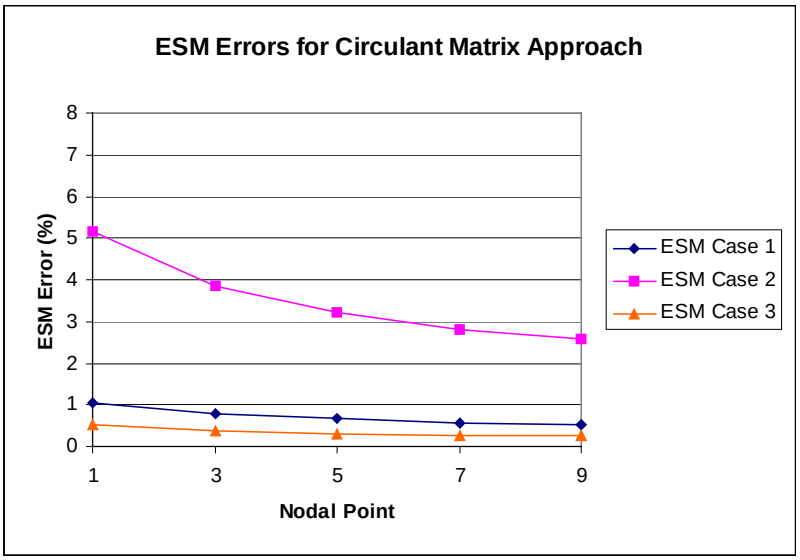

Figure 46. ESM Errors for Circulant Matrix Approach.

of error depending on how well the measurement points in the state vectors correspond. The ESM error at each measurement point, along with the average error for each case, is shown in Table 17. The average error across all measurement points is similar for the two approaches (except for Case 3 where the circulant matrix approach produces less error).

In order to quantify the "smoothness" in the state vector of the product, we use the *variation* metric defined in Eqn. 4-27. If we note that the state vector of the product ($\mathbf{T_p}$) is composed of temperatures at five equally spaced nodal points, or, in other words,

$$T_p = \begin{bmatrix} T_{p,1} \\ T_{p,3} \\ T_{p,5} \\ T_{p,7} \\ T_{p,9} \end{bmatrix}, \tag{4-28}$$

where the subscripts indicate the product node numbers, we can rewrite Eqn. 4-27

Table 17. Errors in Temperature Predictions.

Product Nodal Point	ESM Diagonal Error (%)			ESM Circulant Error (%)		
	Case 1	Case 2	Case 3	Case 1	Case 2	Case 3
1	0	0	0	1.03	5.15	0.51
3	0.73	5.50	5.50	0.77	3.87	0.37
5	1.29	7.94	3.87	0.66	3.21	0.30
7	1.07	3.47	0.95	0.56	2.81	0.26
9	0	0	0	0.52	2.58	0.27
Average	0.62	3.38	2.06	0.71	3.52	0.34

in terms of the specific ESM variables for this example as follows:

$$V(T_p) = \left|T_{p,1} - T_{p,3}\right|^2 + \left|T_{p,3} - T_{p,5}\right|^2 + \left|T_{p,5} - T_{p,7}\right|^2 + \left|T_{p,7} - T_{p,9}\right|^2 + \left|T_{p,9} - T_{p,1}\right|^2 . \quad (4\text{-}29)$$

Equation 4-29 is used to calculate the variation in the actual product state vector as well as the variation in the product state vector as predicted through the ESM diagonal and circulant matrix approaches. The variation in the state vectors is shown in Table 18. Note that we are interested more in the *change* in variation between test cases than in the *magnitude* of the variation. (Note that, since the variation calculated by equation 4-29 is dependent on the number of measurement points that are used, the *magnitude* of variation by itself means very little; the *change* in variation, however, indicates how the spacing between adjacent points in the vector changes from one case to another). Table 18 shows that the change in variation between test cases is much smaller for the circulant matrix approach than it is for the diagonal matrix approach. The results in Table 18 demonstate the ability of a circulant matrix to smooth the variation in a vector.

4.2.2. Cantilever Beam Application

We now turn to a system whose measurement points are equally spaced

Table 18. Variation in Product Temperature Vector.

	$V(\mathbf{T_p})$ Product $(K)^2$	$V(\mathbf{T_p})$ ESM Diagonal $(K)^2$	$V(\mathbf{T_p})$ ESM Circulant $(K)^2$
Case 1	114,168	113,668	114,166
Case 2	114,168	112,880	114,161
Case 3	114,168	116,384	114,202

and conduct a similar evaluation of the diagonal and circulant approaches. We expect that a system with equally spaced measurement points will have a similar value of variation for both the diagonal and circulant matrix techniques (i.e. there will be no "smoothing" required of the circulant matrix since the measurement points are already evenly spaced).

The cantilever beam system presented in Section 3.2.1 involves a load of 20 pounds that is applied to the tip of the product and product specimen beams in equal increments of two pounds (the scaled load on the model and model specimen beams is also applied to the tip of the beams in equal increments). Since there is no variation in the geometric location of the measurement point, and since the measurements are taken at equal increments of load, we can say that the points that make up the state vectors correspond perfectly (there would, of course, be some variation if this system were tested experimentally).

It is important to note that measurement "points" are not restricted to geometric locations; rather, the points that make up a state vector can be measured with respect to spatial location, magnitude of a load, or any other variable against which the state of a product is measured. In this case, the measurement points correspond to the magnitude of the applied load, and the value that is entered in the state vector is the beam deflection at the specified load.

Three test cases in which different sets of points are used in the state vectors are defined in Table 19. (Note that the five "points" that make up the state vector δ_p for the product family, which is given by

$$\delta_p = \begin{bmatrix} \delta_{p,2} \\ \delta_{p,4} \\ \delta_{p,6} \\ \delta_{p,8} \\ \delta_{p,10} \end{bmatrix}, \tag{4-30}$$

include $\delta_{p,4}$, which is the beam deflection under a load of two pounds, $\delta_{p,8}$, which is the beam deflection under a load of four pounds, and so on to $\delta_{p,20}$.) The measurement points in the product and product specimen (i.e. product family) are held constant while the corresponding points in the model and model specimen (i.e. model family) are different for each case. As in the previous study, the first case involves evenly spaced points and the last two cases involve unevenly spaced points. Keep in mind that the difference between this study and the previous study is that, in this case, the increments between points are consistent (i.e. the magnitude of one load step in the product family is always equivalent to the magnitude of one load step in the model family).

Table 19. Measurement Points for Cantilever Beam.

	Product Family	**Model Family**		
Measurement Point	Load Step	Load Step Case 1	Load Step Case 2	Load Step Case 3
1	2	2	2	2
2	4	4	3	3
3	6	6	4	8
4	8	8	7	9
5	10	10	10	10

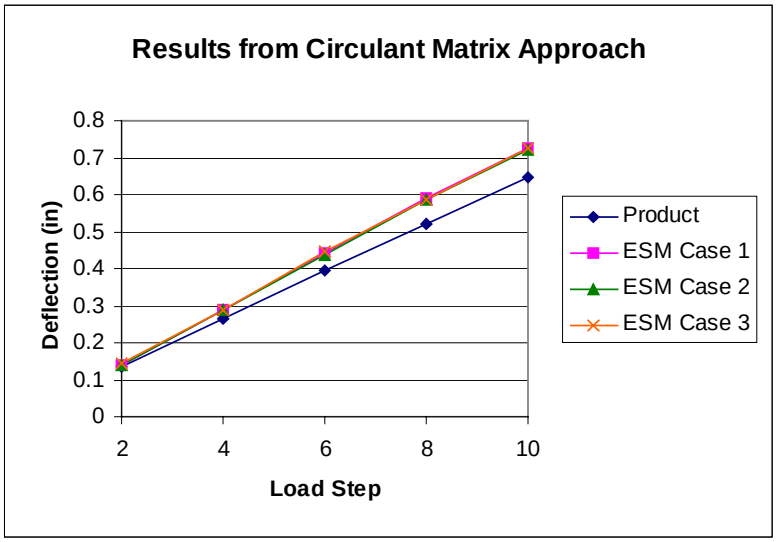

Figure 47. Beam Deflection Using Diagonal Matrix Approach.

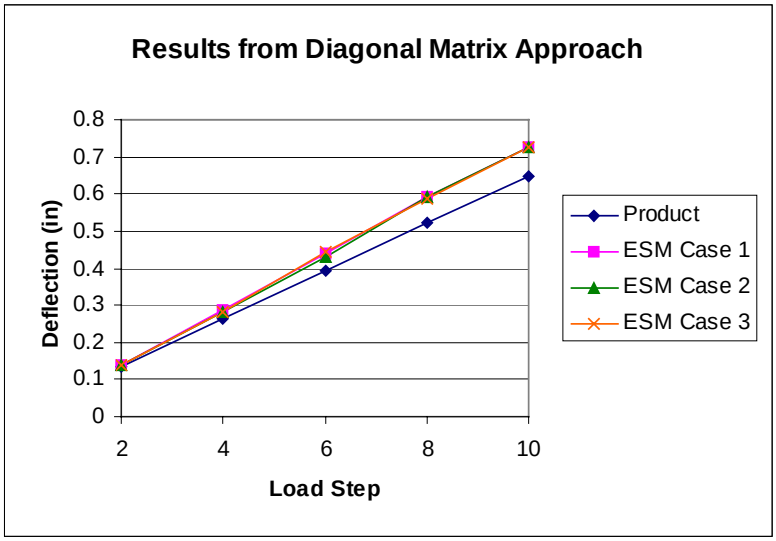

Figure 48. Beam Deflection Using Circulant Matrix Approach.

Figure 47 and Figure 48 show the ESM predictions of cantilever beam deflection using the diagonal and circulant matrix approaches, respectively. The figures, in this case, look identical. This result indicates that point selection does

not have the same impact on ESM results when equal increments are used between measurement points as when unequal increments are used. The ESM error at each measurement point, along with the average error for each case, is shown in Table 20. Note that, for both ESM approaches, error values tend to increase as the load increases (this is due to the specimen distortion described in Chapter 3 in connection with this problem). The average error across all measurement points is slightly better for the diagonal approach than for the circulant approach (although we cannot say that this will always be the case).

The variation in the product state vector is calculated in the same manner as in the previous section. The change in variation in the product state vectors, as shown in Table 21, is very small for both approaches (the small increase in variation in the circulant approach is considered to be caused by numerical noise within the method).

We are now ready to draw conclusions about the differences in the various

Table 20. Errors in Deflection Predictions.

Meas. Point	ESM Diagonal Error (%)			ESM Circulant Error (%)		
	Case 1	Case 2	Case 3	Case 1	Case 2	Case 3
1	3.77	3.77	3.77	6.38	4.75	7.20
2	8.33	6.22	6.22	9.46	8.85	9.10
3	11.86	8.58	12.90	11.89	10.45	12.79
4	13.27	13.07	12.87	12.96	12.48	12.47
5	12.33	12.33	12.33	12.18	11.85	12.60
Average	9.91	8.80	9.62	10.57	9.68	10.83

Table 21. Variation in Product Deflection Vector.

	Product $(in)^2$	ESM Diagonal $(in)^2$	ESM Circulant $(in)^2$
Case 1	0.3291	0.4320	0.4255
Case 2	0.3291	0.4321	0.4255
Case 3	0.3291	0.4322	0.4278

approaches for deriving ESM transformation matrices:

1. The pseudo-inverse approach does not satisfy the basic ESM requirement that **SF** = **FS;** both the diagonal matrix and circulant matrix approaches do satisfy this requirement. For this reason the diagonal matrix and circulant matrix approaches are recommended. Although the pseudo-inverse approach has shown promising results, additional research on separating the error that is due to specimen distortion from the inherent error in the method itself is needed before this approach can be used with confidence.
2. The circulant matrix approach smooths the variation in the state vector. The circulant matrix approach is recommended for situations in which corresponding points between the product / model pair and the specimen pair are difficult to determine. The circulant matrix approach is also recommended when the increments between corresponding points are inconsistent.
3. The diagonal matrix approach is recommended for situations in which corresponding points are easy to determine and in which the

increments between corresponding points are consistent. The diagonal matrix approach is recommended in these situations because of its ease of use, not because it will necessarily yield more accurate results than the circulant approach.

It is important to recognize that the conclusions described above are based on tendencies that were exhibited in the finite element studies presented in this section. No mathematical proof has been found to verify these conclusions, nor are these conclusions gauranteed to hold under all circumstances. Additional research is required to fully characterize the differences in the various methods for deriving transformation matrices. However, the conclusions given above are expected to hold for systems that are similar to those used in the studies (i.e. systems whose behavior is described by simple, monotonic functions).

4.3. ADVANCED EMPIRICAL SIMILITUDE METHOD

Having clarified the differences in the various approaches for deriving ESM transformation matrices, we are now ready to proceed with the *advanced empirical similitude method*. The following sections outline the advanced method and demonstrate its application using the three ESM studies from Chapter 3.

4.3.1. Overview of Advanced ESM

Several sources of specimen distortion that produce errors in the ESM are described and illustrated in Chapter 3. The specimen distortions result in $S \neq S'$ or $F \neq F'$, as shown in Figure 22. In order to clarify the underlying theory of the ESM, the two-dimensional illustration of the ESM, as shown in Figure 22, is

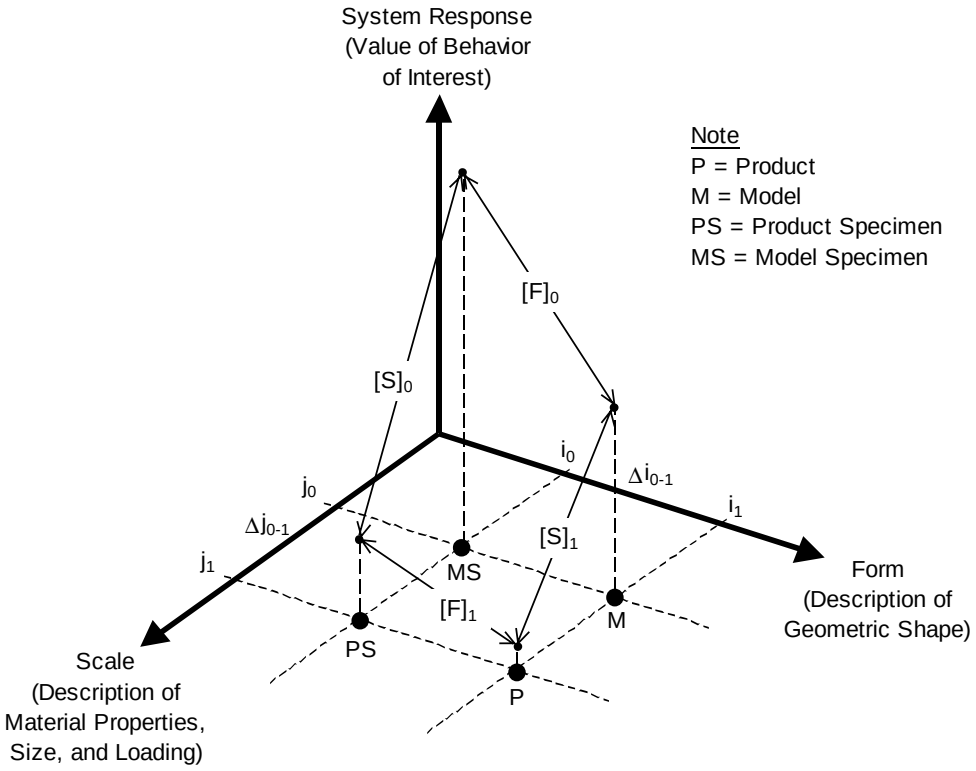

Figure 49. Illustration of Empirical Similarity Method.

converted to a three-dimensional illustration, as shown in Figure 49. In Figure 49, a description of material properties, size, and loading conditions is plotted on the x-axis, a description of geometric shape is plotted on the y-axis, and the system response is plotted on the z-axis. (Note that $[S]_1$ and $[F]_1$ in Figure 49 represent S' and F', respectively, in Figure 22). The four configurations shown in Figure 49 correspond to the traditional ESM systems (viz. product, product specimen, model, and model specimen). Although the system response is shown as a single point in the figure, the response can more generally be represented as a vector.

Figure 49 illustrates that, for the most general case, the transformation matrices that relate the four system states are all different.

The goal of the advanced ESM is to capture the change in the *Scale* transformation matrix as the *Form* parameters change or, equivalently, to capture the change in the *Form* transformation matrix as the *Scale* parameters change. An intermediate specimen pair is presented as a means of capturing the variation in the transformation matrices, as illustrated in Figure 50. By defining an intermediate specimen pair that lies between the original system pairs, the variation in the transformation matrix that occurs from one specimen pair to the

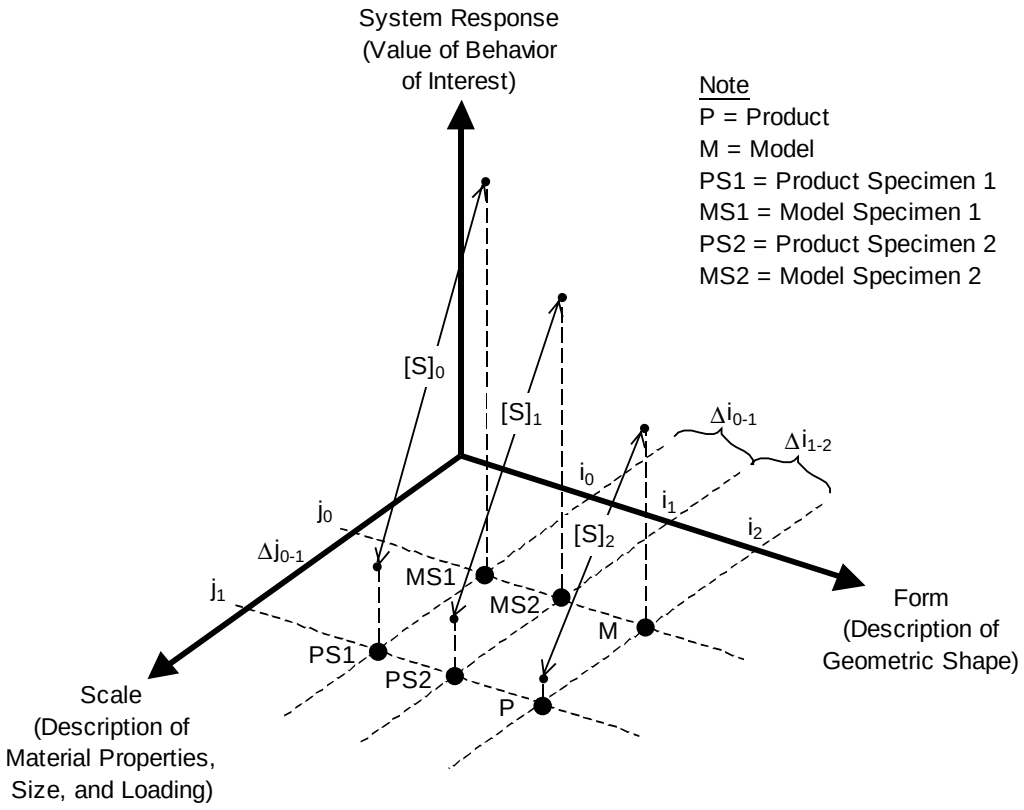

Figure 50. Illustration of Advanced Empirical Similarity Method.

next can be extrapolated to predict the transformation matrix between the model and the product. (An alternate approach is to define the additional specimen pair *outside* of the original system pairs and *interpolate* to predict the transformation matrix between the model and the product). The decision of whether to capture changes in the *Scale* transformation matrix or the *Form* transformation matrix depends on whether it is easier to characterize changes in geometric shape for a particular problem or to characterize changes in material properties, size, and loading conditions.

In the advanced ESM, each transformation matrix signifies a "data point," and an interpolating polynomial is constructed to describe the trend in the data. For a single intermediate specimen pair, a first order polynomial is constructed; for two intermediate specimen pairs, a second order polynomial is constructed; etc. In general, *n* intermediate specimen pairs allow for the construction of an n^{th} order polynomial.

A polynomial know as the *Lagrange interpolating polynomial P* is defined by the following equation [Burden, 1989]:

$$P(x) = \sum_{k=0}^{n} f(x_k) L_{n,k}(x) \tag{4-31}$$

where $f(x_k)$ is the value of a function *f* evaluated at a point x_k, and $L_{n,k}(x)$ is given by the formula

$$L_{n,k}(x) = \prod_{\substack{m=0 \\ m \neq k}}^{n} \frac{x - x_m}{x_k - x_m}. \tag{4-32}$$

Equation 4-31 can also be expressed in the following form:

$$P_n(x) = a_0 + a_1(x - x_0) + a_2(x - x_0)(x - x_1) + \cdots + a_n(x - x_0)(x - x_1)\cdots(x - x_{n-1}) \quad (4\text{-}33)$$

where *n* is the order of the polynomial, and the coefficients are given by

$$a_k = f\{x_0, x_1, x_2, ..., x_k\}. \quad (4\text{-}34)$$

The notation *f{x}* in Eqn. 4-34 is the *divided-difference notation*. The zeroth divided difference of a function *f* with respect to x_m is simply the value of the function evaluated at the point x_m, or

$$f\{x_m\} = f(x_m). \quad (4\text{-}35)$$

The zeroth divided difference of the function with respect to x_{m+1} is likewise given as

$$f\{x_{m+1}\} = f(x_{m+1}). \quad (4\text{-}36)$$

Now, the *first* divided difference of the function with respect to x_m and x_{m+1} is defined as

$$f\{x_m, x_{m+1}\} = \frac{f\{x_{m+1}\} - f\{x_m\}}{x_{m+1} - x_m}. \quad (4\text{-}37)$$

The second divided difference of the function with respect to x_m, x_{m+1}, and x_{m+2} is

$$f\{x_m, x_{m+1}, x_{m+2}\} = \frac{f\{x_{m+1}, x_{m+2}\} - f\{x_m, x_{m+1}\}}{x_{m+2} - x_m}. \quad (4\text{-}38)$$

In general, the k[th] divided difference formula with respect to $x_m, x_{m+1}, \cdots, x_{m+k}$ is given as

$$f\{x_m, x_{mi+1}, \cdots, x_{m+k}\} = \frac{f\{x_{m+1}, x_{m+2}, \cdots, x_{m+k}\} - f\{x_m, x_{m+1}, \cdots x_{m+k-1}\}}{x_{m+k} - x_m}. \quad (4\text{-}39)$$

By writing Eqn. 4-33 in divided-difference notation we obtain the following:

$$P_n(x) = f\{x_0\} + \sum_{k=1}^{n} f\{x_0, x_1, \cdots, x_k\}(x - x_0)\cdots(x - x_{k-1}). \qquad (4\text{-}40)$$

Equation 4-40 is known as *Newton's interpolatory divided-difference formula* (see [Burden, 1989]). Equation 4-40 reflects the form of the Lagrange polynomial that is used in the advanced ESM.

A convenient way to construct the interpolating polynomial shown in Eqn. 4-40 is to set up a table similar to that shown in Table 22. The format of Table 22 allows one to systematically construct the divided differences and enter the first value in each divided difference column into Eqn. 4-40. Although Table 22 is set up for a third order polynomial, it can easily be expanded to accommodate higher order polynomials.

As a simple example of how to construct an interpolating polynomial with a table such as Table 22, let's evaluate the function $f(x) = x^3 + 2x^2 + 3x + 7$ at the point $x = 4$ with a 3rd order polynomial. In order to construct a 3rd order polynomial, we need to know the value of the function at four specific points

Table 22. Structure for Creating Interpolating Polynomials.

		Divided Differences			
Step	x	**Zeroth**	**First**	**Second**	**Third**
1	x_0	$f\{x_0\} = f(x_0)$	$f\{x_0, x_1\} = \frac{f\{x_1\} - f\{x_0\}}{x_1 - x_0}$	$f\{x_0, x_1, x_2\} = \frac{f\{x_1, x_2\} - f\{x_0, x_1\}}{x_2 - x_0}$	$f\{x_1, x_2, x_3, x_4\} = \frac{f\{x_1, x_2, x_3\} - f\{x_0, x_1, x_2\}}{x_3 - x_0}$
2	x_1	$f\{x_1\} = f(x_1)$	$f\{x_1, x_2\} = \frac{f\{x_2\} - f\{x_1\}}{x_2 - x_1}$	$f\{x_1, x_2, x_3\} = \frac{f\{x_2, x_3\} - f\{x_1, x_2\}}{x_3 - x_1}$	
3	x_2	$f\{x_2\} = f(x_2)$	$f\{x_2, x_3\} = \frac{f\{x_3\} - f\{x_2\}}{x_3 - x_2}$		
4	x_3	$f\{x_3\} = f(x_2)$			

Table 23. Example Construction of Interpolating Polynomial.

		Divided Differences			
Step	**x**	**Zeroth**	**First**	**Second**	**Third**
1	0	f{0} = 7	f{0,1} = 6	f{0,1,2}= 5	f{0,1,2,3} = 1
2	1	f{1} = 13	f{1,2} = 16	f{1,2,3} = 8	
3	2	f{2} = 29	f{2,3} = 32		
4	3	f{3} = 61			

(namely x_0, x_1, x_2, and x_3). If we evaluate the function at the points x = 0, 1, 2, and 3, and substitute the resulting values into Table 22, we can calculate the divided differences shown in Table 23. The values in Table 23 are then entered into Eqn. 4-40, and the third order polynomial approximation of the function f at the point x = 4 is given by

$$P_3(4) = 7 + 6(4-0) + 5(4-0)(4-1) + 1(4-0)(4-1)(4-2) \qquad (4\text{-}41)$$

which evaluates to 115. Note that, since a 3rd order polynomial can evaluate a cubic function exactly, the polynomial approximation $P_3(4)$ is identical to the function evaluation $f(4)$. Lower order polynomials, however, give worse approximations to the function (e.g. $P_2(4)$ = 91 and $P_1(4)$ = 31). Figure 51 shows a plot of $f(x)$ along with all three orders of interpolating polynomials. Note that the 3rd order polynomial coincides exactly with the function, and the two curves appear as one in Figure 51.

When applying the Lagrange polynomial to the ESM, the points x_m represent either increments in *form* (i_0, i_1, …) or increments in *scale* (j_0, j_1, …),

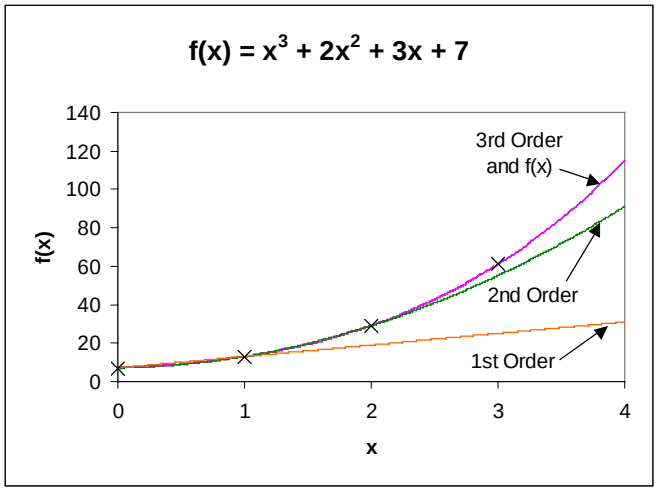

Figure 51. Various Orders of Approximating Polynomials.

depending on the dimension in Figure 50 that is being discretized. The value of the function $f(x_m)$ represents the transformation matrix at the specified point. For example, if the *form* dimension is being discretized, as shown in Figure 50, the first divided difference formula, as shown in Eqn. 4-37, becomes

$$S\{i_0, i_1\} = \frac{[S]_1 - [S]_0}{i_1 - i_0} \tag{4-42}$$

and the first order polynomial prediction of $[S]_2$ becomes

$$[S]_{2,1stOrder} = [S]_0 + S\{i_0, i_1\}(i_2 - i_0) \tag{4-43}$$

which, in this case, is simply a linear extrapolation. This approach can be extended to higher order polynomials, as described in Eqn. 4-40, according to the number of intermediate specimen pairs that are available. Table 24 contains the elements for constructing a second order polynomial approximation of the ESM

Table 24. Construction of Interpolating Polynomial for the ESM.

Step	i	Divided Differences		
		Zeroth	**First**	**Second**
1	i_0	$S\{i_0\} = S_0$	$S\{i_0,i_1\}$	$S\{i_0,i_1,i_2\}$
2	i_1	$S\{i_1\} = S_1$	$S\{i_1,i_2\}$	
3	i_2	$S\{i_2\} = S_2$		

scale transformation matrix. It is important to note that higher order polynomials generally lead to more accurate predictions of the desired transformation matrix.

4.3.2. Application of Advanced ESM

The advanced ESM is now applied to the cantilever beam studies in Chapter 3 that were used to illustrate the effects of specimen distortion. For each case, the beam with large holes is considered as the product beam, and the beams with small holes and medium holes are used as intermediate specimens (see Figure 52). The transformation matrix between the product and the model ($\mathbf{S_3}$) is

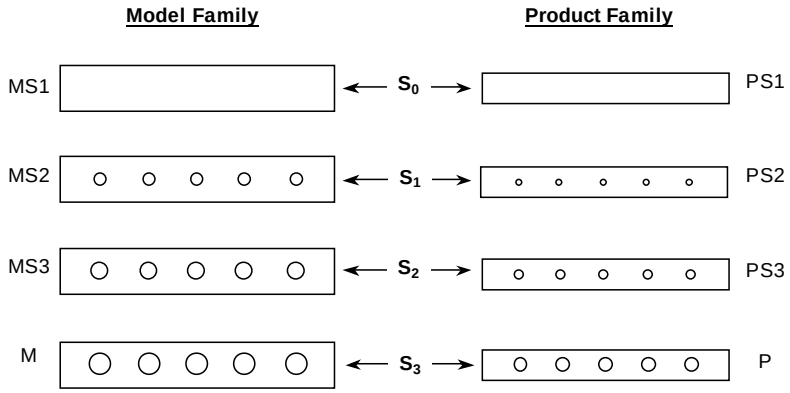

Figure 52. Application of Advanced Empirical Similarity Method.

predicted with both a first order polynomial (using $\mathbf{S_0}$ and $\mathbf{S_1}$) and a second order polynomial (using $\mathbf{S_0}$, $\mathbf{S_1}$, and $\mathbf{S_2}$).

The first step in constructing the divided differences shown in Table 24 is to calculate differences between transformation matrices (e.g. $\mathbf{S_1} - \mathbf{S_0}$). The difference between two matrices is calculated simply by subtracting each corresponding entry. Two matrices must, of course, be the same size in order to calculate their difference. The difference between two 3 x 3 matrices, for example, is given as follows:

$$\begin{bmatrix} a_{11} & a_{12} & a_{13} \\ a_{21} & a_{22} & a_{23} \\ a_{31} & a_{32} & a_{33} \end{bmatrix} - \begin{bmatrix} b_{11} & b_{12} & b_{13} \\ b_{21} & b_{22} & b_{23} \\ b_{31} & b_{32} & b_{33} \end{bmatrix} = \begin{bmatrix} a_{11}-b_{11} & a_{12}-b_{12} & a_{13}-b_{13} \\ a_{21}-b_{21} & a_{22}-b_{22} & a_{23}-b_{23} \\ a_{31}-b_{31} & a_{32}-b_{32} & a_{33}-b_{33} \end{bmatrix} \quad (4\text{-}44)$$

The next step in constructing the divided differences, which is implicit in constructing intermediate specimen pairs, is to quantify the step size of the dimension that is being discretized. In the case of the cantilever beams, the *form* dimension is being discretized, and the parameter that is being changed from one form to the next is the diameter of the holes. The "i" values in Table 24, therefore, are simply equal to the hole diameters, as shown in Table 25. Note that the increments in the steps need not be equal (e.g. $i_1 - i_0 = 0.15$ while $i_2 - i_1 = 0.10$).

Table 25. Step Values for Cantilever Beams.

Step	i	Value
1	i_0	0
2	i_1	0.15
3	i_2	0.25
4	i_3	0.35

We recognize that much more complicated changes in form can exist between a product and a product specimen than simply a variation in a single parameter, as in this example. In general, quantifying a change in form is difficult. Suppose, for example, that instead of going from small holes to large holes, we go from circular holes to non-circular holes (as in Figure 34). Rather than attempting to derive a geometric transformation to describe the change in form, we can instead quantify the *effect that the change in form has on the system parameter whose behavior varies between the product and the product specimen* (or between the model and the model specimen).

For example, in the first ESM study in Chapter 3, the nonlinear stress-strain curve of the model material causes the effective value of Young's modulus to decrease as hole diameters (and, consequently, operating stresses) increase. We could, therefore, use the change in the effective Young's modulus to quantify the change in form, since Young's modulus is the parameter that varies as the form changes. If changing from circular holes to non-circular holes doubles the effective value of Young's modulus, for example, this change in form could be assigned a normalized value (such as one) against which other changes in form are compared. While this procedure presents an alternative to quantifying complex changes in geometric shape, much more research is needed to develop the procedure into a reliable component of the advanced ESM technique.

We return now to the example at hand. With the matrix differences computed and the changes in geometric shape quantified, the transformation matrix between the product and the model ($\mathbf{S_3}$, as shown in Figure 52) can now be

calculated using Eqn. 4-40. First and second order polynomial predictions of $\mathbf{S_3}$ are calculated for each of the three ESM studies in Chapter 3. The improvement in the ESM results obtained from using the "corrected" transformation matrices, as described above, is shown in Figures 53 – 55 for the three ESM studies. The "degree of model distortion" plotted along the abscissa of the three figures is the same as that defined in Chapter 3.

The results from all three ESM studies show significant reductions in prediction error when corrected transformation matrices are used (except for some "numerical noise" where the degree of model distortion is zero). Although Figures 53 – 55 show results obtained from the circulant matrix approach, the diagonal matrix results exhibit similar trends.

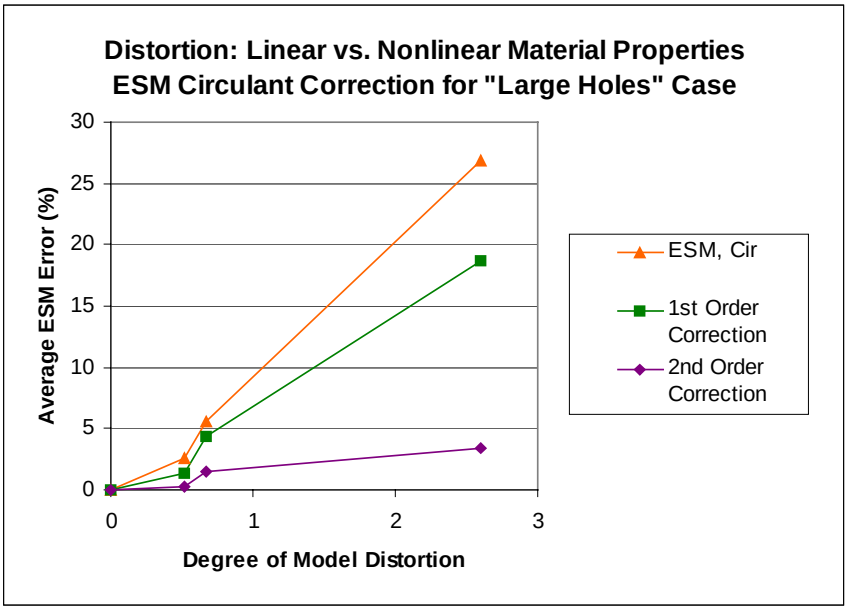

Figure 53. Reduction in Average Error for ESM Study 1.

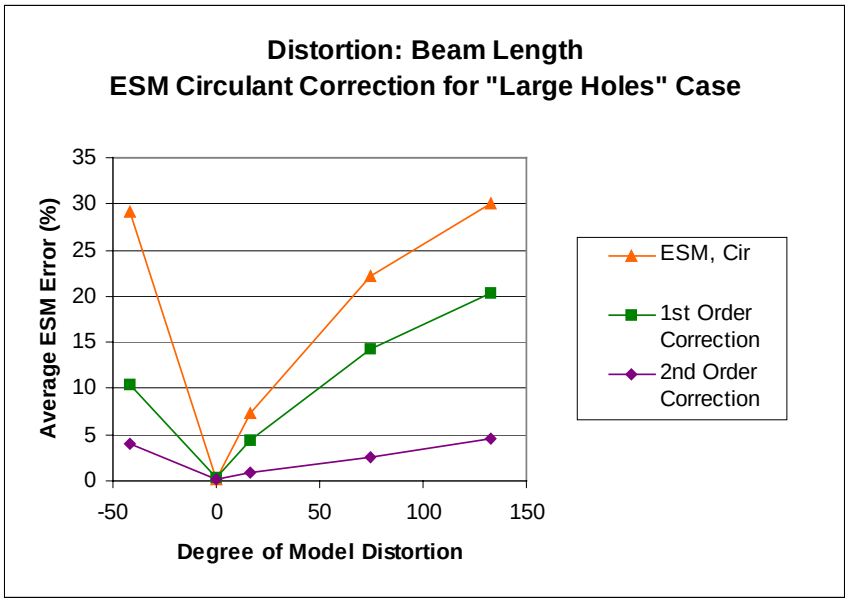

Figure 54. Reduction in Average Error for ESM Study 2.

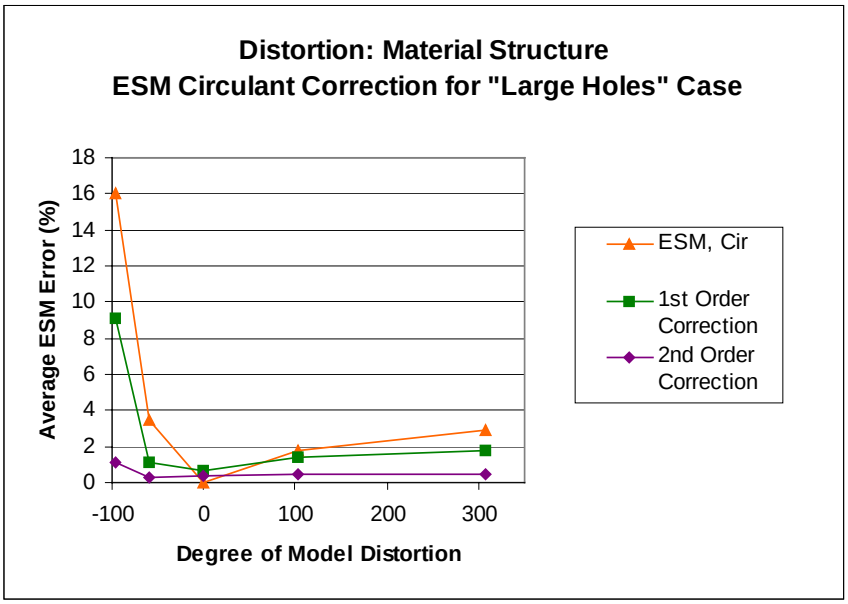

Figure 55. Reduction in Average Error for ESM Study 3.

The three preceding figures confirm that, in general, higher order polynomials produce more accurate predictions of the desired transformation matrix and, consequently, less prediction error. This result agrees with the example of the increasing orders of polynomials shown in Figure 51. This result is true when the function that is being approximated by the polynomial is a "higher order" function. If the function being approximated is a 1^{st} order function, a 1^{st} order polynomial will produce accurate results. However, since higher order polynomials do not produce *less accurate* results, and since the order of the function that describes a particular specimen distortion is typically unknown, a higher order polynomial is generally recommended for higher prediction accuracy.

There are obviously trade offs between the effort required to fabricate and test additional specimen pairs and the improved prediction accuracy that such additional specimen pairs provide. There are, in fact, many different factors that should be considered when deciding if the TSM, the ESM, the advanced ESM, or full scale testing is the most appropriate approach for functional testing of a particular product. The following chapter presents guidelines for choosing among the various approaches to functional testing in product design.

CHAPTER 5

Approach to Functional Testing in Product Development

The selection of an appropriate approach to functional testing in product development is based on several key factors. The "best" approach to functional testing will likely depend on the type of product that is being developed, the nature of the physical phenomenon that governs the behavior of the product, the stage of the design in the development process, and many other similar factors. The selection of an appropriate approach is by no means a trivial task.

This chapter contains two main sections: the first section presents guidelines for selecting an appropriate approach to functional testing; the second section provides numerical and experimental examples of how the guidelines can be used in product design.

5.1. GUIDELINES FOR SELECTING AN APPROACH TO FUNCTIONAL TESTING

Although no formula exists for selecting the "best" approach to functional testing for a given situation, several key questions are important in guiding that selection. The questions address three main issues: (1) what is the level of accuracy that is required for a given situation; (2) what is the level of accuracy that is attainable from the various methods; and (3) what is the level of effort, in terms of time and resources, that is required to implement each method. The method that is selected must provide a balance between *desired accuracy* and

required effort (one would obviously not want to expend an exorbitant amount of effort evaluating a concept that requires little accuracy). The "best" approach to functional testing will likely change as different types of products and different stages in the development process are considered.

The idea of selecting the "best" testing approach for a particular situation, and the fact that the "best" approach may vary as a design moves through the development process, is not a new concept. A similar concept, which is referred to as *prototype partitioning*, is presented in [Moe, 2002] as a method for selecting the best prototyping strategy for different circumstances. The three factors that are evaluated in prototype partitioning include cost flexibility, performance flexibility, and schedule flexibility. It is useful to note the similarities in the process for selecting an appropriate prototyping strategy, as presented in [Moe, 2002], and the process for selecting an appropriate testing strategy, as described in this section.

Each of the three main factors in selecting an appropriate testing approach is discussed in the following sections.

5.1.1. Desired Accuracy

Several factors are critical in determining an appropriate level of accuracy in the prediction of product performance. Such factors include the following:

- **Nature of Product**: The "nature of a product" includes such factors as the target market, development costs, consumer expectations, impact of product failure, etc. Such factors should be considered when determining the required accuracy of functional tests. The impact of

product failure, for example, varies widely among products. Products that support human life obviously demand a high level of accuracy since the impact of product failure is high. Other products, such as high-end consumer products must meet a high level of consumer expectation with respect to product performance in order to remain competitive.

- **Stage in Development Process**: The stage in the development process for which testing information is intended can have a significant impact on the required level of accuracy. Required accuracy is generally low in the early stages of development in which initial concepts are being evaluated, and increases in later stages of development as the product nears production. Therefore, a different approach to functional testing would likely be used in the later stages of development than was used in the initial stages.
- **Intent of Functional Testing**: Testing of physical models can be employed for a number of reasons, including evaluating new concepts, assessing design changes, validating virtual models, etc. [Otto, 2001]. The purpose of functional testing often changes as a design matures and progresses through the development process. The intent of the functional tests is a significant factor in determining the required accuracy of the test results.

5.1.2. Attainable Accuracy

Once the desired accuracy of functional tests has been determined, a testing approach that provides that level of accuracy is selected. The level of accuracy that can be attained from functional tests depends on the particular testing method that is used (i.e. TSM, ESM, advanced ESM, or full-scale tests), as well as on the accuracy of the experimental testing procedure. Figure 37 indicates that an improvement in prediction accuracy occurs as one moves from the TSM to the ESM to the advanced ESM and, finally, to full-scale testing. A measure of the accuracy of each method (which is evaluated by calculating the *error* of each method) is outlined below.

5.1.2.1. TSM Error

The error in the TSM approach can be approximated with the following equation (see [Cho, 1999]):

$$e_{TSM} \approx \left.\frac{\partial f}{\partial d_1}\right|_0 \Delta d_{m,1} + \left.\frac{\partial f}{\partial d_2}\right|_0 \Delta d_{m,2} + \cdots + \left.\frac{\partial f}{\partial d_N}\right|_0 \Delta d_{m,N} \qquad (5\text{-}1)$$

where d_i represents relevant system parameters for the function f, $\Delta d_{m,i}$ represents the deviation of the parameter from its "well-scaled" value (as determined from TSM scaling factors), and the subscript *0* represents the well-scaled point of the model. The error described by Eqn. 5-1 is an approximation since each term in the equation is simply a first order Taylor series expansion of the function *f*.

A review of Eqn. 5-1 reveals that TSM error is dependent on two factors. The first factor, which is given by $\frac{\partial f}{\partial d_i}$, represents the change in the function with respect to each governing parameter. We refer to this factor as the *TSM*

sensitivity. The second factor, which is given by $\Delta d_{m,i}$, represents the deviation of each relevant parameter from its well-scaled value. The value of $\Delta d_{m,i}$ is zero for systems that contain no model distortion. The value of $\Delta d_{m,i}$ increases as the degree of model distortion increases.

As an example of how to use Eqn. 5-1 to estimate TSM error for a particular problem, consider the cantilever beam example given in Section 3.2.1. Recall that the only parameter that is distorted in this system is Young's modulus. The distortion in Young's modulus comes from the fact that the stress-strain curve for the model material is nonlinear. As the size of the holes in the model beam increases, the maximum operating stress in the beam also increases. Figure 56 shows the maximum operating point along the stress-strain curve of Material 2 for each geometric shape (recall that Geometry 1 has small holes, Geometry 2 has medium holes, and Geometry 3 has large holes). The effective value of Young's modulus at the various operating points (as given by the slope of the stress-strain curve) is also shown in Figure 56.

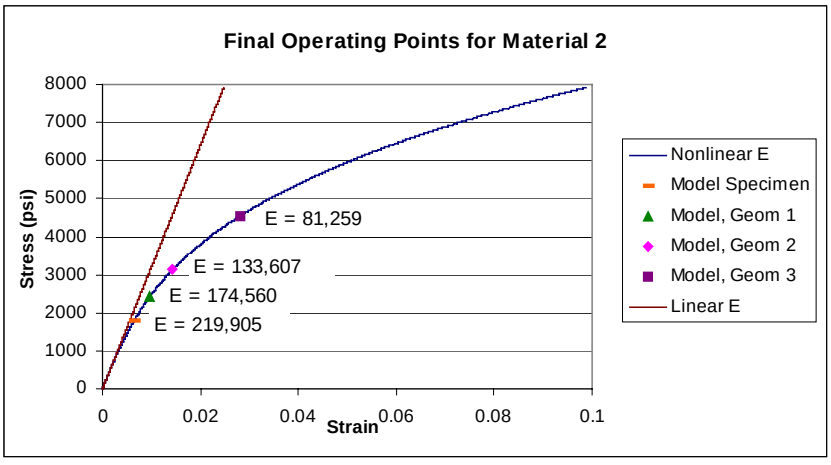

Figure 56. Effective Values of Young's Modulus for Material 2.

Now suppose that we can describe the deflection of the model specimen with the following analytical expression (see [Shigley, 1989]):

$$\delta = \frac{FL^3}{3EI} \tag{5-2}$$

where I is the moment of inertia of the cross section of the beam, and all other parameters are as described in Eqn. 2-15. Although Eqn. 5-2 ignores deflection due to shear stresses and assumes that the beam is limited to small deflections, it is nonetheless useful in illustrating the use of Eqn. 5-1 in estimating TSM error.

Since Young's modulus is the only governing parameter in Eqn. 5-2 that is not well scaled, Eqn. 5-1 reduces to

$$e_{TSM} = \frac{\partial \delta}{\partial E}\Delta E = \frac{FL^3}{3E^2 I}\Delta E\,. \tag{5-3}$$

The values of the governing parameters for both the model and product families, along with the TSM scale factors used in determining those values (see Eqn. 2-30), are shown in Table 26. Note in Table 26 that the scale factor for Young's modulus is calculated assuming a constant value of Young's modulus for the model family. Also note in Table 26 that, since the beam cross section is rectangular, the moment of inertia is calculated by substituting the width and height values of each beam into the following equation (see [Shigley, 1989]):

$$I = \frac{wh^3}{12}\,. \tag{5-4}$$

Suppose we want to estimate the TSM error for the cantilever beam with large holes (Geometry 3). From Figure 56 we see that the "deviated" value of Young's modulus for Geometry 3 is 81,259 psi. If we substitute this value of

Table 26. Parameter Values for TSM Error Study.

	TSM Scale Factor ($K = x_p / x_m$)	Value of Product Parameters (x_p)	Value of Model Parameters (x_m)
Applied Force (F)	10.72	20 lbs	1.87 lbs
Beam Length (L)	0.5814	4.00 in	6.88 in
Beam Width (w)	0.5814	0.50 in	0.86 in
Beam Height (h)	0.5814	0.125 in	0.215 in
Moment of Inertia (I)	$I = wh^3/12$	8.138e-5 in^4	7.123e-4 in^4
Young's Modulus (E)	31.72	10,150 ksi	320 ksi

Young's modulus, along with the other appropriate parameter values from Table 26, into Eqn. 5-3, we get the following expression for TSM error:

$$e_{TSM} = \frac{(1.87lb)(6.88in)^3}{(3)(320{,}000\,psi)^2\,(7.1225\times10^{-4}\,in^4)}(320{,}000\,psi - 81{,}259\,psi) = 0.66in \qquad (5\text{-}5)$$

Note that the value calculated in Eqn. 5-5 represents an absolute error, rather than a percent error (we cannot calculate a percent error at this point since this is an *a priori* estimate of TSM error and we do not yet know the actual deflection of the product). Also note that the value in Eqn. 5-5 represents an upper *error boundary* since the deviation in Young's modulus used in Eqn. 5-5 is the *maximum deviation* (the actual deviation varies along the length of the beam as the cross section changes).

The actual error in the TSM prediction of beam deflection for Geometry 3, as determined from the finite element study described in Section 3.2.1, is found

to be 0.16 inches. This level of error is well within the upper TSM error bound described in Eqn. 5-5 (the two error values are comparable since they are both calculated at a maximum applied load of 1.87 lbs).

5.1.2.2. ESM Error

Errors in the ESM approach occur when there is distortion or inconsistent behavior *within* the product or model families (this is in contrast to TSM errors, which occur when distortions exist *between the product and model*). The ESM captures distortions between the product and the model as long as the same distortion that exists between the product and model also exists between the product specimen and model specimen. If, however, the distortion between the product and model is not the same as that between the specimen pair (this situation is referred to as *specimen distortion*), errors result form the ESM approach.

The level of error in the ESM approach can be approximated with the following equation:

$$e_{ESM} \approx abs\left[\left.\frac{\partial f}{\partial d_1}\right|_0\left(\left.\frac{\partial d_1}{\partial GS}\right|_{ps} - \left.\frac{\partial d_1}{\partial GS}\right|_{ms}\right)\Delta GS + \cdots + \left.\frac{\partial f}{\partial d_N}\right|_0\left(\left.\frac{\partial d_N}{\partial GS}\right|_{ps} - \left.\frac{\partial d_N}{\partial GS}\right|_{ms}\right)\Delta GS\right] \qquad (5\text{-}6)$$

where d_i represents relevant system parameters for the function f, GS represents *geometric shape*, and ΔGS represents the change in geometric shape between the specimen and the corresponding model or product. The subscripts *ps* and *ms* within the parentheses in Eqn. 5-6 indicate evaluation of the partial derivative at the product specimen shape and the model specimen shape, respectively. The

subscript *0* indicates evaluation of the partial derivative at the "well-scaled" (or *nominal*) values of the model parameters.

Equation 5-6 shows that ESM error is governed by three factors. The first factor, which is given by $\frac{\partial f}{\partial d_i}$, represents the change in the function with respect to each governing parameter (this factor is referred to as *TSM sensitivity* in Eqn. 5-1). The second factor, which is given by $\frac{\partial d_i}{\partial GS}$, represents the change in each governing parameter as the geometric shape changes (as from the shape of the model to the shape of the model specimen). The quantity $\left(\left.\frac{\partial d_i}{\partial GS}\right|_{ps} - \left.\frac{\partial d_i}{\partial GS}\right|_{ms} \right)$ in Eqn. 5-6 indicates how a change in geometric shape affects a governing parameter in the product family *differently* than it affects the same parameter in the model family. The term $\frac{\partial d_i}{\partial GS}$ in Eqn. 5-6 is referred to as *ESM sensitivity*. Specimen distortions, which produce errors in the ESM approach, occur when the ESM sensitivity for a particular parameter is different in the product family than in the model family. The value of $\left(\left.\frac{\partial d_i}{\partial GS}\right|_{ps} - \left.\frac{\partial d_i}{\partial GS}\right|_{ms} \right)$ is zero for systems that contain no specimen distortion. The (absolute) value of $\left(\left.\frac{\partial d_i}{\partial GS}\right|_{ps} - \left.\frac{\partial d_i}{\partial GS}\right|_{ms} \right)$ increases as the degree of specimen distortion increases.

The third factor in Eqn. 5-6, which is given by ΔGS, represents the change in geometric shape between the specimen and the corresponding model or product. It should be noted that ΔGS in Eqn. 5-6 is the same as Δi in Figure 49. Evaluation of the term ΔGS requires a *discretization of geometric shape* (i.e. we

need to determine a *value* that describes *how much* the geometric shape changes between the specimen and the corresponding model or product). Difficulties associated with this requirement are discussed in more detail later in the chapter.

In order to demonstrate how to use Eqn. 5-6 for estimating ESM error, we again consider the cantilever beam example from Section 3.2.1. The ESM setup for this example is shown in Figure 25. We must keep in mind that, for ESM error, we are concerned with changes in the governing parameters *within the product and model families* (i.e. changes in governing parameters that are caused by the change in geometric shape between the model and model specimen, or between the product and product specimen).

A review of Eqn. 5-2 shows that deflection of the cantilever beam is dependent on four governing parameters: applied force *F*; beam length *L*; Young's modulus *E*; and moment of inertia *I*. Since the same force of 20 lbs is applied to both the product and the product specimen (and the same *scaled* force of 1.87 lbs is applied to the model and the model specimen), the ESM sensitivity for force ($\frac{\partial F}{\partial GS}$) is *zero* for both the product and the model. Likewise, since the beam length does not change between the product and the product specimen, or between the model and the model specimen, the ESM sensitivity for length ($\frac{\partial L}{\partial GS}$) is also zero for both the product and the model.

We now consider the moment of inertia of the product and model beams. We can easily see from Figure 25 that the moment of inertia *does* change as we change shape from the specimen to the model or product. However, since the change in shape between the product specimen and the product is identical to the

change in shape between the model specimen and the model (i.e. the model specimen and the product specimen are geometrically similar, as are the model and the product), the ESM sensitivity for moment of inertia ($\frac{\partial I}{\partial GS}$) is *the same* for both the product and the model. With equal ESM sensitivities for moment of inertia, the value of $\left(\left.\frac{\partial I}{\partial GS}\right|_{ps} - \left.\frac{\partial I}{\partial GS}\right|_{ms} \right)$ in Eqn. 5-6 goes to zero.

Finally, we consider the Young's modulus of the product and model beams. Since the value of Young's modulus is the same (10,150 ksi) for both the product and the product specimen, the ESM sensitivity for Young's modulus ($\frac{\partial E}{\partial GS}$) is zero for the product family. However, since the Young's modulus for the model family varies as the geometric shape changes (see Figure 56), the ESM sensitivity for Young's modulus ($\frac{\partial E}{\partial GS}$) is *not zero* for the model family. This ESM sensitivity for Young's modulus in the model family is the source of specimen distortion (and of ESM error) in this example.

In light of the above discussion, we can now express Eqn. 5-6 in the following simplified form (for this specific example):

$$e_{ESM} \approx \frac{\partial \delta}{\partial E} \left.\frac{\partial E}{\partial GS}\right|_{ms} \Delta GS \qquad (5\text{-}7)$$

The term $\frac{\partial \delta}{\partial E}$ in Eqn. 5-7, which is the same TSM sensitivity described in Eqn. 5-3, is given by

$$\frac{\partial \delta}{\partial E} = \frac{FL^3}{3E^2 I}. \qquad (5\text{-}8)$$

The term $\left.\frac{\partial E}{\partial GS}\right|_{ms} \Delta GS$ in Eqn. 5-7 represents the change in the value of Young's modulus as the geometric shape changes from the model specimen to the model. The value of this term can often be very difficult to determine either analytically or experimentally. For this example, however, the changes in Young's modulus that result from changes in geometric shape have been determined from the finite element study in section 3.2.1, and are shown in Figure 56. Although we do not evaluate the quantity $\left.\frac{\partial E}{\partial GS}\right|_{ms} \Delta GS$ analytically, we understand that it represents the change in Young's modulus between the model specimen and the model, and we can determine that change from the graph in Figure 56. Equation 5-7 can therefore be written as follows:

$$e_{ESM} \approx \frac{FL^3}{3E^2 I}(E_{ms} - E_m) \qquad (5\text{-}9)$$

Substituting in the appropriate values for Young's modulus from Figure 56, along with the other required parameter values listed in Table 26, Eqn. 5-9 is evaluated as follows:

$$e_{ESM} = \frac{(1.87lb)(6.88in)^3}{(3)(320{,}000\,psi)^2(7.1225\times10^{-4}\,in^4)}(219{,}905\,psi - 81{,}259\,psi) = 0.39in \qquad (5\text{-}10)$$

As in the case of the TSM, the ESM error described by Eqn. 5-10 represents an absolute error, rather than a percent error (we cannot calculate a percent error at this point since this is an *a priori* estimate of ESM error and we do not yet know the actual deflection of the product). Also, the ESM error described by Eqn. 5-10 is an approximation since the values of Young's modulus used in the equation are

maximum values. The actual value of Young's modulus varies along the length of the beam (i.e. the stress level and, consequently, the effective value of Young's modulus, as determined by the slope of the nonlinear stress-strain curve of the material, varies along the length of the beam).

The actual error in the ESM prediction of beam deflection for Geometry 3, as determined from the finite element study in Section 3.2.1, is 0.10 inches. This level of error is well below the ESM error estimate shown in Eqn. 5-10 (the two error values are comparable since they are both calculated at a maximum applied load of 1.87 lbs).

It is important to highlight the difference in the TSM error estimation described by Eqn. 5-5 and the ESM error estimation described by Eqn. 5-10. Both equations contain the same term describing the TSM sensitivity for Young's modulus ($\frac{\partial \delta}{\partial E}$). The distinction between the two equations lies in the fact that the TSM error estimation involves the difference between the Young's modulus of the model and the "well-scaled" value of Young's modulus (as determined from TSM scale factors), while the ESM error estimation involves the difference between the Young's modulus of the model and that of the model specimen. In this example, the ESM error in Eqn. 5-10 is much smaller than the TSM error in Eqn. 5-5. This result is generally true for situations in which the nonlinearity in the system can be described with a monotonically increasing or decreasing function. In such cases, the model specimen captures (at least some of) the nonlinearity (as shown in Figure 56) and, therefore, gives a better prediction of product behavior than the TSM.

5.1.2.3. Advanced ESM Error

The error in the advanced ESM depends on the order of the (Lagrange) polynomial that is used in the method. A Lagrange polynomial of degree *n* has an error formula of the following form:

$$\frac{f^{(n+1)}(\xi(x))}{(n+1)!}(x-x_0)(x-x_1)\cdots(x-x_n) \qquad (5\text{-}11)$$

where $f^{(n+1)}$ represents the (n+1)th derivative of the function *f*, and ($\xi(x)$) is some number in the interval [*a,b*] which contains the numbers $x_0, x_1, \ldots, x_n$ and in which $f \in C^{n+1}[a,b]$ (see [Burden, 1989]). Higher order polynomials involve higher order derivatives of the function and, in general, lower values of error. The error formula in Eqn. 5-11 can be used only in those situations in which the governing function that describes the behavior of interest (along with its first n + 1 derivatives) is known. In practice, this information is generally unknown (that is why we are evaluating the behavior experimentally instead of analytically). The formula in Eqn. 5-11 serves primarily as a qualitative evaluation of the error in the advanced ESM and illustrates the fact that the error is on the order of the (n+1)th derivative of the governing function *f*.

5.1.2.4. Experimental Error

It is important at this point to make a note about experimental error and highlight the impact that such error can have on prediction accuracy. It is noted in the previous section that higher order polynomials tend to increase the prediction accuracy that is attainable with the advanced ESM approach. While this statement is true in theory, the practical application of the advanced ESM technique

demands that we consider the impact of experimental error on prediction accuracy.

In order to assess the impact of experimental error on the accuracy of the advanced ESM technique, let's consider the polynomial curve fit of the function $f(x) = x^3 + 2x^2 + 3x + 7$ that is discussed in section 4.3.1. Recall that, since the function is 3rd order, a 3rd order Lagrange polynomial fits the curve perfectly, while 2nd and 1st order polynomials yield less accurate results (see Figure 51).

Now suppose that we include the effects of experimental error (i.e. random error or repeatability error in the experimental setup) by attaching a tolerance value to each functional evaluation. The impact of such experimental error on the prediction accuracy of the polynomial will depend on the nature of the function being evaluated as well as on the magnitude of the error.

In order to illustrate the potential impact of experimental error on the prediction accuracy of a polynomial, let's assume that each evaluation of the function $f(x) = x^3 + 2x^2 + 3x + 7$ includes a tolerance of ±1.0. Let's assume also that the function is evaluated at the points $x = 0$, 1, 2, and 3 (as in Section 4.3.1.), and that the value of the function at the point $x = 4$ is to be predicted using 1st, 2nd, and 3rd order polynomials.

Table 27 shows the results of the polynomial predictions when the maximum tolerance (either +1.0 or –1.0) is applied to each functional evaluation (the polynomial predictions are calculated using the procedure outlined in section 4.3.1.). Note that the 1st order polynomial matches the actual function value at the first two points, the 2nd order polynomial matches the actual function value at the

Table 27. Polynomial Predictions Including Experimental Error.

				Polynomial Predictions		
x	***f(x)*** **Theoretical**	**Experimental Error**	***f(x)*** **Measured**	**1st Order**	**2nd Order**	**3rd Order**
0	7.0	+ 1.0	8.0	8.0	8.0	8.0
1	13.0	- 1.0	12.0	12.0	12.0	12.0
2	29.0	+ 1.0	30.0	16.0	30.0	30.0
3	61.0	- 1.0	60.0	20.0	62.0	60.0
4	115.0	n/a	n/a	24.0	108.0	100.0

first three points, and the 3rd order polynomial matches the actual function value at the first four points (as required for polynomial curve fits). Note also that, in this case, the 2nd order prediction of the value *f*(4) is closer to the theoretical value than the 3rd order prediction! This result is also shown in the plot in Figure 57.

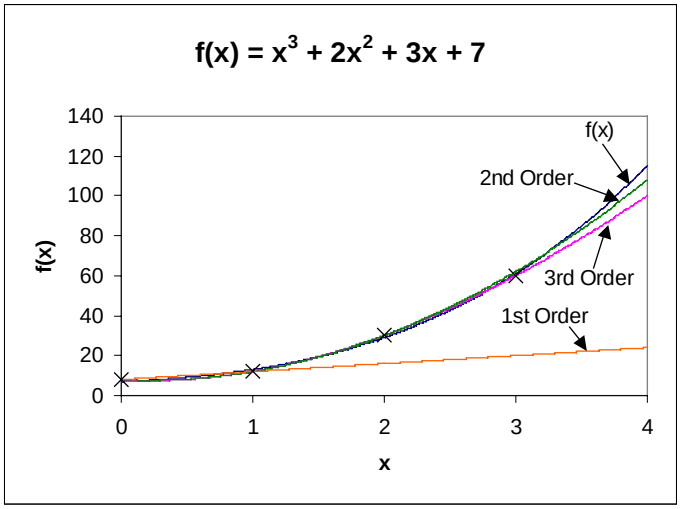

Figure 57. Polynomial Curve Fits when Experimental Error is Considered.

The prediction error illustrated in Figure 57, which results when experimental data (with inherent experimental error) is fit to a polynomial curve, is affected by the magnitude of the experimental error as well as by the step size used in creating the curve. In order to illustrate this concept more clearly, consider the simple linear function $f(x) = x$. Let's suppose that each data point involves ten percent experimental error (except for $f(0)$, which we assume to be exactly equal to zero). Let's also suppose that $f(1)$ is used as the second data point, and that the measured value of this point is ten percent below the actual value. The first order polynomial approximation of the function is shown in Figure 58. If we want to predict the value of $f(4)$ with the first order polynomial, our prediction is off by ten percent.

Now let's suppose that we approximate the curve with a second order polynomial. Recall that, with no experimental error, a second order polynomial fits a linear curve as well as a first order polynomial. We want to see, however, how experimental error and different step sizes affect prediction error. The first

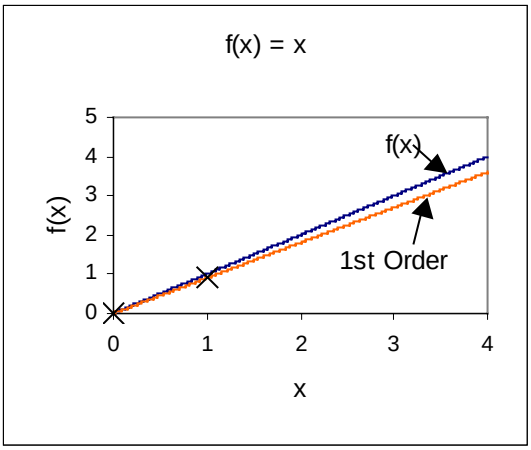

Figure 58. First Order Polynomial Including Experimental Error.

two data points for the second order polynomial are the same as those used in the first order case. Let's suppose, however, that the measured value of the third data point is ten percent *above* the actual value. The magnitude of the prediction error that results from such experimental error varies depending on the step size between the second and third data points. Let's consider three cases that represent three different step sizes between the second and third data points: Case 1 has a step size of 2.0; Case 2 has a step size of 1.0; and Case 3 has a step size of 0.5. The second order polynomial for each of these cases is shown in Figure 59. Note that the prediction error for *f(4)* increases as the step size decreases, or, in other words, as the distance between the third data point and *f(4)* increases (20% error for Case 1, 50% error for Case 2, and 110% error for Case 3).

The results in Figure 59 show that higher order polynomials can produce greater prediction error than lower order polynomials when experimental error is included. The results in Figure 59 also indicate that data points close to the

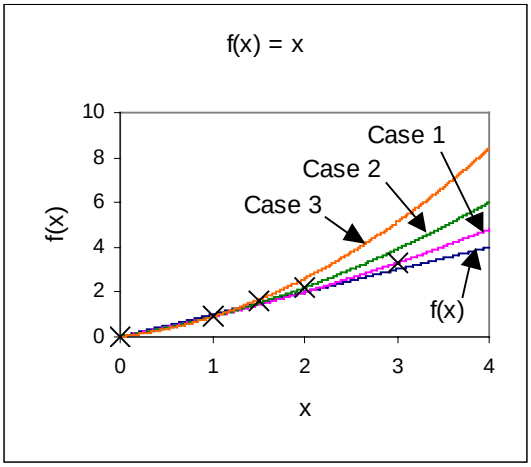

Figure 59. Second Order Polynomials Including Experimental Error.

"prediction point" tend to produce less error than points that are farther away. It should also be obvious that, for a given set of data points, prediction error will tend to increase as the magnitude of the experimental error increases. We can propose, therefore, that the magnitude of the experimental error, the location of the data points, and the nature of the function itself can affect the prediction error for higher order polynomials. The example given in this section can easily be repeated for different analytical functions, different step sizes, and different magnitudes of experimental error in order to explore this idea more fully.

The fact that experimental error can, in some cases, cause higher order polynomials to produce *less accurate* predictions of a functional behavior than lower order polynomials has obvious implications to the advanced ESM technique. Since the impact that experimental error has on prediction accuracy depends on the nature of the functional behavior that is being predicted, the location of the data points, and the magnitude of the experimental error, it is difficult (if not impossible) to determine *a priori* the "best" order polynomial to use in the advanced ESM technique. In general, however, prediction error is reduced when experimental error is reduced or when data points that are close to the "prediction point" are used.

5.1.2.5. Summary of Attainable Accuracy

As indicated in the preceding sections, and as illustrated in Figure 37, the accuracy of predicted product behavior tends to increase as we move from the TSM to the ESM to the advanced ESM and, finally, to full-scale testing. This increase in accuracy is due to the fact that each successive method involves

additional information that more accurately reflects the behavior of the product. The additional information in the advanced methods does, however, require additional effort (such as in time and money required to fabricate and test specimen pairs). The increased effort that is required to obtain increased accuracy in functional testing is illustrated qualitatively in Figure 60. Although the trend shown in Figure 60 is roughly linear, the actual placement of each method on the graph varies with each situation (full-scale testing, for example, may require less effort in some situations than the advanced ESM). The decision of which method to use for a given situation requires that a balance between the *desired accuracy* of the test results and the *required effort* to conduct the tests be found.

It is also important at this point to make a note regarding the use of the error formulas that are presented in the preceding sections. The error formulas for all of the similitude techniques rely on knowledge of the function that describes the behavior of interest, and of how that function is affected by changes in the

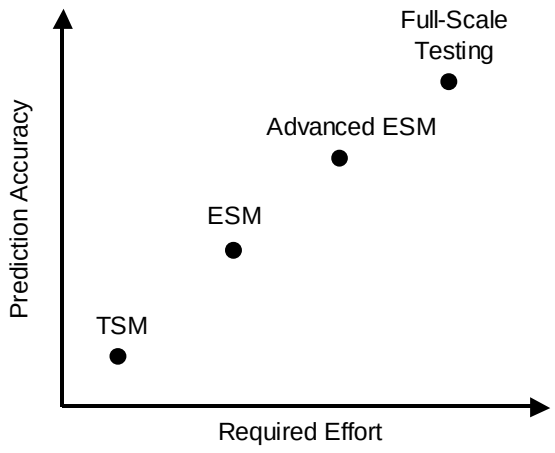

Figure 60. Accuracy vs. Effort in Functional Testing.

various system parameters. Such in-depth knowledge of a system is rarely available in situations where physical testing is an essential element of product evaluation (otherwise the behavior of the system would simply be evaluated analytically). The error formulas presented in the preceding sections do, however, give the designer or engineer a better understanding of the source of the error and allow for a more informed engineering decision to be made regarding the type of similitude, if any, that should be used in a given situation.

5.1.3. Required Effort

We turn now to an evaluation of the effort that is required to implement the various approaches to functional testing. As in the case of accuracy, no formula exists for determining precisely the level of effort that is needed for each testing approach; instead, a determination of required effort is guided by considering several key factors. Such factors include the following:

- **Difficulty in Constructing the Product**: The easier it is to fabricate the product, the sooner one will move from similitude techniques to full-scale testing of the product. The value of similitude techniques increases as the difficulty in product construction increases.
- **Difficulty in Constructing a Well-Scaled Model**: The accuracy of the TSM approach depends on one's ability to construct a well-scaled model (i.e. a model that exhibits no *model distortions*). The ESM, however, captures the effects of model distortions in a simplified specimen pair. Therefore, the more difficult it is to construct a well-scaled model (whether that difficulty comes from a lack of availability

of specific materials, a lack of knowledge of governing parameters, nonlinearities in governing parameters, or any other factor), the sooner one will move from the TSM approach to the ESM approach.

- **System Complexity**: The higher the level of complexity, the more difficult it is to identify all of the relevant parameters that influence the behavior of the system. Since the TSM relies on one's ability to identify all of the governing parameters explicitly (whereas the ESM captures the effects of the governing parameters implicitly), the higher the level of complexity of a system, the sooner one will move from the TSM approach to the ESM approach.
- **Difficulty in Obtaining Product and Model Specimens**: The difficulty involved in constructing, or otherwise obtaining, product and model specimens will determine whether the ESM or the advanced ESM should be used in place of full-scale testing. In some cases, construction of a specimen pair may be as difficult as constructing the full-scale product. In these cases, full-scale testing would obviously be preferred over the ESM technique. In other cases, however, product specimens may be readily available (e.g. previous versions of a product) or easily constructed (relative to the full-scale product). In these cases, the ESM or advanced ESM techniques may be used.
- **Difficulty in Testing**: If the level of difficulty in performing functional tests is relatively high, the approaches which involve the fewest tests (viz. TSM and full-scale testing) should be considered.

When determining the approach that is most appropriate for a specific situation, the factors that indicate the effort required for each approach must be considered together with the factors that indicate the available accuracy from each method. After considering these factors, the approach that gives the desired level of accuracy at the minimal effort is selected.

In order to facilitate the selection of an appropriate approach to functional testing, the guidelines presented above are formalized into a step-by-step procedure, as shown in Table 28. The procedure requires that, for a given situation, an assessment be made of the *required accuracy* of the functional tests, the *achievable accuracy* of the various testing methods, and the *required effort* to implement the various methods. Each assessment is then assigned a value from low to high, as shown in Table 28. Some of the categories list several factors that should be considered when making the assessment.

Once all of the appropriate assessments have been made, the values of the assessments are entered into the template shown in Table 29. Note that the numbers in the cells of the template correspond to the steps shown in Table 28. Each cell is filled in with the assessment value (i.e. low, medium, high) assigned to that step. Note that the cell corresponding to the desired level of effort is not used since we assume that the method that requires the least effort, and which also meets the requirement for accuracy, will be selected as the best method.

The completed template is now used to create a 2D graph similar to that shown in Figure 61. The dotted line in Figure 61 represents the required accuracy of the tests. The method that is above the line (i.e. that meets the required level of

accuracy) and that requires the lowest level of effort (i.e. that is farthest to the left on the graph) is selected as the best method for the given situation.

Table 28. Procedure for Selecting an Appropriate Testing Approach.

Step	Assessment
1. Determine the required accuracy of the tests	Low - High
• Consider the nature of the product	
• Consider the stage in the development process	
• Consider the underlying purpose of the tests	
• Consider other aspects that may affect required accuracy	
2. Evaluate the accuracy of the various techniques	
2a. Evaluate TSM error	Low - High
2b. Evaluate ESM error	Low - High
2c. Evaluate advanced ESM error	Low - High
• Consider magnitude of experimental error	
• Consider location of data points	
2d. Evaluate full-scale testing error	Low - High
3. Evaluate the required effort for the various techniques	
3a. Evaluate TSM effort	Low - High
• Evaluate the difficulty in constructing a well-scaled model	
• Evaluate the level of system complexity	
3b. Evaluate ESM effort	Low - High
• Evaluate the difficulty in obtaining specimens	
• Evaluate the difficulty in performing functional tests	
3c. Evaluate advanced ESM effort	Low - High
• Evaluate the difficulty in obtaining specimens	
• Evaluate the difficulty in performing functional tests	
3d. Evaluate full-scale testing effort	Low - High
• Evaluate difficulty in fabricating the product	

Table 29. Summary of Selection Procedure.

	Accuracy	**Effort**
Required	1	n/a
TSM	2a	3a
ESM	2b	3b
Advanced ESM	2c	3c
Full-Scale Testing	2d	3d

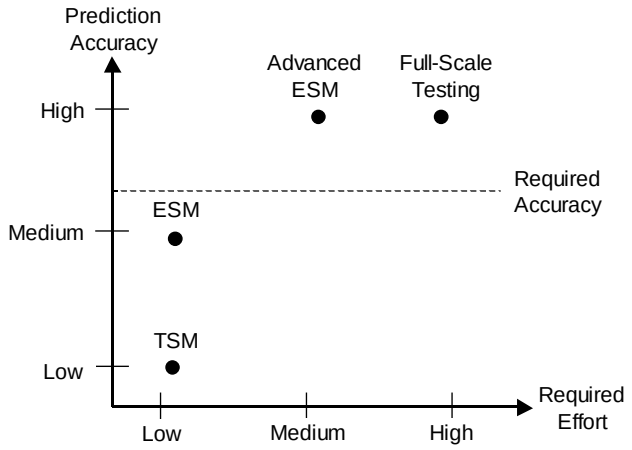

Figure 61. Graph for Selecting Appropriate Testing Method.

The procedure for selecting an appropriate approach to functional testing, as outlined in this section, is now illustrated in three practical examples.

5.2. APPLICATIONS OF FUNCTIONAL TESTING

Three specific examples (two experimental and one numerical) are now considered in which various approaches to functional testing are compared. The

examples expand on several important aspects of functional testing that have been introduced earlier. The first example involves experimental testing of the static deflection of a cantilever beam. The second example involves a numerical evaluation of steady state temperature in a heat transfer problem. The third example uses similitude techniques in the evolution of a headphone design.

5.2.1. Experimental Evaluation of Static Deflection

The product whose behavior is to be predicted in this case is a cantilever beam with six evenly spaced holes along its length. The dimensions of the beam are shown in Figure 62. The product beam is to be made of 6061 aluminum. A total load of 3.0 lbs is to be applied five inches from the fixed end. The static deflection of the beam at the point where the load is applied is to be monitored at five different increments of load (up to 3.0 lbs). The state vector of interest is, therefore, a deflection vector with five entries, each of which corresponds to a particular load.

The goal of this experiment is to use a rapid prototype (RP) model beam, along with an appropriate similitude technique, to predict the deflection of the

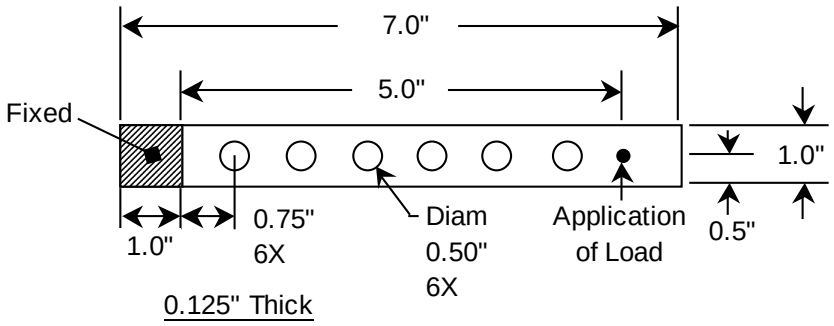

Figure 62. Dimensions of Product Beam.

product beam. A polymeric material called Duraform™ is used in the selective laser sintering (SLS) process to create the model beam (and any model specimens).

In order to select the best testing approach for this situation, we follow the procedure outlined in the previous section. Each step in the procedure is summarized below.

Step 1: Determine the required accuracy of the tests. Since this is somewhat of a "hypothetical" problem, we do not evaluate the various product characteristics suggested in Table 28. Let's suppose, however, that we want a relatively accurate prediction of beam deflection (less than 10% error). We will consider this level of accuracy to be in the "medium" category.

Step 2: Evaluate the accuracy of the various techniques. We consider the accuracy of each method below:

TSM: We look first at the TSM approach. Since the complexity of the system (i.e. beam) is relatively low, the governing parameters can be easily determined, and the TSM scale factors can be created. There are, however, several potential sources of model distortion that could produce errors in the TSM results. These potential model distortions include the following (see Figure 16):

- **Nonlinear Material Behavior**: Since Duraform™ is a polymeric material, and since polymeric materials generally have a nonlinear stress-strain relationship, we can assume that the model beam will exhibit (at least to some extent) variable values of Young's modulus. In addition, since aluminum has a relatively linear stress-strain

relationship, we can expect the product beam to maintain a constant value of Young's modulus. This difference in material behavior is a source of model distortion.

- **Distinct Material Structures**: Since the selective laser sintering process (along with most other rapid prototyping processes) creates parts layer by layer, the resulting part structure exhibits a form of orthotropy known as *transverse isotropy* (see Section 3.2.3. and [Cho, 1998b]). Aluminum, on the other hand, has an isotropic material structure. These distinct material structures between the model and the product represent an additional source of model distortion.
- **Unknown Material Property Values**: Although most rapid prototyping materials have published material property information, it is well known that many factors (such as processing parameters, environmental conditions, elapsed time after processing, etc.) can affect the final material properties of an RP part [Dulieu-Barton, 2000; Watson, 1999]. Any difference between the actual material properties of an RP part and the published values (which are used to construct TSM scaling factors) will result in model distortion and TSM error.

The model distortions described above cause the TSM error (see Eqn. 5-1) to increase. Because of the number and magnitude of the model distortions, we consider the accuracy of the TSM to be in the "low" category in this case.

ESM: Beams with no holes are selected for the specimen pair. We find, however, that potential specimen distortions may exist among the model family.

These potential sources of specimen distortions include the following (see Figure 23):

- **Distinct Operating Point along a Nonlinear Material Property Curve**: Since the stress-strain curve of the model material will likely be nonlinear, and since the holes will cause the model beam to experience a higher operating stress than the model specimen, we expect the model and model specimen to have distinct values of effective Young's modulus (see Section 3.2.1.).
- **Functionally Coupled Parameters**: Since total deflection is the summation of deflection due to normal stresses and deflection due to shear stresses, and since both components of deflection involve material property and geometric information, we expect total deflection to be a "functionally coupled value" in which geometry and material property information can not be isolated, as required by the ESM. This source of specimen distortion is illustrated numerically in Section 3.2.3.

The specimen distortions described above cause the ESM error (see Eqn. 5-6) to increase. Since the magnitude of the ESM error that results from the specimen distortions is assumed to be smaller than the TSM error, we assign the accuracy of the ESM approach to the "medium" category.

Advanced ESM: The advanced ESM (with a single intermediate specimen pair) should correct for the specimen distortion described in the previous section and provide a more accurate prediction than the ESM approach.

The advanced ESM is therefore assigned to the "high" category for accuracy. It should be noted, however, that since the testing process involves experimental error, additional specimen pairs could result in less accurate predictions (as illustrated in Section 5.1.2.4.). If the experimental error is anticipated to be significant, a single intermediate specimen pair is recommended for the advanced ESM approach.

Full-scale testing: The accuracy of full-scale testing is assumed to be high.

Step 3: Evaluate the required effort for the various techniques. As in Step 1, evaluating the specific characteristics of the product is not relevant in this example since we are considering a "hypothetical" product. Let's assume, however, that fabrication of the product falls in the "high" effort category, fabrication of product specimens falls in the "medium" effort category, and fabrication of all models and model specimens falls in the "low" effort category.

The assessments described above allow us to fill in the selection template as shown in Table 30. The corresponding 2D graph is shown in Figure 63. With

Table 30. Assessments for Deflection Example.

	Accuracy	**Effort**
Required	Medium	n/a
TSM	Low	Low
ESM	Medium	Medium
Advanced ESM	High	Medium
Full-Scale Testing	High	High

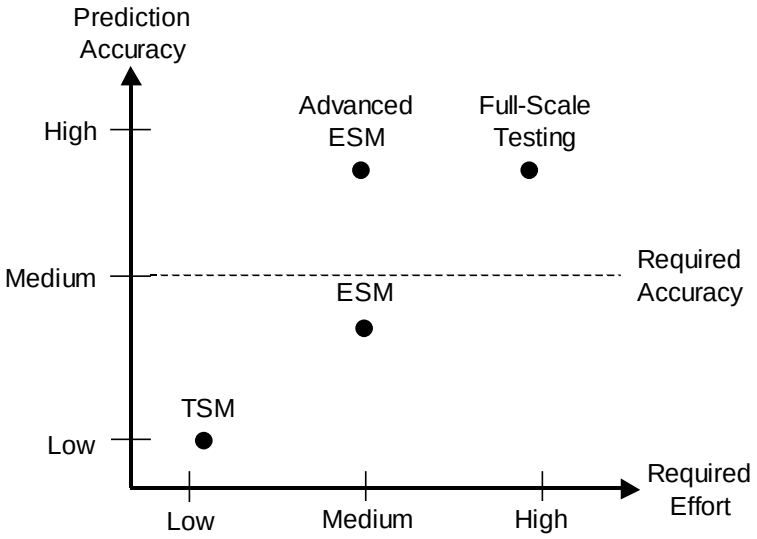

Figure 63. Selection Graph for Deflection Example.

the use of Table 30 and Figure 63, we select the advanced ESM technique (with a single intermediate specimen pair) as the best approach for this situation.

We now proceed with setting up the experiment. The size of the model beam is chosen to be the same as that of the product beam since the SLS process can create a beam with the dimensions shown in Figure 62 (if the product beam were longer than approximately 10 inches, the size of the model beam would need to be scaled down in order to fit within the build chamber of the SLS machine). The beams in the original specimen pair have an overall size equal to that shown in Figure 62, but contain no holes. The beams in the intermediate specimen pair have an overall size equal to that shown in Figure 62, but contain holes that are half as large as those in the product and model beams. The advanced ESM setup is shown in Figure 64 (note that *MS* in Figure 64 denotes *model specimen* and *PS* denotes *product specimen*).

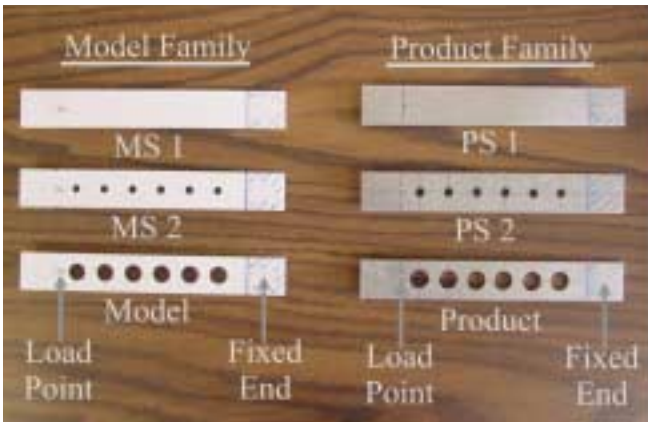

Figure 64. Advanced ESM Setup for Beam Experiments.

The beams are prepared for testing by fixing (i.e. clamping) one end of the beam and applying the load five inches from the fixed end. Calipers are mounted to a stand and are used to measure the static deflection of the beam at each increment of the load. The experimental setup is shown in Figure 65.

Although the ESM does not require that a "properly scaled" load be applied to the model beam (as long as the same load that is applied to the model

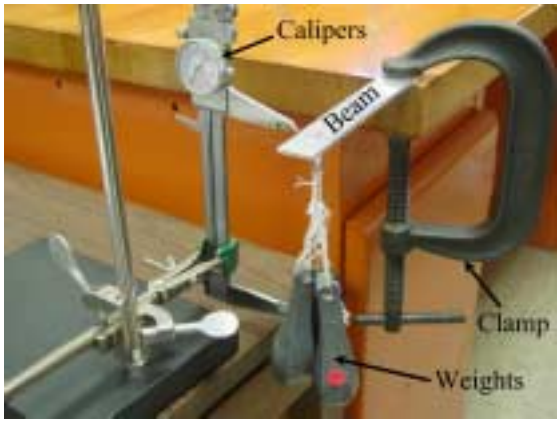

Figure 65. Experimental Setup for Beam Experiments.

beam is also applied to the model specimens), the examples in Section 3.2 illustrate the fact that, when specimen distortions are present, ESM error is reduced by minimizing the level of model distortion. Therefore, the force to be applied to the model beam (as well as to the model specimens) is determined from TSM scale factors, along with published material property values for both the product and the model. The TSM scale factors for the deflection of a cantilever beam, which are developed in Chapter 2, are as follows:

$$K_\delta = K_h \quad if \quad K_w = K_h, \quad K_F = K_h^2 K_E, \quad and \; K_L = K_h \tag{5-12}$$

where K is the TSM scale factor (defined in Eqn. 2-31 as the product parameter divided by the model parameter). The scale factors and parameter values for both the model and product systems are shown in Table 31 (note that the values shown in Table 31 are the *ideal* values upon which the TSM scale factors are based; any deviation from these ideal values in the actual experiment constitutes a source of model distortion).

Table 31. Parameter Values for Beam Experiment.

	TSM Scale Factor ($K = x_p / x_m$)	Value of Product Parameters (x_p)	Value of Model Parameters (x_m)
Applied Force (F)	46.1	3.00 lbs	0.065 lbs
Beam Length (L)	1.00	7.00 in	7.00 in
Beam Width (w)	1.00	1.00 in	1.00 in
Beam Height (h)	1.00	0.125 in	0.125 in
Young's Modulus (E)	46.1	10,150 ksi	220 ksi

Table 32. Deflection of Model Beams.

Applied Force (lbs)	**δ_{ms1} (in)**	**δ_{ms2} (in)**	**δ_{model} (in)**
0.0156	0.026	0.024	0.038
0.0313	0.048	0.053	0.084
0.0469	0.075	0.081	0.121
0.0625	0.099	0.113	0.159
0.0750	0.124	0.137	0.205

The deflection results for the model beams are shown in Table 32, while those for the product beams are shown in Table 33. Note that the actual weights applied to the beams are not exactly equal to those prescribed by the TSM scale factors. Note also that deflection values tend to increase as the size of the holes in the beams increases, as expected. There are a few exceptions, however, where apparent experimental error causes the deflection of the intermediate specimen (with small holes) to be slightly less than that of the original specimen (with no holes).

Table 33. Deflection of Product Beams.

Applied Force (lbs)	**δ_{ps1} (in)**	**δ_{ps2} (in)**	**$\delta_{product}$ (in)**
0.675	0.019	0.019	0.027
1.35	0.041	0.040	0.056
1.99	0.061	0.060	0.086
2.37	0.070	0.073	0.100
3.02	0.089	0.093	0.128

In order to estimate the experimental error in the testing procedure, the maximum load is applied to each beam randomly, and the static deflection of the beam is measured. This process continues until all beams have been measured a total of eight times. The average beam deflection (and standard deviation) is then calculated. Three standard deviations is assumed to be the tolerance value on all measurements of beam deflection. The results of this "repeatability" study are shown in Table 34.

Several interesting observations can be made about the results shown in Table 34. We see from the values in Table 34 that the repeatability of the

Table 34. Results of Study on Experimental Repeatability.

Test	MS1	MS2	Model	PS1	PS2	Product
1	0.135	0.133	0.208	0.086	0.097	0.127
2	0.138	0.143	0.209	0.086	0.096	0.127
3	0.128	0.14	0.234	0.084	0.09	0.127
4	0.133	0.146	0.211	0.092	0.091	0.123
5	0.132	0.152	0.203	0.088	0.094	0.124
6	0.128	0.143	0.201	0.085	0.094	0.126
7	0.136	0.139	0.212	0.085	0.096	0.128
8	0.133	0.141	0.212	0.086	0.094	0.13
Ave	**0.133**	**0.142**	**0.211**	**0.0865**	**0.094**	**0.127**
Std Dev (σ)	**0.0036**	**0.0055**	**0.0101**	**0.0025**	**0.0024**	**0.0022**
Tol (3σ)	**0.0107**	**0.0165**	**0.0302**	**0.0075**	**0.0073**	**0.0066**
Error @ 3σ	**8.0 %**	**11.6 %**	**14.3 %**	**8.7 %**	**7.8 %**	**5.2 %**

experiment is relatively good, with a maximum error (calculated as $\frac{3\sigma}{Ave}\times 100\%$) less than 15% and an average error less than 10%. The repeatability of the product family, however, tends to be better than that of the model family.

We can also see that, although the repeatability measurements were taken days after the measurements for Table 32 and Table 33 were taken, all of the values of deflection at maximum force shown in Table 32 and Table 33 are within the $\pm 3\sigma$ range of the average values shown in Table 34. The average deflection (at maximum load) for each beam in the model family, however, is greater in Table 34 (whose measurements were taken at a later time) than the corresponding values in Table 32. In other words, the average value of deflection appears to have increased in the later measurements of the model family. The same phenomenon does not occur in the product family, however. This observation indicates that *elapsed time since processing* may have an effect on the material properties of the model family (i.e. the RP beams). In other words, leaving the model beams exposed to the environment may, over time, affect material behavior. Further research is needed to more fully characterize the impact of such factors on the material properties of RP parts.

The deflection results in Table 32 and Table 33 are used to construct the "first order" advanced ESM prediction of the deflection of the product (as outlined in Section 4.3.). The TSM predictions and the traditional ESM predictions of the deflection of the product are also calculated in order to compare their results with the advanced ESM (see Appendix A for intermediate calculations for all three similitude techniques). The results from all three

Table 35. Deflection Predictions for Experimental Study.

Load Inc.	$\delta_{product}$	δ_{TSM}	Error TSM,%	δ_{ESM}	Error ESM,%	$\delta_{1st\ O}$	Error 1^{st} O,%
1	0.027	0.038	40.7	0.028	2.1	0.032	18.4
2	0.056	0.084	50.0	0.071	26.8	0.054	4.3
3	0.086	0.121	40.7	0.098	14.5	0.081	5.6
4	0.1	0.159	59.0	0.112	12.1	0.093	6.8
5	0.128	0.205	60.2	0.148	15.4	0.131	2.5
		Ave.	**50.1**		**17.2**		**7.5**

approaches, along with the actual deflection values for the product, are shown in Table 35 (note in Table 35 that *1^{st} O* refers to the advanced ESM with a first order polynomial prediction of the scale transformation matrix). Although the results from the traditional ESM shown in Table 35 are from the circulant matrix approach, the diagonal matrix approach produces similar results. The results in Table 35 are illustrated graphically in Figure 66.

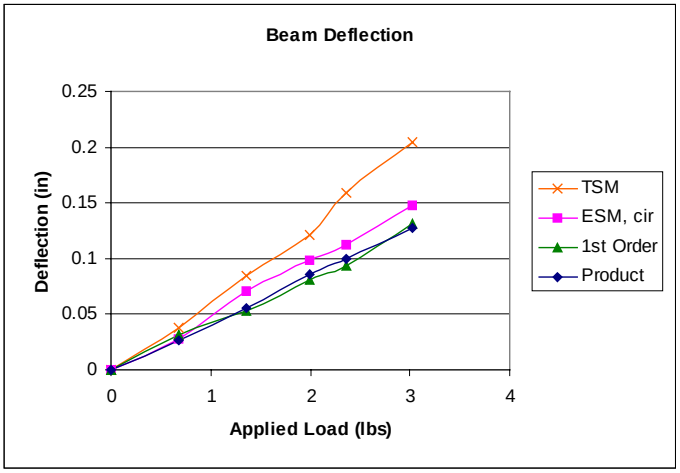

Figure 66. Beam Deflection Results for Experimental Study.

The results of this study show that, in this case, the prediction errors do in fact decrease as we move from the TSM to the ESM to the advanced ESM approaches. The error from the first order advanced ESM is below the ten percent error that was established as the desired accuracy for this problem.

It should be noted, however, that without actually constructing and testing the product, we do not know what the error is for a particular method. Suppose that we assume in this case that we can obtain a higher level of accuracy by including an additional intermediate specimen pair in the advanced ESM technique. While the original specimen pair has no holes and the first intermediate specimen pair has 0.25" diameter holes, the second intermediate specimen pair is constructed with 0.375" diameter holes (recall that the product and model beams have 0.50" diameter holes). With two intermediate specimen pairs, a second order polynomial can be used in the advanced ESM technique. The setup for the "second order" advanced ESM approach is shown in Figure 67.

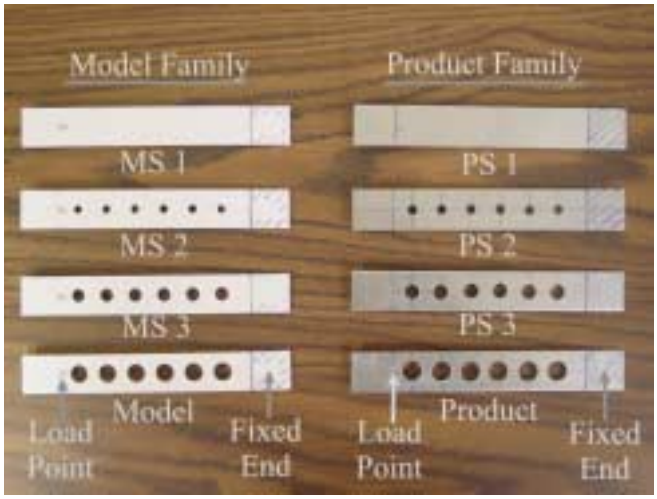

Figure 67. Second Order Advanced ESM Setup.

Table 36. Deflection of Model Beams.

Applied Force (lbs)	**δ_{ms1} (in)**	**δ_{ms2} (in)**	**δ_{ms3} (in)**	**δ_{model} (in)**
0.0156	0.026	0.024	0.027	0.038
0.0313	0.048	0.053	0.060	0.084
0.0469	0.075	0.081	0.094	0.121
0.0625	0.099	0.113	0.123	0.159
0.0750	0.124	0.137	0.154	0.205

Table 36 and Table 37 show the deflections of all four beams in the model family and product family, respectively. Note that the difference in deflection between specimens (which is caused by changes in hole sizes) is on the same order as the repeatability error of the experiment (as shown in Table 34). The repeatability error has the potential to cause higher order polynomial approximations of the scale transformation matrix to be less accurate than lower order approximations, as demonstrated in Section 5.1.2.4. The results of the second order advanced ESM approach, as summarized in Table 38, show that this

Table 37. Deflection of Product Beams.

Applied Force (lbs)	**δ_{ps1} (in)**	**δ_{ps2} (in)**	**δ_{ps3} (in)**	**$\delta_{product}$ (in)**
0.675	0.019	0.019	0.028	0.027
1.35	0.041	0.040	0.052	0.056
1.99	0.061	0.060	0.072	0.086
2.37	0.070	0.073	0.088	0.100
3.02	0.089	0.093	0.112	0.128

Table 38. Results for Second Order Advanced ESM.

Load Inc.	$\delta_{product}$	δ_{TSM}	Error TSM (%)	δ_{ESM}	Error ESM (%)	δ_{1stO}	Error 1^{st}O (%)	δ_{2ndO}	Error 2^{nd}O (%)
1	0.027	0.038	40.7	0.028	2.1	0.032	18.4	0.052	92.2
2	0.056	0.084	50.0	0.071	26.8	0.054	4.3	0.091	62.0
3	0.086	0.121	40.7	0.098	14.5	0.081	5.6	0.102	18.0
4	0.1	0.159	59.0	0.112	12.1	0.093	6.8	0.136	36.4
5	0.128	0.205	60.2	0.148	15.4	0.131	2.5	0.168	31.1
		Ave.	**50.1**		**17.2**		**7.5**		**47.9**

situation does, in fact, occur in this case (i.e. the second order prediction is worse than the first order prediction). The results in Table 38 are plotted in Figure 68.

The findings in this study confirm the fact that the order of polynomial that can be used with the advanced ESM technique is limited by the level of experimental error. As additional specimen pairs are introduced, and the step size

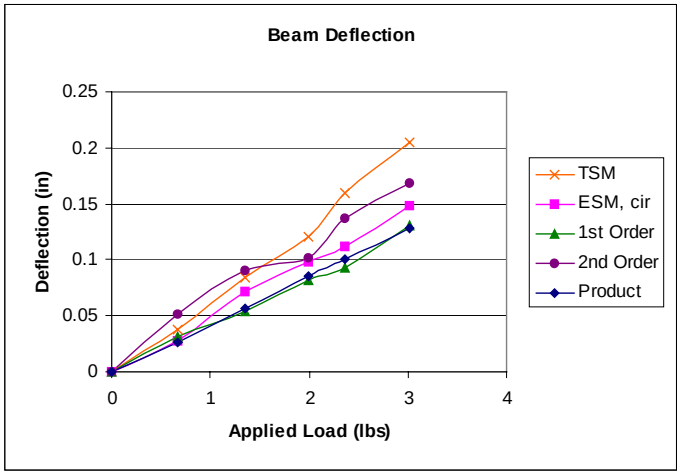

Figure 68. Results of Second Order Advanced ESM.

between specimen pairs is reduced, the level of experimental error that can be present in the advanced ESM technique is reduced.

Although a method for determining the precise number of intermediate specimen pairs that can be used in the advanced ESM does not exist, a general guideline is as follows: if intermediate specimen pairs are close together or are far from the point of interest, prediction accuracy is very sensitive to experimental error; if intermediate specimen pairs are far apart or are close to the point of interest, prediction accuracy is not as sensitive to experimental error. This concept is illustrated in Section 5.1.2.4. Further research is needed to develop a more definitive method for selecting the proper order of polynomial to use with the advanced ESM technique.

5.2.2. Numerical Evaluation of Steady State Temperature Distribution

The next example, which is similar to that presented in Section 4.2.1, deals with the steady state temperature distribution in a two-dimensional cross section. One of the objectives of this example is to evaluate the effect of using different geometric shapes as specimen pairs. As was stated earlier with regard to the advanced ESM, the quantification of changes in geometric shape is generally not a straightforward process. One approach to quantifying changes in geometric shape is developed more fully in this example.

The goal of this example is to use a polymeric model, along with an appropriate similitude technique, to predict the steady state temperature of a steel product. The geometric shape of the product is such that direct fabrication and testing of the product is difficult (thereby necessitating the use of similitude

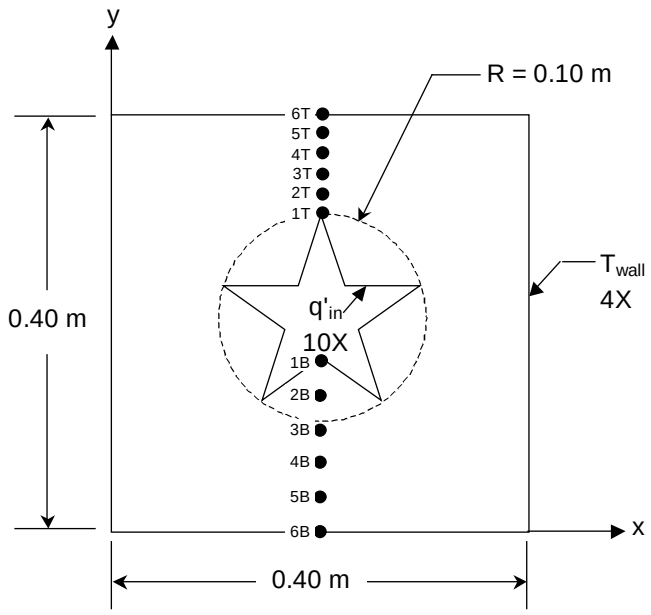

Figure 69. Setup for Heat Transfer Example.

techniques). The cross sectional shape of the product (and model) is shown in Figure 69. Also shown in Figure 69 is the setup of the problem with regard to the load (heat generation q' along the inside surfaces) and the boundary condition (temperature T_{wall} along the outside surfaces). The steady state temperature is to be measured at six points above (labeled 1T through 6T) and six points below (labeled 1B through 6B) the star shape in the center of the cross section.

In order to carry out the process for selecting an appropriate testing procedure, we first need some background information on the problem. First, we determine that the functional equation that describes the steady state temperature of the product is as follows:

$$T = f(x,y,q',k,T_{wall}) \qquad (5\text{-}13)$$

where T is the steady state temperature at a particular point, x is the position of the point in the x-direction, y is the position of the point in the y-direction, q' is the heat generation, k is the coefficient of thermal conduction, and T_{wall} is the temperature that is maintained along the outer surfaces. One set of dimensionless parameters that can be formed from Eqn. 5-13 is the following:

$$\pi_1 = \frac{T}{T_{wall}} \quad ; \quad \pi_2 = \frac{x}{y} \quad ; \quad \pi_3 = \frac{kT_{wall}}{yq'} \tag{5-14}$$

so that the TSM model law becomes

$$K_T = K_{Twall} \quad ; \quad K_x = K_y \quad ; \quad K_k K_{Twall} = K_y K_{q'}. \tag{5-15}$$

The finite element model that is used to evaluate the steady state temperature at the specified points is shown in Figure 70. Note that the specified

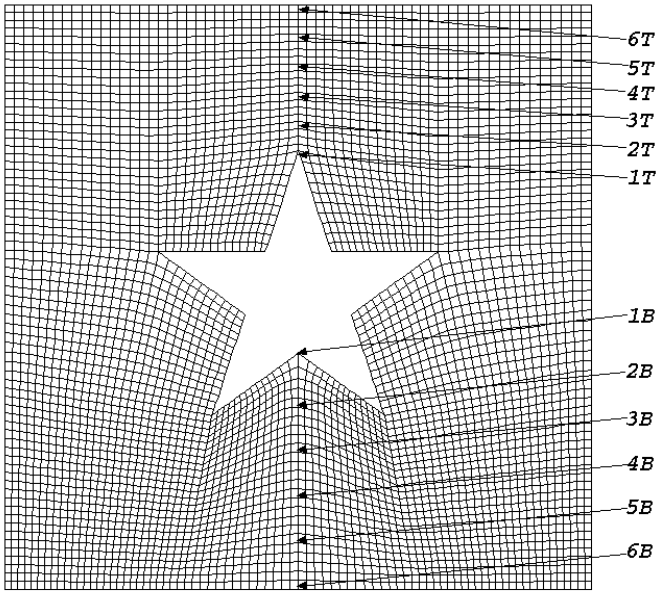

Figure 70. Finite Element Model for Heat Transfer Example.

points are separated by an equal number of nodes on both the top and the bottom of the cross section (every fourth node on the top, and every fifth node on the bottom). The same mesh (with different parameter values assigned to the elements) is used to evaluate both the product and the model since the model, in this case, is the same size as the product.

The finite element model shown in Figure 70 is comprised of two-dimensional, four node thermal elements. As in previous examples, ABAQUS™ software is used to create and solve the model. The parameter values for both the product and the model are listed in Table 39. The coefficient of thermal conduction of the model is typical of unfilled polymeric material [Barlow, 1996]. The coefficient of thermal conduction of the product, which is a function of temperature, as described in Table 40, is identical to that for steel (see [Holman, 1990]).

We are now ready to select the best approach for predicting product behavior. Again we use the selection process outlined in Section 5.1. A summary

Table 39. Parameter Values for Heat Transfer Problem.

	k (W/m·°C)	**q' (W/m2)**	**T_{wall} (°C)**
Product	35-73	100,000	25
Model	0.2	100	25

Table 40. Temperature-Dependent Values of *k* for Steel.

Temp (°C)	0	100	200	300	400	600	800	1000
k (W/m·°C)	73	67	62	55	48	40	36	35

of this process is as follows:

Step 1: Determine the required accuracy of the tests. As in the previous example, we do not present a rigorous evaluation of the various product characteristics suggested in Table 28 since this is a "hypothetical" problem. Let's suppose, however, that we again want a relatively accurate prediction of temperature (less than 10% error). We will consider this level of accuracy to be in the "medium" category.

Step 2: Evaluate the accuracy of the various techniques. We consider the accuracy of each method below:

TSM: Since the model is designed to have the same dimensions as the product, the value of K_x and K_y in Eqn. 5-15 is equal to one. Likewise, since the outside surfaces of both the product and the model are maintained at room temperature (T_{wall} = 25°C), the value of K_{Twall} in Eqn. 5-15 is also equal to one. As a result, the third relationship in Eqn. 5-15 can be simplified to $K_k = K_{q'}$. A review of the parameter values in Table 39, however, shows that this relationship is not satisfied (i.e. model distortions exist). The TSM similarity constraints are, therefore, violated, and we expect TSM predictions of product performance to be inaccurate. We therefore consider the TSM prediction accuracy for this case to be in the "low" category.

ESM: Since the coefficient of thermal conductivity of the product material is not constant, and the product and product specimen may operate at different values of thermal conductivity, specimen distortions will likely exist in this problem (see Figure 23). Since the ESM error that results from the variation in

thermal conductivity is expected to be lower than the TSM error, the ESM technique is considered to be in the "medium" category for accuracy.

Advanced ESM: The advanced ESM technique should effectively correct for the specimen distortions described in the previous paragraph. The accuracy of the advanced ESM technique is considered to be "high."

Full-Scale Testing: The accuracy of full-scale testing is also assumed to be in the "high" category.

Step 3: Evaluate the required effort for the various techniques. Again, evaluating the specific characteristics of the product is not relevant in this example since we are considering a "hypothetical" product. We will assume, however, that the required effort is "low" for the TSM, "medium" for the ESM and advanced ESM, and "high" for full-scale testing.

The selection matrix that results from the above assessments is shown in Table 41, and the corresponding 2D selection graph is shown in Figure 71. Using the selection matrix and graph, we choose the advanced ESM technique as the best approach for this situation.

Table 41. Assessments for Temperature Example.

	Accuracy	**Effort**
Required	Medium	n/a
TSM	Low	Low
ESM	Medium	Medium
Advanced ESM	High	Medium
Full-Scale Testing	High	High

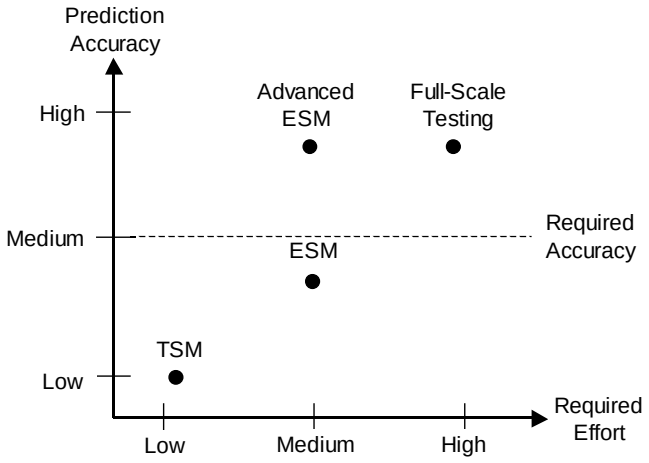

Figure 71. Selection Graph for Temperature Example.

A single intermediate specimen pair is used with the original specimen pair to produce a "first-order correction" with the advanced ESM. The geometric shape of the original and intermediate specimen pairs is shown in Figure 72. As with the product / model pair, the steady state temperature of each specimen pair

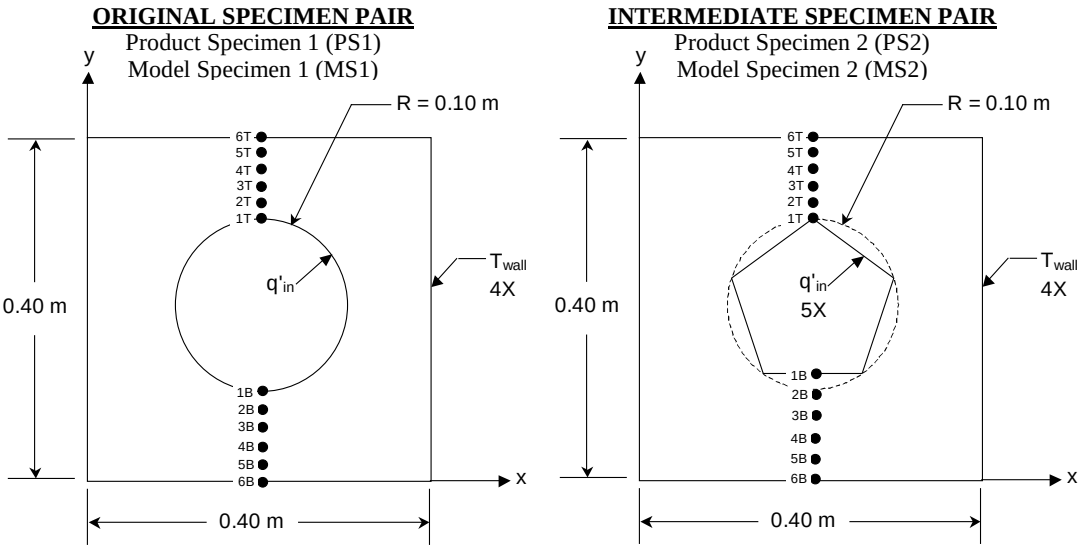

Figure 72. Geometry of Intermediate Specimen Pairs.

is to be measured at six points above and six points below the shape at the center of the cross section.

The finite element models of the original and intermediate specimen pairs are shown in Figure 73. The points in the models at which the temperature is measured are all separated by an equal number of nodes (every fourth node on both the top and the bottom of the cross sections). The same mesh (with different parameter values assigned to the elements) is used to evaluate corresponding product and model specimens since the overall sizes are the same. The parameter values used for the product specimens are the same as those listed for the product in Table 39. Likewise, the parameter values used for the model specimens are the same as those listed for the model in Table 39.

It is important to point out that the changes in geometry between the product / model pair and each specimen pair are considered to be pure *shape*

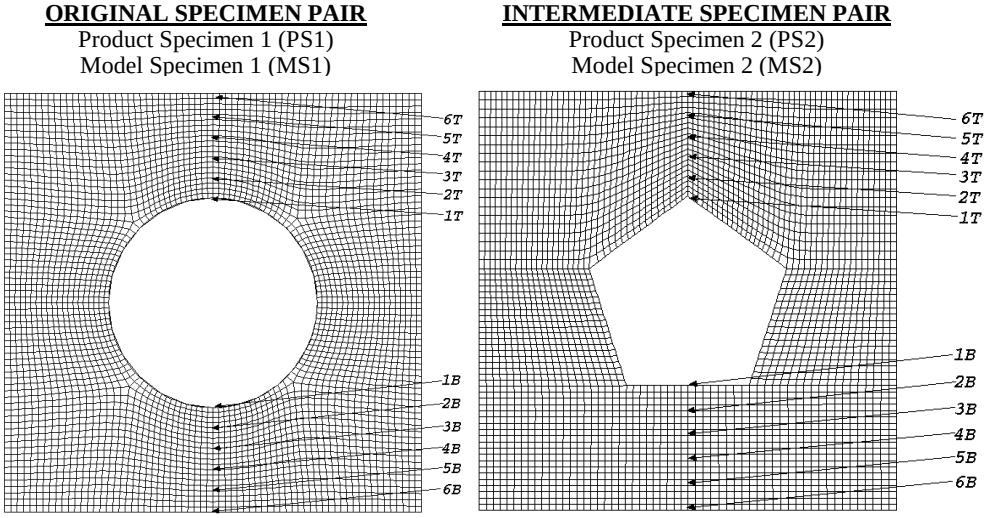

Figure 73. Finite Element Models for Intermediate Specimen Pairs.

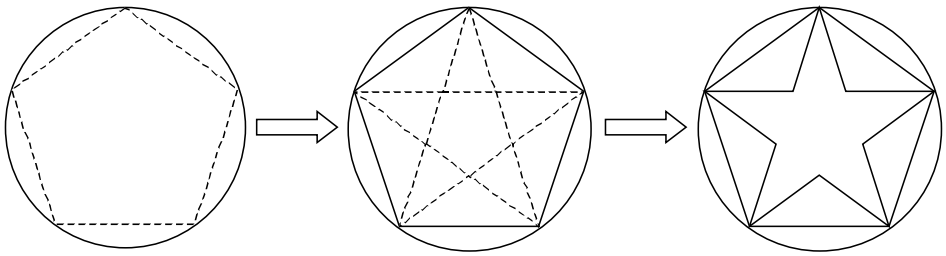

Figure 74. Relationship Among Geometric Shapes.

changes (and not *size changes*). The geometric shapes at the center of the cross sections are considered to have the same size since each shape *can be inscribed within a circle of the same diameter*. Figure 74 shows how a regular pentagon is inscribed within a circle, and then a star is inscribed within the pentagon. The three shapes are, therefore, considered to be of *equal size*.

In order to utilize the advanced ESM technique, the "step size" between the three different geometric shapes described above must be determined (as indicated in Figure 50). In considering this situation, we recognize the similarities between the need for "discretized" geometric shapes in the advanced ESM and the use of shape factors in fluid flow and heat transfer applications [Gerhart, 1992; Holman, 1990]. For example, the geometric shape of a body submersed in a moving fluid has a significant effect on the coefficient of drag on the body. The coefficient of drag of several two dimensional shapes is shown in Figure 75.

In order to estimate shape factors for the heat transfer problem (similar to the coefficients of drag shown in Figure 75), we solve the finite element models shown in Figure 70 and Figure 73 and evaluate the effect of the various geometric shapes on steady state temperature. The calculated temperatures at the lower

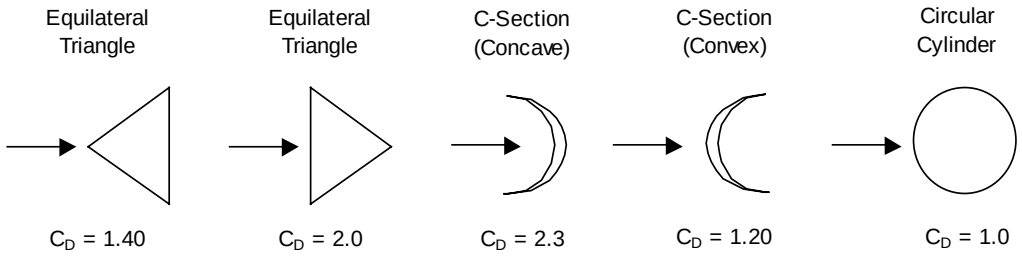

Figure 75. Drag Coefficients for Various 2D Shapes [Gerhart, 1992].

points of the cross section are shown in Table 42, and those at the upper points of the cross section are shown in Table 43. Since the temperature at the outer boundaries (points 6B and 6T) is maintained at 25°C, it is not shown in the tables.

Table 42. Steady State Temperatures for Lower Points.

Point	T (°C) Product	T (°C) PS1	T (°C) PS2	T (°C) Model	T (°C) MS1	T (°C) MS2
1B	269.7	136.4	154.7	104	63	68.9
2B	194.5	109.3	120.8	81.5	54.1	57.9
3B	141	85	92.3	64.5	45.9	48.4
4B	96.7	63.5	67.7	49.8	38.6	40
5B	59.5	43.8	45.7	37.1	31.7	32.3

Table 43. Steady State Temperatures for Upper Points

Point	T (°C) Product	T (°C) PS1	T (°C) PS2	T (°C) Model	T (°C) MS1	T (°C) MS2
1T	165.1	136.4	133.1	72.2	63	61.9
2T	125	109.3	104.2	59.3	54.1	52.4
3T	95.2	85	81	49.4	45.9	44.6
4T	70.2	63.5	61.1	40.9	38.5	37.7
5T	47	43.8	42.7	32.8	31.7	31.3

The six geometric shapes that are important in this study are illustrated in Table 44. (It is important to note that the top of each geometric shape has a different impact on temperature than the bottom of the shape, except in the case of the circle where both sides are identical). The “Shape Factor Rank” shown in

Table 44. Descriptions of Relevant Geometric Shapes.

Illustration	Description	Name	Shape Factor Rank
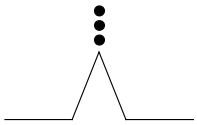	Top of Star in Product and Model	P/M-T	4
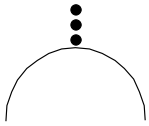	Top of Circle in First Specimens (PS1 and MS1)	S1-T	2
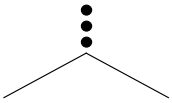	Top of Pentagon in Second Specimens (PS2 and MS2)	S2-T	1
	Bottom of Star in Product and Model	P/M-B	5
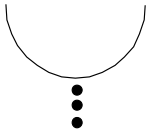	Bottom of Circle in First Specimens (PS1 and MS1)	S1-B	2
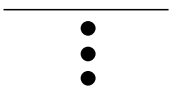	Bottom of Pentagon in Second Specimens (PS2 and MS2)	S2-B	3

Table 44 indicates, in sequential order, which shapes produce the largest increase in temperature. For example, the points above the top of the pentagon experience the lowest steady state temperature, while the points below the star experience the highest temperature. The values in Table 42 and Table 43 can be used to verify that the rankings shown in Table 44 hold for both the product and model families. The rankings shown in Table 44 also make intuitive sense since the shapes that expose the points to more of the heat flux produce higher values of temperature, and have a higher ranking, and the shapes that expose the points to less of the heat flux produce lower values of temperature, and have a lower ranking.

In order to develop a quantifiable shape factor for each geometric shape shown in Table 44, we first establish the top of the pentagon (S2-T) as the "base shape" against which all other shapes are compared, and assign it a value of one. The temperatures above and below the other geometric shapes are now normalized by divided the temperature of each point by the temperature of the corresponding point in S2-T. The average value of these normalized temperatures, for both the product and model families, is shown in Table 45. The shape factor that is used for each geometric shape is the average of the product and model families, as shown in Table 45.

It is important to note here that the purpose of deriving shape factors in this problem is to *illustrate how such shape factors can be used in the advanced ESM*. More advanced methods for developing shape factors than that presented here have been proposed in the literature [Nickolay, 1998; Kolodziej, 2001]. The

shape factors developed in this section, however, serve our present purpose of demonstrating the use of such shape factors in the advanced ESM.

The shape factors shown in Table 45 are now used as the "description of geometric shape" required by the advanced ESM (i.e. the values of *i* shown in

Table 45. Shape Factors for Various Geometric Shapes.

Illustration	**Ave. Normalized Temperature (Product Family)**	**Ave. Normalized Temperature (Model Family)**	**Shape Factor (Ave. Between Product & Model Families)**
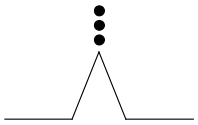	1.17	1.11	1.14
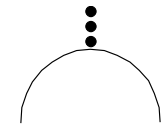	1.04	1.02	1.03
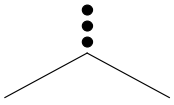	1.00	1.00	1.00
	1.72	1.44	1.58
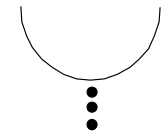	1.04	1.02	1.03
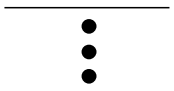	1.13	1.08	1.10

Figure 50 and in Table 24). Using the values in Table 42 and Table 43, the steady state temperature at the specified points in the product are now predicted with the TSM, the ESM, and the advanced ESM (see Appendix B for details). Results for the points on the lower half of the cross section are shown in Table 46, while results for the points on the upper half of the cross section are shown in Table 47.

The results shown in Table 46 and Table 47 include only the first five points defined for each cross section since the sixth point is maintained at 25°C in

Table 46. Predictions of Steady State Temperature for Lower Points.

Point	**$T_{product}$**	**T_{TSM}**	**Error TSM,%**	**T_{ESM}**	**Error ESM,%**	**$T_{1st\ O}$**	**Error 1^{st} O,%**
1B	269.7	104.0	61.4	235.8	12.6	277.1	2.7
2B	194.5	81.5	58.1	167.5	13.9	202.2	4.0
3B	141.0	64.5	54.3	117.3	16.8	147.2	4.4
4B	96.7	49.8	48.5	74.0	23.5	105.9	9.5
5B	59.5	37.1	37.6	37.9	36.2	69.2	16.3
		Ave.	**39.7**		**22.6**		**7.4**

Table 47. Predictions of Steady State Temperature for Upper Points.

Point	**$T_{product}$**	**T_{TSM}**	**Error TSM,%**	**T_{ESM}**	**Error ESM,%**	**$T_{1st\ O}$**	**Error 1^{st} O,%**
1T	165.1	72.2	56.3	159.1	3.7	163.8	0.8
2T	125.0	59.3	52.6	119.9	4.0	124.9	0.1
3T	95.2	49.4	48.1	90.7	4.8	96.1	0.9
4T	70.2	40.9	41.7	66.0	6.0	70.8	0.9
5T	47.0	32.8	30.2	42.5	9.5	46.7	0.7
		Ave.	**34.5**		**6.1**		**0.7**

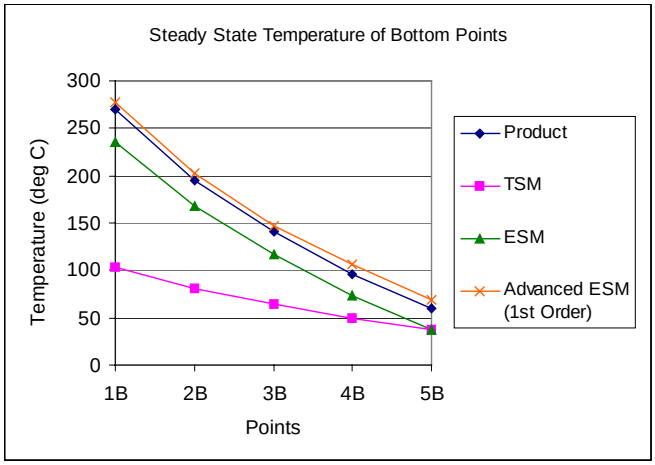

Figure 76. Plot of Results for Bottom Points.

each case. The ESM results listed in the tables are obtained from the circulant matrix approach, although results from the diagonal matrix approach show similar trends. The results in Table 46 and Table 47 are shown graphically in Figure 76 and Figure 77, respectively. Note that the curve for the product and the curve for the advanced ESM are so similar that they appear as one line in Figure 77.

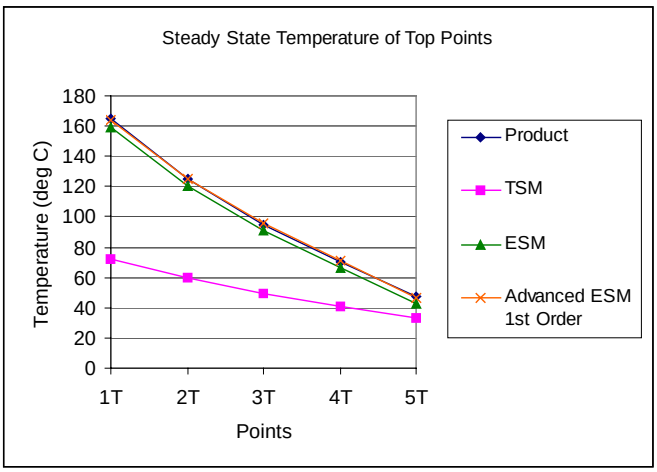

Figure 77. Plot of Results for Top Points.

Despite the relatively simple method used to define the shape factors for the various geometric shapes, the results from the advanced ESM show amazing accuracy. As expected (and as illustrated in previous examples) the accuracy of the similitude predictions increases as we move from the TSM to the ESM to the advanced ESM.

Now suppose that we need to analyze the steady state temperature for the same geometric shapes but with different material properties. Let's suppose that the product material in this case is aluminum, and the model material is a different type of polymer than that used in the previous example. The parameters used in this case are shown in Table 48. Note that the coefficient of thermal conductivity for the product is again a function of temperature, as shown in Table 49, but that, for steel, the value of the coefficient *decreases* with increased temperature, but for aluminum, the value of the coefficient *increases* with increased temperature. The coefficients of thermal conductivity shown in Table 49 are taken from [Holman, 1990]. Note that higher values of heat generation are used with the new materials.

Table 48. Modified Parameters for Heat Transfer Problem.

	k (W/m·°C)	**q' (W/m2)**	**T_{wall} (°C)**
Product	202-249	500,000	25
Model	0.4	300	25

Table 49. Temperature-Dependent Values of *k* for Aluminum.

Temp (°C)	0	100	200	300	400
k (W/m·°C)	202	206	215	228	249

Table 50. Steady State Temperatures for Lower Points, Second Study.

Point	T (°C) Product	T (°C) PS1	T (°C) PS2	T (°C) Model	T (°C) MS1	T (°C) MS2
1B	386.3	207.4	234.8	143.5	82.0	90.9
2B	291.2	165.7	183.7	109.8	68.6	74.3
3B	214.4	126.9	138.6	84.2	56.4	60.0
4B	145.7	91.3	98.3	62.3	45.3	47.5
5B	84.5	57.7	60.9	43.2	35.0	36.0

The calculated temperatures for the second heat transfer study are shown in Table 50 and Table 51. Table 50 shows the results for the lower points, while Table 51 shows the results for the upper points. Note that the "shape factor rank" listed in Table 44 holds for the results shown in Table 50 and Table 51, despite the change in material properties (i.e. the points at the top of the pentagon still have the lowest temperature, the points at the bottom of the star still have the highest temperature, etc.).

Table 51. Steady State Temperatures for Upper Points, Second Study.

Point	T (°C) Product	T (°C) PS1	T (°C) PS2	T (°C) Model	T (°C) MS1	T (°C) MS2
1T	249.7	207.4	202.5	95.9	82.0	80.4
2T	190.1	165.7	157.6	76.4	68.6	66.0
3T	143.5	126.9	120.4	61.6	56.4	54.3
4T	102.5	91.3	87.2	48.8	45.3	44.1
5T	63.2	57.7	55.9	36.7	35.0	34.4

The temperature values in Table 50 and Table 51 are used to create TSM, ESM, and advanced ESM predictions of the temperature of the product (the same shape factors shown in Table 45 are used in the advanced ESM). The prediction results for the lower and upper points are shown in Table 52 and Table 53, respectively. The results shown in the tables, which are again from the circulant matrix approach, are plotted in Figure 78 and Figure 79.

Table 52. Predictions of Steady State Temperature for Lower Points.

Point	**$T_{product}$**	**T_{TSM}**	**Error TSM,%**	**T_{ESM}**	**Error ESM,%**	**$T_{1st\ O}$**	**Error 1^{st} O,%**
1B	386.3	143.5	62.9	373.9	3.2	405.1	4.9
2B	291.2	109.8	62.3	268.6	7.7	308.9	6.1
3B	214.4	84.2	60.7	187.1	12.7	232.6	8.5
4B	145.7	62.3	57.2	116.8	19.8	159.5	9.5
5B	84.5	43.2	48.9	54.3	35.7	98.9	17.1
		Ave.	**45.8**		**19.0**		**9.2**

Table 53. Predictions of Steady State Temperature for Upper Points.

Point	**$T_{product}$**	**T_{TSM}**	**Error TSM,%**	**T_{ESM}**	**Error ESM,%**	**$T_{1st\ O}$**	**Error 1^{st} O,%**
1T	249.7	95.9	61.6	245.6	1.6	251.1	0.6
2T	190.1	76.4	59.8	184.7	2.8	190.2	0.05
3T	143.5	61.6	57.1	137.6	4.1	142.9	0.4
4T	102.5	48.8	52.4	96.5	5.8	104.0	1.4
5T	63.2	36.7	41.9	57.0	9.8	62.8	0.7
		Ave.	**42.2**		**5.6**		**0.6**

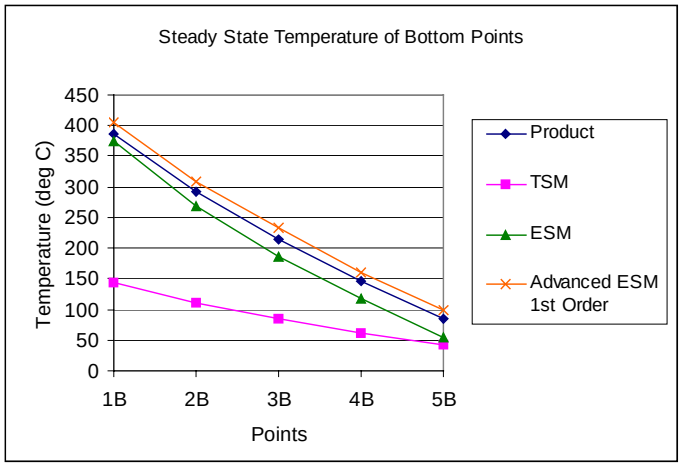

Figure 78. Plot of Results for Bottom Points.

We see from Figure 78 and Figure 79 that the prediction accuracy again improves as we move from the TSM to the ESM to the advanced ESM. Again, the curve for the product and the curve for the advanced ESM are so similar that they appear as one line in Figure 79. It is interesting to note that the same shape factors

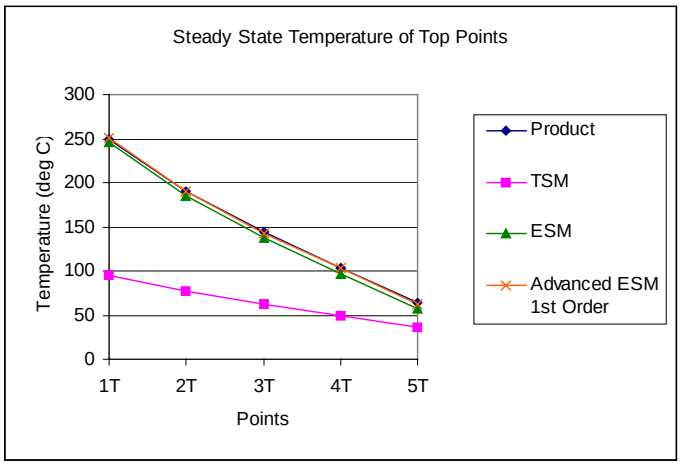

Figure 79. Plot of Results for Top Points.

that were developed for the advanced ESM using material properties for steel produce extremely accurate results for a product made out of aluminum (even when the thermal conductivity characteristics of aluminum are quite different from those of steel).

The heat transfer example presented above effectively illustrates how shape factors can be used to quantify changes in geometric shape when implementing the advanced ESM technique. The advanced ESM results for both cases (using material properties of steel and using material properties of aluminum) show remarkable accuracy.

5.2.3. Evolution of Headphone Design

Many examples in this research have dealt with the deflection of a cantilever beam. Besides being an excellent way to demonstrate the concepts of system distortion, this example also has practical application in mechanical design. For example, many products in today's market involve compliant members or components that behave like a cantilever beam. Figure 80 shows several products that contain compliant members. The cantilever beam examples presented in this research enhance our understanding of how such products perform and the types of system distortion that may occur during testing.

In this section, the use of the ESM in the evolution of a compliant headphone design is presented. The ESM technique is very well suited for product evolution since the existing product can often be used as the product specimen for the new design. The functional performance of the new design can be predicted with the ESM as follows:

Ice Cream Scoop

Headphones

Retention Tabs on CD Case

Plastic Clip

Integral Belt Clip

Retention Tabs on Ear Thermometer

Compliant Wrist Band

Actuation Lever in Garage Door Remote

Plastic Clip

Figure 80. Products with Compliant Members.

- Use the existing product as the product specimen for the new design.
- Create a rapid prototype of the current product with the (already existing) solid model of the current design. This rapid prototype can be used as the model specimen.

- Modify the solid model to reflect the evolved design. Create a rapid prototype of the evolved design. This rapid prototype can be used as the model.
- Use the ESM, along with the model, model specimen, and product specimen described above, to predict the functional behavior of the new design.

The approach described above may be easier to implement than the TSM in many instances, if information on the governing parameters of the system is not readily available.

Many styles of headphones exist on the market today. Several different styles are shown in Figure 81. The headphone design that will be modified in this example is shown in Figure 82. This product is used as the product specimen for the new design. Let's suppose that we want to modify the existing product to include a slot in the compliant member along the top of the headphone. The solid

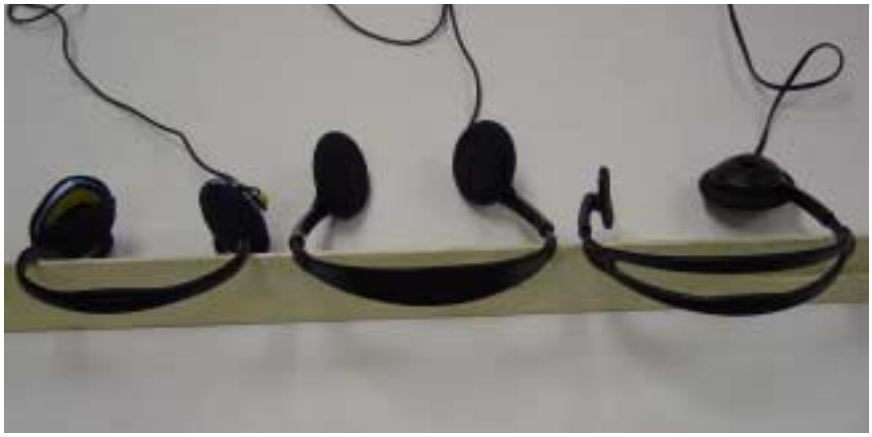

Figure 81. Various Headphone Designs.

Figure 82. Current Headphone Design.

models of the original design (which was reverse-engineered since the actual solid model was not available) and the modified design are shown in Figure 83. The solid models shown in Figure 83 are used to create rapid prototype parts with the selective laser sintering process. The original design serves as the model specimen, while the modified design serves as the model.

Original Design Modified Design

Figure 83. Solid Models of Headphone Designs.

In order to simulate the behavior of the product, a second headphone (of the existing design) was obtained and a slot was machined similar to that shown in Figure 83. The overall ESM setup for this problem is shown in Figure 84. Figure 84 shows, from left to right, the product, product specimen, model, and model specimen.

The behavior of interest in this case is the reaction force of the headphones under a specific displacement. The displacement is intended to represent the width of a human head. The reaction force produced from the given displacement (6.35” in this case) is recorded for each set of headphones shown in Figure 84. The experimental setup is shown in Figure 85.

It is important to note that the procedure described in the preceding paragraphs is designed to give a quick (back-of-the-envelope type) prediction of product performance. In keeping with this principle, a single force value is used for each system in this example, which results in state vectors with a dimension of

Figure 84. ESM Setup for Headphone Redesign.

Figure 85. Experimental Setup for Headphone Tests.

one (i.e. a single value). Although all previous examples of the ESM have state vectors with dimension greater than one, it is not *required* that state vectors have a dimension greater than one. Representing system states with a single value greatly simplifies the calculation of the ESM transformation matrices since such transformation matrices also become single values (i.e. 1 x 1 matrices). When state vectors have a dimension of one, the transformation matrices can be calculated by simply dividing through by the appropriate state value. For example,

$$X_{ps} = S\, X_{ms} \quad \Rightarrow \quad S = \frac{X_{ps}}{X_{ms}} \tag{5-16}$$

where X represents the measured behavior of the system.

The reaction force from an imposed 6.35” displacement is measured five times for each set of headphones shown in Figure 84. The measured values of

Table 54. Measurements of Reaction Force of Headphones.

Measurement	**F_p (oz.)**	**F_{ps} (oz.)**	**F_m (oz.)**	**F_{ms} (oz.)**
1	9.05	12.85	7.50	8.35
2	9.00	12.55	7.35	8.45
3	9.05	12.90	7.25	8.40
4	9.05	12.95	7.35	8.65
5	9.00	12.80	7.25	8.50
Ave.	**9.03**	**12.81**	**7.34**	**8.47**
Std. Dev.	0.027	0.156	0.102	0.115

force, along with the average value and standard deviation, are shown in Table 54. The average value is used as the state value for each system. The ESM prediction of product behavior is calculated as follows:

$$
\begin{aligned}
&F_{ps} = SF_{ms} \quad \Rightarrow \quad S = \frac{F_{ps}}{F_{ms}} = \frac{12.81oz.}{8.47oz.} = 1.512 \\
&F_p = SF_m = (1.512)(7.34oz.) = 11.10oz. \\
&Error_{TSM} = \frac{11.10oz. - 9.03oz.}{9.03oz.} \times 100\% = 23.0\%
\end{aligned}
\tag{5-17}
$$

Note again the simplicity in calculating ESM transformations when the state vectors have a dimension of one.

The relatively high error in the ESM prediction is attributed to the inaccuracy of the machined slot in the new “product” headphones. Since the slot was machined by hand, the dimensions of the slot were not as accurate as they would be in the actual product. The example is effective, however, in demonstrating the power of the ESM approach in product evolution processes.

The inaccuracy of the machined slot described in the previous paragraph suggests that experimental error will prevent the advanced ESM approach from producing more accurate results than the ESM approach. In addition, the process of creating an intermediate product specimen (with a smaller slot – also machined by hand) destroys the simplicity of the approach that is being demonstrated in this example. If, however, an accurate intermediate product specimen were available, the advanced ESM technique could be used to obtain a more accurate prediction of product performance. The advanced ESM technique is, therefore, presented below in order to illustrate how the technique can be applied in this example.

The setup for the advanced ESM technique is shown in Figure 86. Figure 86 shows, from left to right, the product, intermediate product specimen, original product specimen, model, intermediate model specimen, and original model specimen. The slot in the intermediate specimen pair is half as wide as the slot in the product / model pair (which is 0.30”). The five individual force measurements, along with the average force and the standard deviation, are shown in Table 55.

The results in Table 54 and Table 55 are entered into the polynomial

Figure 86. Advanced ESM Setup for Headphone Redesign.

Table 55. Results for Intermediate Specimen Pair.

Measurement	F_{ps2} (oz.)	F_{ms2} (oz.)
1	11.15	8.95
2	11.05	8.90
3	11.00	8.85
4	11.05	8.80
5	10.75	8.75
Ave.	**11.00**	**8.85**
Std. Dev.	0.150	0.079

construction table shown in Table 56. The first order approximation to the scale transformation matrix that relates the model to the product is determined as follows:

$$S_2 = 1.512 - 1.793\,(0.30 - 0) = 0.974, \tag{5-18}$$

so the advanced ESM prediction of product performance becomes

$$F_p = SF_m = (0.974)(7.34oz.) = 7.149oz.$$
$$Error_{TSM} = \frac{9.03oz. - 7.149oz.}{9.03oz.} \times 100\% = 20.8\% \tag{5-19}$$

Table 56. Polynomial Construction Table for Advanced ESM.

		Divided Differences	
Step	**i**	**Zeroth**	**First**
1	0	$S\{i_0\} = 1.512$	$S\{i_0,i_1\} = -1.793$
2	0.15	$S\{i_1\} = 1.243$	
3	0.30		

The relatively large error from the advanced ESM is expected since the accuracy of the machined slots in the product and the intermediate product specimen is low. However, an additional source of error that is not expected is shown in Figure 87. The plot in Figure 87 shows an anomaly between the first and second points in the model family: the reaction force actually goes *up* as the small slot is introduced. This anomaly may be due to experimental error or it may be a result of the rapid prototyping process (for example, does the process create a "crust" around the edges which actually causes the stiffness of the part to increase when the width of the slot is small?). Additional research is needed to explore the source of such inconsistencies in the model behavior.

In summary, this chapter presents general guidelines for selecting an appropriate approach to functional testing. The guidelines are formalized in a step-by-step procedure that assesses the required accuracy of the tests, the accuracy that is attainable with the various techniques, and the effort required to implement the various techniques. A selection matrix and 2D selection graph are

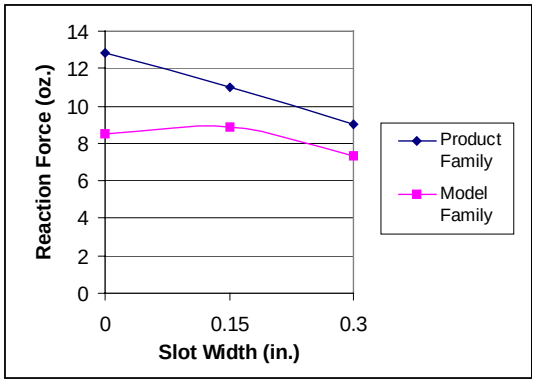

Figure 87. Advanced ESM Setup for Headphone Redesign.

presented as useful tools in implementing the formalized procedure. Finally, the procedure is illustrated with experimental and numerical examples. The first experimental example serves to illustrate the impact of experimental error on prediction accuracy, and the numerical example illustrates the use of shape factors in the advanced ESM technique. The final example illustrates the application of the ESM in a product evolution process and encourages the use of similitude techniques in design (see also [Schnittger, 1988]).

CHAPTER 6

Conclusions and Future Work

The advent of rapid prototyping technologies has led to significant improvements in many aspects of the product development process. Among these enhancements is the ability to quickly evaluate the *fit* and *form* of a product. Limited material properties and sizes that are available from common RP systems, however, have prevented rapid prototypes from being widely used in *functional* testing. Using rapid prototypes in place of traditional prototypes in functional evaluations of product performance could significantly reduce overall design costs and improve time to market.

Similitude techniques are proposed as a means of correlating the behavior of rapid prototypes with the behavior of a product. The research presented in this dissertation expands our understanding of current similitude techniques and extends those techniques to provide more accurate predictions of product performance. As the field of similitude methods has advanced, many topics for additional study and research have been revealed. The following sections outline the major contributions of this work and highlight several areas for further study.

6.1. RESEARCH CONTRIBUTIONS

The major contributions of this research include the following:

- **Compilation of Model Distortions**: Although the concept of *distortion* between a product and a model is not new, the compilation of model distortions that is presented in this document is believed to be the most comprehensive in the literature. In addition to the descriptions of model distortion that are presented, the explanations and examples that are used throughout the document serve to clarify the impact that such distortions can have on predicted product behavior.
- **Identification and Classification of Specimen Distortions**: The idea of *specimen distortion*, which occurs when a specimen in the ESM exhibits different behavior than the model or product it represents, is developed in this research. Several sources of specimen distortion are identified and organized in a classification structure.
- **Illustrations of the Effects of Specimen Distortions**: Several examples that illustrate the impact of specimen distortions on the accuracy of predicted product behavior are presented in this work. The examples indicate that prediction accuracy can be affected by the degree of model distortion as well as by the nature of the shape change between the model or product and the respective specimen.
- **Development of diagonal matrix approach**: The diagonal matrix approach to deriving the ESM transformation matrices was developed in this work.

- **Development of an Advanced ESM technique**: An advanced ESM technique, which employs intermediate specimen pairs to capture the effects of specimen distortions, is developed in this dissertation. The advanced technique fits multiple transformation matrices to a polynomial curve in order to more accurately estimate the unknown transformation matrix between the model and the product (or between the product specimen and the product).
- **Creation of Error Estimate for ESM Technique**: An analytical method for estimating ESM error is presented in this work. Such a method for estimating ESM error has not been found elsewhere in the literature. An example demonstrating use of the method is also presented.
- **Development of a Systematic Method for Selecting an Appropriate Approach to Functional Testing**: A systematic procedure that directs the selection of an appropriate approach to functional testing is developed. The procedure is illustrated with numerical and experimental examples.

The results described in the preceding paragraphs are considered to be significant contributions to the study of similitude techniques. The contributions include not only clarification of existing techniques, but also the creation and evaluation of an advanced technique. The results expand the understanding of, and range of application for, similitude techniques in engineering design. The replacement of full-scale testing (i.e. direct product testing) with scale model

testing and similitude techniques holds great potential to decrease product development costs and improve time to market.

In addition to the contributions described above, the research presented in this dissertation also revealed many areas for further research, as described below.

6.2. AREAS OF FURTHER RESEARCH

The traditional similitude method (or at least parts of it) has been in use for centuries. However, use of advanced similitude techniques, such as the empirical similitude method, is relatively new. More specifically, the concept of using advanced similitude techniques in connection with rapid prototypes in order to accurately predict product behavior is a new area of research. As a consequence, many topics in this field remain unexplored. Several areas for further research include the following:

- **Comprehensive Evaluation of RP System Capabilities**: Although several isolated studies on various aspects of RP system capabilities have been reported in the literature, a comprehensive study of such RP capabilities is noticeably absent. Factors such as operating parameters and environmental conditions have been shown to affect the material properties of rapid prototypes. Reliable information on the range and repeatability of material properties must be established before rapid prototypes can be used with confidence in functional testing.
- **Expansion of Distortion Structures:** The classification structures that describe sources of model and specimen distortion are not presented as comprehensive compilations of all possible sources of distortion

(although they are believed to be the most comprehensive descriptions to date). Additional sources of distortion may be revealed as research in this field continues. Such additional sources of distortion should be added to the basic "distortion structures" presented in this work.

- **Development of Polynomial ESM**: Although the circulant matrix and diagonal matrix approaches are evaluated in this work, the polynomial ESM is not included in the evaluation since it fails to meet the basic ESM requirement that **SF** = **FS**. A method for isolating the error in the polynomial approach from the error that results from specimen distortions would allow the polynomial approach to be included as an alternative, reliable ESM technique.
- **Development of Lumped ESM**: The focus of this research is on single part systems. A lumped ESM technique, which deals with multiple part systems, is not addressed (see [Cho, 1999, 1999c]). Although the lumped ESM technique is not developed here, it nonetheless represents an exciting extension to current research in similitude techniques.
- **Polynomial Curve Fitting of Experimental Data**: The advanced ESM technique relies on curve fitting of experimental data. Measurements that are used as data points in the curve fitting process contain inherent experimental error. The way in which experimental error in state vectors propagates into transformation matrices, and the way in which the resultant error in transformation matrices propagates

through the polynomial curve fitting process, represents an additional area of further research.

- **Decomposition of Transformation Matrices**: Geometric transformation matrices can be decomposed into "component" matrices that represent different physical phenomena (e.g. reflection, expansion, contraction, and shear. See, for example, [Mortenson, 1995]). A decomposition of the ESM transformation matrices into similar "component" matrices may yield insights into the effect that various types of specimen distortion have on the transformation matrices. Subsequent studies may focus on pairing different ESM techniques (e.g. circulant matrix, diagonal matrix, polynomial) to the type of specimen distortion for which they are best suited.
- **Quantification of Changes in Geometric Shape through the use of Shape Factors:** An example presented in this dissertation illustrates the use of shape factors as a means of quantifying changes in geometric shape. Such quantification of geometric shape is necessary when implementing the advanced ESM technique for products that have different geometric shapes than their specimens. Research on developing such shape factors would contribute to the extension of the advanced ESM approach.
- **Continuous Shape Transformations through Conformal Mapping:** The concept of using discrete shape factors could be extended to

include continuous geometric transformation through the use of conformal mapping techniques.

- **Development of Mathematical Foundation for Circulant Matrix Technique:** The mathematical foundations of the circulant matrix approach could be developed more fully. Such a development could lead to a better understanding of how to select among the various techniques for deriving ESM transformation matrices.
- **Distortion Between Systems with Grossly Different Scales:** Recent advances in fields such as nanotechnology present additional possibilities for the application of similitude techniques. Evaluating the behavior of extremely small structures (micro or nano scale) by performing tests on large-scale models is an exciting area for further research. However, unique distortions will likely exist between two systems with such widely different scales. Investigation into the existence and impact of such distortions is necessary before similitude techniques can be used in these types of applications (see [Wang, 1989]).

The topics listed above represent areas in the field of advanced similitude methods that are ripe for further research and study. The continued advancement of similitude methods holds the potential to dramatically improve the way in which products are designed and evaluated. Such improvements in design processes are needed in order to keep pace with ongoing advances in engineering and technology.

Appendix A

Similitude Calculations for Beam Deflection

Data

Product

$F_{product}$	Distance	$\delta_{product}$
0	5.492	0
0.675	5.465	0.027
1.35	5.436	0.056
1.990625	5.406	0.086
2.365625	5.392	0.1
3.021875	5.364	0.128

PS1

F_{ps1}	Distance	δ_{ps1}
0	5.466	0
0.675	5.447	0.019
1.35	5.425	0.041
1.990625	5.405	0.061
2.365625	5.396	0.07
3.021875	5.377	0.089

PS2

F_{ps2}	Distance	δ_{ps2}
0	5.492	0
0.675	5.473	0.019
1.35	5.452	0.04
1.990625	5.432	0.06
2.365625	5.419	0.073
3.021875	5.399	0.093

Model

F_{model}	Distance	δ_{model}
0	5.246	0
0.015625	5.208	0.038
0.03125	5.162	0.084
0.046875	5.125	0.121
0.0625	5.087	0.159
0.075	5.041	0.205

MS1

F_{ms1}	Distance	δ_{ms1}
0	5.241	0
0.015625	5.215	0.026
0.03125	5.193	0.048
0.046875	5.166	0.075
0.0625	5.142	0.099
0.075	5.117	0.124

MS2

F_{ms2}	Distance	δ_{ms2}
0	5.243	0
0.015625	5.219	0.024
0.03125	5.19	0.053
0.046875	5.162	0.081
0.0625	5.13	0.113
0.075	5.106	0.137

TSM Approach

$\lambda_\delta =$ 1

$F_{product}$	$\delta_{product}$	$\delta_{product,TSM}$	$Error_{\delta,TSM}$ (%)
0	0	0	n/a
0.675	0.027	0.038	40.74074
1.35	0.056	0.084	50.00000
1.990625	0.086	0.121	40.69767
2.365625	0.1	0.159	59.00000
3.021875	0.128	0.205	60.15625
		Average	**50.11893**

Diagonal Matrix Approach

S Matrix

0.73076923	0	0	0	0
0	0.85416667	0	0	0
0	0	0.81333333	0	0
0	0	0	0.707070707	0
0	0	0	0	0.71774194

δ_{model}	$S*\delta_{model}$	$\delta_{product}$	$Error_{\delta,S}$ (%)
0.03800	0.02776923	0.027	2.849002849
0.08400	0.07175	0.056	28.125
0.12100	0.09841333	0.086	14.43410853
0.15900	0.11242424	0.1	12.42424242
0.20500	0.1471371	0.128	14.95085685
		Average	**17.48355195**

Circulant Matrix Approach

Using MS1 and PS1

cir(δ_{ps})

0.019	0.089	0.07	0.061	0.041
0.041	0.019	0.089	0.07	0.061
0.061	0.041	0.019	0.089	0.07
0.07	0.061	0.041	0.019	0.089
0.089	0.07	0.061	0.041	0.019

cir(δ_{ms})

0.026	0.124	0.099	0.075	0.048
0.048	0.026	0.124	0.099	0.075
0.075	0.048	0.026	0.124	0.099
0.099	0.075	0.048	0.026	0.124
0.124	0.099	0.075	0.048	0.026

cir(δ_{ms})$^{-1}$

-7.5844119	0.45939984	0.74719461	0.203150909	8.86283855
8.86283855	-7.5844119	0.45939984	0.747194612	0.20315091
0.20315091	8.86283855	-7.5844119	0.459399842	0.74719461
0.74719461	0.20315091	8.86283855	-7.584411871	0.45939984
0.45939984	0.74719461	0.20315091	8.862838551	-7.5844119

S = cir(δ_{ps})cir(δ_{ms})$^{-1}$

0.72332363	-0.0028582	0.07313679	0.003245433	-0.0441595
-0.0441595	0.72332363	-0.0028582	0.073136791	0.00324543
0.00324543	-0.0441595	0.72332363	-0.002858176	0.07313679
0.07313679	0.00324543	-0.0441595	0.723323634	-0.0028582
-0.0028582	0.07313679	0.00324543	-0.04415951	0.72332363

δ_{model}	$S*\delta_{model}$	$\delta_{product}$	$Error_{\delta,cir}$ (%)
0.038	0.02755909	0.027	2.070693823
0.084	0.07102935	0.056	26.83812171
0.121	0.09847468	0.086	14.5054413
0.159	0.11213105	0.1	12.13104538
0.205	0.14768756	0.128	15.38090628
		Average	**17.21387867**

Using MS2 and PS2 (For use in Advanced ESM Method)

cir(δ_{ps})

0.019	0.093	0.073	0.06	0.04
0.04	0.019	0.093	0.073	0.06
0.06	0.04	0.019	0.093	0.073
0.073	0.06	0.04	0.019	0.093
0.093	0.073	0.06	0.04	0.019

cir(δ_{ms})

0.024	0.137	0.113	0.081	0.053
0.053	0.024	0.137	0.113	0.081
0.081	0.053	0.024	0.137	0.113
0.113	0.081	0.053	0.024	0.137
0.137	0.113	0.081	0.053	0.024

cir(δ_{ms})$^{-1}$

-6.7967181	0.89487437	0.27247383	0.55772819	7.5226221
7.5226221	-6.7967181	0.89487437	0.27247383	0.55772819
0.55772819	7.5226221	-6.7967181	0.89487437	0.27247383
0.27247383	0.55772819	7.5226221	-6.7967181	0.89487437
0.89487437	0.27247383	0.55772819	7.5226221	-6.7967181

S = cir(δ_{ps})cir(δ_{ms})$^{-1}$

0.66332377	-0.0215781	0.06590635	-0.0056355	-0.0034871
-0.0034871	0.66332377	-0.0215781	0.06590635	-0.0056355
-0.0056355	-0.0034871	0.66332377	-0.0215781	0.06590635
0.06590635	-0.0056355	-0.0034871	0.66332377	-0.0215781
-0.0215781	0.06590635	-0.0056355	-0.0034871	0.66332377

δ_{model}	$S*\delta_{model}$	$\delta_{product}$	$Error_{\delta,cir}$ (%)
0.038	0.02975751	0.027	10.2129959
0.084	0.06229957	0.056	11.2492372
0.121	0.08983499	0.086	4.45929312
0.159	0.10265409	0.1	2.65408608
0.205	0.13946119	0.128	8.95405709
		Average	**6.82916837**

Advanced ESM, Circulant Matrix Approach

S^1 (Between MS1 and PS1)			"x" =	0
0.72332363	-0.0028582	0.07313679	0.003245433	-0.0441595
-0.0441595	0.72332363	-0.0028582	0.073136791	0.00324543
0.00324543	-0.0441595	0.72332363	-0.002858176	0.07313679
0.07313679	0.00324543	-0.0441595	0.723323634	-0.0028582
-0.0028582	0.07313679	0.00324543	-0.04415951	0.72332363

S^2 (Between MS2 and PS2)			"x" =	0.25
0.66332377	-0.0215781	0.06590635	-0.005635471	-0.0034871
-0.0034871	0.66332377	-0.0215781	0.065906352	-0.0056355
-0.0056355	-0.0034871	0.66332377	-0.021578112	0.06590635
0.06590635	-0.0056355	-0.0034871	0.663323773	-0.0215781
-0.0215781	0.06590635	-0.0056355	-0.003487131	0.66332377

ΔS^{1-2} (Difference Between S^1 and S^2)				
-0.2399994	-0.0748797	-0.0289218	-0.035523618	0.16268952
0.16268952	-0.2399994	-0.0748797	-0.028921759	-0.0355236
-0.0355236	0.16268952	-0.2399994	-0.074879741	-0.0289218
-0.0289218	-0.0355236	0.16268952	-0.239999442	-0.0748797
-0.0748797	-0.0289218	-0.0355236	0.162689518	-0.2399994

S^3 (1^{st} order approximation)			"x" =	0.5
0.60332391	-0.040298	0.05867591	-0.014516376	0.03718525
0.03718525	0.60332391	-0.040298	0.058675912	-0.0145164
-0.0145164	0.03718525	0.60332391	-0.040298047	0.05867591
0.05867591	-0.0145164	0.03718525	0.603323913	-0.040298
-0.040298	0.05867591	-0.0145164	0.037185249	0.60332391

Advanced ESM - 1st Order

δ_{model}	$S^3*\delta_{model}$	$\delta_{product}$	$Error_{\delta,1st}$ (%)
0.038	0.03195593	0.027	18.3552979
0.084	0.0535698	0.056	4.339647363
0.121	0.0811953	0.086	5.586855071
0.159	0.09317713	0.1	6.82287321
0.205	0.13123483	0.128	2.527207901
		Average	**7.52637629**

Appendix B

Similitude Calculations for Steady State Temperature

Data

Product

Step	T(bot)	T(top)
0	269.7	165.1
1	194.5	125
2	141	95.2
3	96.7	70.2
4	59.5	47
5	25	25

PS1

Step	T(bot)	T(top)
0	136.4	136.4
1	109.3	109.3
2	85	85
3	63.5	63.5
4	43.8	43.8
5	25	25

PS2

Step	T(bot)	T(top)
0	154.7	133.1
1	120.8	104.2
2	92.3	81
3	67.7	61.1
4	45.7	42.7
5	25	25

Model

Step	T(bot)	T(top)
0	104	72.2
1	81.5	59.3
2	64.5	49.4
3	49.8	40.9
4	37.1	32.8
5	25	25

MS1

Step	T(bot)	T(top)
0	63	63
1	54.1	54.1
2	45.9	45.9
3	38.6	38.5
4	31.7	31.7
5	25	25

MS2

Step	T(bot)	T(top)
0	68.9	61.9
1	57.9	52.4
2	48.4	44.6
3	40	37.7
4	32.3	31.3
5	25	25

TSM Approach (Bottom)

$\lambda_T =$ 1

Step	$T_{product}$	$T_{product,TSM}$	$Error_{T,TSM}$ (%)
0	269.7	104	61.43864
1	194.5	81.5	58.09769
2	141	64.5	54.25532
3	96.7	49.8	48.50052
4	59.5	37.1	37.64706
5	25	25	0.00000
		Average	**39.70012**

TSM Approach (Top)

$\lambda_T =$ 1

Step	$T_{product}$	$T_{product,TSM}$	$Error_{T,TSM}$ (%)
0	165.1	72.2	56.26893
1	125	59.3	52.56000
2	95.2	49.4	48.10924
3	70.2	40.9	41.73789
4	47	32.8	30.21277
5	25	25	0.00000
		Average	**34.52398**

ESM Diagonal Matrix, Using MS1 and PS1 (Bottom)

S Matrix

2.16507937	0	0	0	0
0	2.02033272	0	0	0
0	0	1.85185185	0	0
0	0	0	1.64507772	0
0	0	0	0	1.38170347

T_{model}	$S*T_{model}$	$T_{product}$	$Error_{T,S}$ (%)
104.00000	225.168254	269.7	16.51158548
81.50000	164.657116	194.5	15.34338486
64.50000	119.444444	141	15.28762805
49.80000	81.9248705	96.7	15.27934802
37.10000	51.2611987	59.5	13.84672481
		Average	**14.93927143**

ESM Diagonal Matrix, Using MS1 and PS1 (Top)

S Matrix

2.16507937	0	0	0	0
0	2.02033272	0	0	0
0	0	1.85185185	0	0
0	0	0	1.649350649	0
0	0	0	0	1.38170347

T_{model}	$S*T_{model}$	$T_{product}$	$Error_{T,S}$ (%)
72.20000	156.31873	165.1	5.318758232
59.30000	119.80573	125	4.155415896
49.40000	91.4814815	95.2	3.906006847
40.90000	67.4584416	70.2	3.905353905
32.80000	45.3198738	47	3.57473656
		Average	**3.885378302**

ESM Diagonal Matrix, Using MS2 and PS2 (Bottom)

S Matrix

2.24528302	0	0	0	0
0	2.08635579	0	0	0
0	0	1.90702479	0	0
0	0	0	1.6925	0
0	0	0	0	1.41486068

T_{model}	$S*T_{model}$	$T_{product}$	$Error_{T,S}$ (%)
104.00000	233.509434	269.7	13.41882315
81.50000	170.037997	194.5	12.57686553
64.50000	123.003099	141	12.76375945
49.80000	84.2865	96.7	12.83712513
37.10000	52.4913313	59.5	11.77927518
		Average	**12.48925632**

ESM Diagonal Matrix, Using MS2 and PS2 (Top)

S Matrix

2.15024233	0	0	0	0
0	1.98854962	0	0	0
0	0	1.8161435	0	0
0	0	0	1.620689655	0
0	0	0	0	1.36421725

T_{model}	$S*T_{model}$	$T_{product}$	$Error_{T,S}$ (%)
72.20000	155.247496	165.1	5.967597843
59.30000	117.920992	125	5.663206107
49.40000	89.7174888	95.2	5.758940347
40.90000	66.2862069	70.2	5.575203851
32.80000	44.7463259	47	4.795051322
		Average	**5.448100407**

ESM Circulant Matrix, Using MS1 and PS1 (Bottom)

$cir(\delta_{ps})$

136.4	43.8	63.5	85	109.3
109.3	136.4	43.8	63.5	85
85	109.3	136.4	43.8	63.5
63.5	85	109.3	136.4	43.8
43.8	63.5	85	109.3	136.4

$cir(\delta_{ms})$

63	31.7	38.6	45.9	54.1
54.1	63	31.7	38.6	45.9
45.9	54.1	63	31.7	38.6
38.6	45.9	54.1	63	31.7
31.7	38.6	45.9	54.1	63

$cir(\delta_{ms})^{-1}$

0.0269948	0.0005522	0.00026444	0.00044377	-0.0239689
-0.0239689	0.0269948	0.0005522	0.000264439	0.00044377
0.00044377	-0.0239689	0.0269948	0.000552196	0.00026444
0.00026444	0.00044377	-0.0239689	0.026994799	0.0005522
0.0005522	0.00026444	0.00044377	-0.023968877	0.0269948

$S = cir(\delta_{ps})cir(\delta_{ms})^{-1}$

2.74326549	-0.1977084	-0.2144251	-0.218063279	-0.2356577
-0.2356577	2.74326549	-0.1977084	-0.214425106	-0.2180633
-0.2180633	-0.2356577	2.74326549	-0.197708357	-0.2144251
-0.2144251	-0.2180633	-0.2356577	2.743265488	-0.1977084
-0.1977084	-0.2144251	-0.2180633	-0.235657687	2.74326549

T_{model}	$S*T_{model}$	$T_{product}$	$Error_{T,cir}$ (%)
104	235.753509	269.7	12.5867598
81.5	167.547031	194.5	13.85756767
64.5	117.254894	141	16.84050083
49.8	74.0073522	96.7	23.46706085
37.1	37.937	59.5	36.24033614
		Average	**22.60136637**

ESM Circulant Matrix, Using MS1 and PS1 (Top)

$cir(\delta_{ps})$

136.4	43.8	63.5	85	109.3
109.3	136.4	43.8	63.5	85
85	109.3	136.4	43.8	63.5
63.5	85	109.3	136.4	43.8
43.8	63.5	85	109.3	136.4

$cir(\delta_{ms})$

63	31.7	38.5	45.9	54.1
54.1	63	31.7	38.5	45.9
45.9	54.1	63	31.7	38.5
38.5	45.9	54.1	63	31.7
31.7	38.5	45.9	54.1	63

$cir(\delta_{ms})^{-1}$

0.02705468	0.0004227	0.00033516	0.000444988	-0.0239694
-0.0239694	0.02705468	0.0004227	0.000335163	0.00044499
0.00044499	-0.0239694	0.02705468	0.000422696	0.00033516
0.00033516	0.00044499	-0.0239694	0.027054682	0.0004227
0.0004227	0.00033516	0.00044499	-0.023969364	0.02705468

$S = cir(\delta_{ps})cir(\delta_{ms})^{-1}$

2.74334676	-0.2049466	-0.2065562	-0.217985855	-0.235642
-0.235642	2.74334676	-0.2049466	-0.206556205	-0.2179859
-0.2179859	-0.235642	2.74334676	-0.204946556	-0.2065562
-0.2065562	-0.2179859	-0.235642	2.743346763	-0.2049466
-0.2049466	-0.2065562	-0.2179859	-0.235642023	2.74334676

T_{model}	$S*T_{model}$	$T_{product}$	$Error_{T,cir}$ (%)
72.2	159.067749	165.1	3.653695257
59.3	119.944664	125	4.044268577
49.4	90.6518217	95.2	4.777498187
40.9	66.0000004	70.2	5.982905408
32.8	42.5295895	47	9.511511692
		Average	**6.079045966**

ESM Circulant Matrix, Using MS2 and PS2 (Bottom)

$cir(\delta_{ps})$

154.7	45.7	67.7	92.3	120.8
120.8	154.7	45.7	67.7	92.3
92.3	120.8	154.7	45.7	67.7
67.7	92.3	120.8	154.7	45.7
45.7	67.7	92.3	120.8	154.7

$cir(\delta_{ms})$

68.9	32.3	40	48.4	57.9
57.9	68.9	32.3	40	48.4
48.4	57.9	68.9	32.3	40
40	48.4	57.9	68.9	32.3
32.3	40	48.4	57.9	68.9

$cir(\delta_{ms})^{-1}$

0.02331951	0.00041065	0.0002653	0.000158025	-0.0201131
-0.0201131	0.02331951	0.00041065	0.000265298	0.00015803
0.00015803	-0.0201131	0.02331951	0.000410652	0.0002653
0.0002653	0.00015803	-0.0201131	0.023319513	0.00041065
0.00041065	0.0002653	0.00015803	-0.020113084	0.02331951

$S = cir(\delta_{ps})cir(\delta_{ms})^{-1}$

2.77315276	-0.1857925	-0.1988088	-0.212897753	-0.2314113
-0.2314113	2.77315276	-0.1857925	-0.19880879	-0.2128978
-0.2128978	-0.2314113	2.77315276	-0.185792466	-0.1988088
-0.1988088	-0.2128978	-0.2314113	2.77315276	-0.1857925
-0.1857925	-0.1988088	-0.2128978	-0.231411328	2.77315276

T_{model}	$S*T_{model}$	$T_{product}$	$Error_{T,cir}$ (%)
104	241.254966	269.7	10.54691664
81.5	172.162373	194.5	11.48464088
64.5	121.238693	141	14.01511162
49.8	78.2567953	96.7	19.07260047
37.1	42.1024454	59.5	29.2395875
		Average	**18.45298512**

ESM Circulant Matrix, Using MS2 and PS2 (Top)

$cir(\delta_{ps})$

133.1	42.7	61.1	81	104.2
104.2	133.1	42.7	61.1	81
81	104.2	133.1	42.7	61.1
61.1	81	104.2	133.1	42.7
42.7	61.1	81	104.2	133.1

$cir(\delta_{ms})$

61.9	31.3	37.7	44.6	52.4
52.4	61.9	31.3	37.7	44.6
44.6	52.4	61.9	31.3	37.7
37.7	44.6	52.4	61.9	31.3
31.3	37.7	44.6	52.4	61.9

$cir(\delta_{ms})^{-1}$

0.02782905	0.00044673	0.00021453	-0.00018581	-0.0239166
-0.0239166	0.02782905	0.00044673	0.000214534	-0.0001858
-0.0001858	-0.0239166	0.02782905	0.000446733	0.00021453
0.00021453	-0.0001858	-0.0239166	0.027829049	0.00044673
0.00044673	0.00021453	-0.0001858	-0.023916615	0.02782905

$S = cir(\delta_{ps})cir(\delta_{ms})^{-1}$

2.73538067	-0.2062409	-0.2086225	-0.226233761	-0.2421554
-0.2421554	2.73538067	-0.2062409	-0.208622482	-0.2262338
-0.2262338	-0.2421554	2.73538067	-0.206240936	-0.2086225
-0.2086225	-0.2262338	-0.2421554	2.735380669	-0.2062409
-0.2062409	-0.2086225	-0.2262338	-0.242155364	2.73538067

T_{model}	$S*T_{model}$	$T_{product}$	$Error_{T,cir}$ (%)
72.2	157.762789	165.1	4.444100885
59.3	118.583027	125	5.133578167
49.4	89.1558427	95.2	6.34890468
40.9	64.6716865	70.2	7.875090488
32.8	41.378475	47	11.96069144
		Average	**7.829566194**

Advanced ESM, Diagonal Matrix (Bottom)

Shape	Coef.
Cup	1.5797653
Flat w/Point	1.14034883
Flat	1.10355825
Circle	1.0304175
Point	1

S^1 (Between MS1 and PS1)			"i" =	1.0304175
2.16507937	0	0	0	0
0	2.02033272	0	0	0
0	0	1.85185185	0	0
0	0	0	1.64507772	0
0	0	0	0	1.38170347

S^2 (Between MS2 and PS2)			"i" =	1.10355825
2.24528302	0	0	0	0
0	2.08635579	0	0	0
0	0	1.90702479	0	0
0	0	0	1.6925	0
0	0	0	0	1.41486068

$S\{i_1,i_2\}$ (Divided Difference Between S^1 and S^2)				
1.09656587	0	0	0	0
0	0.9026851	0	0	0
0	0	0.75433926	0	0
0	0	0	0.64837013	0
0	0	0	0	0.45333428

S^3 (1^{st} order approximation)			"i" =	1.5797653
2.76747541	0	0	0	0
0	2.51622079	0	0	0
0	0	2.26624646	0	0
0	0	0	2.001258423	0
0	0	0	0	1.63074166

T_{model}	$S*T_{model}$	$T_{product}$	$Error_{T,S,1st}$ (%)
104	287.817443	269.7	6.717627982
81.5	205.071995	194.5	5.435472762
64.5	146.172897	141	3.668721099
49.8	99.6626695	96.7	3.063774025
37.1	60.5005156	59.5	1.681538845
		Average	**4.113426943**

Advanced ESM, Diagonal Matrix (Top)

Shape	Coef.
Cup	1.5797653
Flat w/Point	1.14034883
Flat	1.10355825
Circle	1.0304175
Point	1

S^1 (Between MS1 and PS1)			"i" =	1.0304175
2.16507937	0	0	0	0
0	2.02033272	0	0	0
0	0	1.85185185	0	0
0	0	0	1.649350649	0
0	0	0	0	1.38170347

S^2 (Between MS2 and PS2)			"i" =	1
2.15024233	0	0	0	0
0	1.98854962	0	0	0
0	0	1.8161435	0	0
0	0	0	1.620689655	0
0	0	0	0	1.36421725

$S\{i_1,i_2\}$ (Divided Difference Between S^1 and S^2)				
0.4877797	0	0	0	0
0	1.04489519	0	0	0
0	0	1.17394114	0	0
0	0	0	0.942253461	0
0	0	0	0	0.57487361

S^3 (1^{st} order approximation)			"i" =	1.14034883
2.21870164	0	0	0	0
0	2.13519944	0	0	0
0	0	1.98090477	0	0
0	0	0	1.752933829	0
0	0	0	0	1.44490009

T_{model}	$S*T_{model}$	$T_{product}$	$Error_{T,S,1st}$ (%)
72.2	160.190258	165.1	2.97379876
59.3	126.617327	125	1.293861363
49.4	97.8566955	95.2	2.790646518
40.9	71.6949936	70.2	2.129620505
32.8	47.392723	47	0.835580897
		Average	**2.004701608**

Advanced ESM, Circulant Matrix (Bottom)

S^1 (Between MS1 and PS1)			"i" =	1.0304175
2.74326549	-0.1977084	-0.2144251	-0.218063279	-0.2356577
-0.2356577	2.74326549	-0.1977084	-0.214425106	-0.2180633
-0.2180633	-0.2356577	2.74326549	-0.197708357	-0.2144251
-0.2144251	-0.2180633	-0.2356577	2.743265488	-0.1977084
-0.1977084	-0.2144251	-0.2180633	-0.235657687	2.74326549

S^2 (Between MS2 and PS2)			"i" =	1.10355825
2.77315276	-0.1857925	-0.1988088	-0.212897753	-0.2314113
-0.2314113	2.77315276	-0.1857925	-0.19880879	-0.2128978
-0.2128978	-0.2314113	2.77315276	-0.185792466	-0.1988088
-0.1988088	-0.2128978	-0.2314113	2.77315276	-0.1857925
-0.1857925	-0.1988088	-0.2128978	-0.231411328	2.77315276

$S\{i_1,i_2\}$ (Divided Difference Between S^1 and S^2)				
0.4086268	0.16291727	0.21351047	0.070624459	0.05805736
0.05805736	0.4086268	0.16291727	0.213510468	0.07062446
0.07062446	0.05805736	0.4086268	0.162917267	0.21351047
0.21351047	0.07062446	0.05805736	0.408626804	0.16291727
0.16291727	0.21351047	0.07062446	0.058057358	0.4086268

S^3 (1^{st} order approximation)			"i" =	1.5797653
2.96774372	-0.1082101	-0.0971336	-0.179265888	-0.203764
-0.203764	2.96774372	-0.1082101	-0.097133601	-0.1792659
-0.1792659	-0.203764	2.96774372	-0.108210115	-0.0971336
-0.0971336	-0.1792659	-0.203764	2.967743723	-0.1082101
-0.1082101	-0.0971336	-0.1792659	-0.203764005	2.96774372

T_{model}	$S*T_{model}$	$T_{product}$	$Error_{T,S,1st}$ (%)
104	277.07402	269.7	2.734156375
81.5	202.212087	194.5	3.965083143
64.5	147.176531	141	4.380518463
49.8	105.924199	96.7	9.538986003
37.1	69.2229544	59.5	16.34109991
		Average	**7.391968778**

Advanced ESM, Circulant Matrix (Top)

S^1 (Between MS1 and PS1)			"i" =	1.0304175
2.74334676	-0.2049466	-0.2065562	-0.217985855	-0.235642
-0.235642	2.74334676	-0.2049466	-0.206556205	-0.2179859
-0.2179859	-0.235642	2.74334676	-0.204946556	-0.2065562
-0.2065562	-0.2179859	-0.235642	2.743346763	-0.2049466
-0.2049466	-0.2065562	-0.2179859	-0.235642023	2.74334676

S^2 (Between MS2 and PS2)			"i" =	1
2.73538067	-0.2062409	-0.2086225	-0.226233761	-0.2421554
-0.2421554	2.73538067	-0.2062409	-0.208622482	-0.2262338
-0.2262338	-0.2421554	2.73538067	-0.206240936	-0.2086225
-0.2086225	-0.2262338	-0.2421554	2.735380669	-0.2062409
-0.2062409	-0.2086225	-0.2262338	-0.242155364	2.73538067

$S\{i_1,i_2\}$ (Divided Difference Between S^1 and S^2)				
0.26189181	0.04255378	0.06793051	0.271156605	0.21413139
0.21413139	0.26189181	0.04255378	0.06793051	0.2711566
0.2711566	0.21413139	0.26189181	0.042553778	0.06793051
0.06793051	0.2711566	0.21413139	0.261891811	0.04255378
0.04255378	0.06793051	0.2711566	0.21413139	0.26189181

S^3 (1^{st} order approximation)			"i" =	1.14034883
2.77213688	-0.2002686	-0.1990885	-0.188177248	-0.2121023
-0.2121023	2.77213688	-0.2002686	-0.199088514	-0.1881772
-0.1881772	-0.2121023	2.77213688	-0.200268563	-0.1990885
-0.1990885	-0.1881772	-0.2121023	2.772136879	-0.2002686
-0.2002686	-0.1990885	-0.1881772	-0.212102273	2.77213688

T_{model}	$S*T_{model}$	$T_{product}$	$Error_{T,S,1st}$ (%)
72.2	163.78398	165.1	0.797104611
59.3	124.865732	125	0.107414539
49.4	96.0584122	95.2	0.901693525
40.9	70.8006357	70.2	0.85560638
32.8	46.6898115	47	0.659975565
		Average	**0.664358924**

References

ABAQUS/Standard User's Manual, Version 6.2, 2001, Hibbitt, Karlsson & Sorensen, Inc.

Astarita, G., 1997, "Dimensional analysis, scaling, and orders of magnitude," *Chemical Engineering Science*, 52, no. 24, pp. 4681-4698.

Barlow, J. W., Beaman, J. J., and Balasubramanian, B., 1996, "A rapid mould-making system: material properties and design considerations," *Rapid Prototyping Journal*, **2**, no. 3, pp. 4-15.

Barr, D. I. H. 1979. "Echelon Matrices in Dimensional Analysis," *International Journal of Mechanical Engineering Education*, **7**, no. 2, pp. 85-89.

Barr, D. I. H., 1982, "A survey of procedures for dimensional analysis," *International Journal of Mechanical Engineering Education*, **11**, no. 3, pp. 147-159.

Barr, D. I. H., 1984, "Consolidation of basics of dimensional analysis," *Journal of Engineering Mechanics*, **110**, no. 9, pp. 1357-1375.

Beaman, J. J., Barlow, J. W., Bourell, D. L., Crawford, R. H., Marcus, H. L., and McAlea, K. P., 1997, Solid Freeform Fabrication: A New Direction in Manufacturing, Kluwer, Massachusetts.

Bridgman, P. W. 1931. Dimensional Analysis, Yale University Press, New Haven.

Burden, R. L., and Faires, J. D., 1989, Numerical Analysis, PWS Kent, Boston.

Cho, U., and Wood, K., 1997, "Empirical Similitude Method for the Functional Test with Rapid Prototypes," *Proceedings of the Solid Freeform Fabrication Symposium*, Austin TX, September, 1997, pp. 559-567.

Cho, U., Wood, K. L., and Crawford, R. H., 1998, "Online Functional Testing with Rapid Prototypes: a Novel Empirical Similarity Method," *Rapid Prototyping Journal*, **4**, No. 3, pp. 128-138.

Cho, U., Wood, K. L., and Crawford, R. H., 1998b, "Novel empirical similarity method for the reliable product test with rapid prototypes," *Proceedings of DETC*, Atlanta, GA, Sept. 13-16, 1998.

Cho, U., 1999, Novel Empirical Similarity Method for Rapid Product Testing and Development, Doctoral dissertation, The University of Texas at Austin.

Cho, U., Wood, K. L., and Crawford, R. H., 1999b, "Error measures for functional product testing," *Proceedings of DETC*, Las Vegas, NV, Sept. 13-16, 1999.

Cho, U., Wood, K. L., and Crawford, R. H., 1999c, "System-level functional testing for scaled prototypes with configurational distortions," *Proceedings of DETC*, Las Vegas, NV, Sept. 1999.

Chua, C. K., Teh, S. H., and Gay, R. K. L., 1999, "Rapid Prototyping Versus Virtual Prototyping in Product Design and Manufacturing," *International Journal of Advanced Manufacturing Technology*, **15**, pp. 597-603.

Davis, P. J., 1979, Circulant Matrices, John Wiley, New York.

Deb, M. K., and Deb, A., 1986, "The matrix method: a powerful technique in dimensional analysis," *Journal of the Franklin Institute*, 321, no. 4, pp. 233-240.

DeVor, R. E., Chang, T., and Sutherland, J. W., 1992, Statistical Quality Design and Control, Macmillan, New York.

Dornfeld, W. H., 1995, "Direct dynamic testing of scaled stereolithographic models," *Sound and Vibration*, Aug. 1995, pp. 12-17.

Dulieu-Barton, J. M., and Fulton, M. C., 2000, "Mechanical Properties of a Typical Stereolithography Resin," *Strain*, **36,** No. 2, pp. 81-87.

Farrar, C. R., Baker, W. E., and Dove, R. C., 1994, "Dynamic Parameter Similitude for Concrete Models," *ACI Structural Journal*, Jan-Feb, pp. 90-99.

Fuhrmann, P. A., 1996, A Polynomial Approach to Linear Algebra, Springer, New York.

Gerhart, P. M., Gross, R. J., and Hochstein, J. I., 1992, Fundamentals of Fluid Mechanics, Addison-Wesley, Massachusetts.

Holman, J. P., 1990, Heat Transfer, McGraw-Hill, New York.

Huntley, H. E., 1955, Dimensional Analysis, Rinehart, New York.

Kochan, D., 1993, Solid Freeform Manufacturing, Elsevier, Amsterdam.

Kolodziej, J. A., and Strek, T., 2001, "Analytical approximations of the shape factors for conductive heat flow in circular and regular polygonal cross-sections," *International Journal of Heat and Mass Transfer*, **44**, pp. 999-1012.

Langhaar, H. L., 1951, Dimensional Analysis and Theory of Models, John Wiley & Sons, New York.

Moe, R. E., 2002, Prototype Partitioning Derived from Requirement Flexibility, Masters thesis, The University of Texas at Austin.

Mortenson, M. E., 1995, Geometric Transformations, Industrial Press, New York.

Murphy, G., 1950, Similitude in Engineering, The Ronald Press Company, New York.

Nickolay, M., Fischer, L., and Martin, H., 1998, "Shape factors for conductive heat flow in circular and quadratic cross-sections," *International Journal of Heat and Mass Transfer*, **41**, no. 11, pp. 1437-1444.

Otto, K. N., and Wood, K. L., 2001, Product Design: Techniques in Reverse Engineering and New Product Development, Prentice Hall, New Jersey.

Schnittger, J. R., 1988, "Dimensional analysis in design," *Journal of Vibration, Acoustics, Stress, and Reliability in Design*, **110**, July, 1988, pp. 401-407.

Shigley, E. J., and Mischke, C. R. 1989, Mechanical Engineering Design, McGraw-Hill.

Strang, G. 1988. Linear Algebra and its Applications, Harcourt Brace Jovanovich, San Diego.

Szirtes, T., 1998, Applied Dimensional Analysis and Modeling, McGraw-Hill, New York.

Szucs, E. 1980. Similitude and Modeling, Elsevier, Amsterdam.

Taylor, E. S., 1974, Dimensional Analysis for Engineers, Oxford University Press, Belfast.

Timoshenko, S. P., and Goodier, J. N., 1970, Theory of Elasticity, McGraw-Hill, Auckland.

Ullman, D. G., 1997, The Mechanical Design Process, McGraw-Hill, New York.

Ulrich, K. T., and Eppinger, S. D., 2000, Product Design and Development, McGraw-Hill, Boston.

Usmani, R. A., 1987, Applied Linear Algebra, Marcel Dekker, New York.

Vosniadou, S., and Ortony, A., 1989, Similarity and Analogical Reasoning, Cambridge University Press, Cambridge.

Wang, Z., and Almenas, K., 1989, "A methodology quantifying the range of applicability of scaling laws," *Nuclear Science and Engineering*, **102**, pp. 101-113.

Watson, D. A., 1999, Process Optimization for Selective Laser Sintering Through the Use of Design Rules and Constraints, Master's Thesis, University of Texas at Austin.

Webster's Universal College Dictionary, 1997, Gramercy, New York.

Wood, J. J., 2002, Design Methodology Using Empirical and Virtual Analysis with Application to Compliant Systems, Doctoral dissertation, Colorado State University.

Wood, J. J., and Wood, K. L. 2002b. "Empirical Analysis using Advanced Similarity Methods," *Proceedings of DETC 2002*.

Wood, K. L., Beaman, J. J., Crawford, R. H., and Bourell, D. L., 1999, CyPhy Process for Rapid Engineering Design and Evaluation, Proposal submitted to the National Science Foundation.

Vita

Alan James Dutson was born in Idaho Falls, Idaho on August 6, 1970, the son of William Daniel Dutson and Faun Arlene Dutson. He graduated from Bonneville high school in Idaho Falls, Idaho in 1988. After high school, he attended Brigham Young University in Provo, Utah where he received Bachelor of Science and Master of Science degrees in mechanical engineering in August 1994 and December 1995, respectively. He worked for Motorola in Fort Worth, Texas from January 1996 to August 1999. In August 1999 he entered The University of Texas at Austin to pursue a PhD in mechanical engineering. Alan is married to Joanna Moody Dutson and they have five children.

Permanent address: 777 Engleman Drive
Rexburg, ID 83440

This dissertation was typed by the author.